# Rapid Synthesis of Thiol-Co-Capped CdTe/CdSe/ZnSe Multi-Core-Shell QDs and Their Encapsulation in Liposomes and Chitosan Nanoparticles; Comparative Bio-compatibility Studies Using Hela and Vero Cells''.

A thesis presented by

**Daramola Abiodun Olamide**

Submitted in fulfilment for the award of the degree of

**PhD in Chemistry**

Department of Chemistry

**Rhodes University.**

**Supervisor: Prof. R.W.M Krause**

**Co-supervisor: Dr P.F Tseki**

## Abstract

The common method that has been used to reduce the toxicity posed to living cells by CdTe Quantum Dots (QDs) is through the synthesis of CdTe multi-core-shells nanoparticles. In this process, the surface of CdTe QDs is usually coated by less toxic ZnS or ZnSe shells. This heterostructure compound does not only reduce the toxicity of CdTe QDs but can also be used in applications such as deep tissue imaging. The heterostructures can be in numerous forms such as CdTe/CdSe/ZnSe or CdTe/CdSe/ZnS or CdTe/CdS/ZnS multi-core-shell QDs. However, the drawbacks attributed to the fabrication of these compounds is long synthesis times (6- 24 h) in achieving the highest wavelength emission maxima. Others are the use of toxic reagents and poor reproducibility of synthesized materials. An additional problem is that the ZnSe or ZnS coating is insufficient to completely protect the highly toxic Cd metal from escaping into immediate solution. This limits their use in biochemistry and with living systems. Liposomes and biopolymers such as chitosan are known to be environmentally friendly compounds that have been used in various studies as delivery systems for QDs and model drugs for drug delivery applications. They are generally non-toxic and highly bio-compatible. In this study, the rapid synthesis of thiol-co-capped CdTe/CdSe/ZnSe multi-core-shell QDs with a maximum reaction time of 35 mins, gave reliable QDs with emission maxima at 625 nm. The multi-core-shell QDs were encapsulated in two different bio-compatible environments, namely liposome and chitosan nanoparticles (CNP) at 14 different formulations (F) for liposome and 12 different formulations for CNP. Cytotoxicity and florescence imaging studies using HeLa and Vero cells, were used to investigate the improved bio-compatibility. Various characterization techniques were used to elucidate the optical properties, morphology and physico-chemical properties of the QDs and

nanocomposites. Two of the best formulations, QD-liposome vesicles (LVs)-F12 and QD-CNP-F9 (with chitosan), demonstrated high loading efficiencies of 42 ± 6 % and 59 ± 5 %, respectively. While the plain CdTe QDs showed high toxicity, some of the encapsulated materials, QD-LVs-F1 and F12, depicted no-toxicity against the cells ($IC_{50}$ > 0.5 mg/ml). The QDs also retained most of their fluorescence and properties and could easily be tracked in cells and visualized around the nucleus, indicating the successful internalization of the QDs in the cytosol.

These results shows that encapsulation of CdTe multi-core-shell QDs in liposomes produce better bio-compatibility compared to multi-core-shell QDs and better than CNP coating. These particles therefore show good promise in cell-labelling, drug delivery studies. Their core-shell nanoparticles have also shown good behavior in enhancing the memory of a device which is based on some recent collaborated works.

## Declaration

I declare that this thesis is my own work and has been submitted for the degree of PhD in Science at Rhodes University. It has not been submitted before for any degree or examination at any other University. I also state that all the sources used in this study have been duly acknowledged.

CANDIDATE: Daramola Abiodun Olamide.

SIGNATURE: _____

DATE: _____

SUPERVISOR: Prof Rui Maçedo Krause

SIGNATURE: _____

DATE: _____

CO-SUPERVISOR: Dr Potlaki Foster Tseki

SIGNATURE: _____

DATE: _____

## Dedication

I hereby dedicate this study to my wife and my lovely daughters.

## Acknowledgement

Firstly, I acknowledge the Almighty God for giving me another grace to start and finish my PhD program.

I acknowledge my supervisors Prof. R.W.M Krause and Dr P.F Tseki for their advice throughout the study. Their interest in the study, valuable suggestions and fruitful criticism assisted me to gain more confidence in the study.

I also want to say a big thank you to Dr X. Siwe Noundou who has been guiding me since the very first day I started my post graduate program. He has really contributed to various skills achieved during both Masters and PhD program.

A special thank also goes to our collaborator (Prof Edkins) who assisted for the biological evaluation aspect of the study. We really appreciate her for carefully spending enough time in assessing the interactions of our QDs and their composite with the cells. I equally want to say a big thank you to Prof Edkins' post-doctoral student Dr Laura Dingle who did a fantastic work in evaluating the toxicity and cellular imaging studies of our QDs and their composite. I would also like to acknowledge Mr Marvin from the Rhodes University Electron Beam Lab for TEM microscopy work in analyzing the morphology and the elemental composition of all the materials produced in this study. We appreciate the Rhodes University XRD unit for some structural morphology measurement and I would also like to thank the Center of Excellence in Strong Materials at University of Witwatersrand for additional Electron Microscope Analysis. I equally want to thank WSU Chemistry Department who gave me the opportunity to use their lab in carrying out the synthesis and the analysis of the compounds produced in this study.

## List of Chapters

## Table of content.



## Table of chapters

## Table of Figures.

## List of Tables.

## Table of Acronyms

| Abbreviation | Full Names |
|---|---|
| CNP | Chitosan nanoparticles |
| CS | Core-shell |
| CSS | Core-shell-shell |
| EDX | Energy dispersive X- ray |
| F | Formulations |
| FTIR | Fourier transmission infrared |
| GSH | Glutathione |
| IC | Inhibitory concentration |
| LV | Liposomes vesicles |
| MPA | Mercaptopropionoic acid |
| PL | Photoluminescence |

| | |
|---|---|
| QDs | Quantum dots |
| TEM | Transmission electron microscope |
| TGA | Thioglycolic acid |
| TGA | Thermogravimetry analysis |
| UV-vis | Ultra-violent - visible |
| XRD | X-ray diffraction |

# CHAPTER 1.

## 1. Introduction and literature review.

Semiconductor nanoparticle also known as quantum dots (QDs) are good candidates in various medical applications due to their high optical and photo-physical properties [1 - 3]. These possess characteristics such as good chemical and photo-stability, high quantum yield and size dependent tunable light emission properties [4 - 6]. The light emission properties allow them to emit light from blue to the near infra-red wavelength (> 650 nm) comparable to organic dyes. This photo-physical property places them as suitable candidates for clinical procedures in routine medical processes including deep tissue imaging [7 – 11].

The common method that has generally been used to prepare QDs are the organic and aqueous phase syntheses.

### 1.1. Organic synthesis

The synthesis of nano-particles in organic phase involves the use of an organic solvent maintained relatively at high temperature under an inert atmosphere. Tri-*n*-octyl phosphine oxide (TOPO), tri-octyl phosphine (TOP), hexadecyl amine (HDA) among others have been reported as common organic solvents used for the synthesis of nano-crystals in the past years with excellent optical properties [12- 14]. However, some of the main draw backs that arise from this synthetic route is that nano-particle that are synthesized in organic phase are usually insoluble in water. Secondly, most of these organic solvents are very toxic which disallows them in the

production of QDs that can be used in biological evaluations. Thirdly the reaction is usually carried out under vigorous high temperature reaction condition (> 400$^{o}$C) and finally, QDs obtained this way are deemed not cost effective [13].

A slightly different approach that has been demonstrated to overcome some of these problems posed by nanoparticle synthesized in organic media is to modify their surfaces with water soluble ligands. This is used to increase the aqueous solubility of the synthesized nanoparticles which is commonly achieved through a ligand exchange process [2 and 4]. However, a few challenges encountered when using surface modification process is the reduction in fluorescence quantum yield of synthesized material and the formation of thick surface coating layer which tends to increases the size of the QD particles. Therefore, this does not permit such materials to be used in areas where size limits transportation such as the brain or cell nucleus [2]. In view of the observed practical challenges, it seems preferable that direct aqueous synthesis is the best option for preparing nanoparticles especially those intended for bio-medical applications like drug delivery processes.

**1.2. Aqueous synthesis.**

The aqueous synthesis method for synthesizing semiconductor nanoparticles uses water as the solvent, usually at much lower temperatures than the organic solvent synthesis, but sometimes under very high pressures instead. This synthetic route is also referred to as a “green synthesis” method due to the use of more environmentally friendly materials, lower cost of materials, ambient reaction conditions and the aqueous solubility of the synthesized QDs product [15- 16]. For possible biological applications, less toxic and water soluble QDs are desirable. This is not

possible with the organic capped QDs unless the materials undergo further surface modification processes**.**

### 1.3. Cadmium telluride Quantum Dots (CdTe QDs)

One of the common QDs that has found application in diverse fields is CdTe QDs, this is due to the outstanding optical properties compared to other QDs such as CdS, CdSe, ZnS, ZnSe etc [17 – 20].

However, one of the major problems associated with the synthesis of this type of QDs is the instability of the tellurium (Te) source [1, 19]. The use of Te powder or $H_2Te$ gas as a source for tellurium leads to either unstable or highly poisonous QDs [17]. In contrast, the source of Te such as potassium and sodium tellurites show huge potential for successful preparation of CdTe QDs which possess high emission intensity (PLQY 98 %) and good photo-stability [18, 20]. Therefore, these tellurium sources have softened the problem of instability and toxicity of the tellurium sources.

Another major concern regarding the use of these nanoparticles is their inherent toxicity profile [21- 23]. QDs, such as CdSe and CdTe, are heavy metal chalcogenide compounds that may leach out toxic metals into the surrounding environment. This challenge has led researchers to develop more chemically benign methods to make suitable QDs for biological applications [24, 26- 28]. In an effort to reduce the toxicity of these QDs, some of the standard approaches used, include surface modifications of the QDs utilizing thiol-ligand containing molecules or less-heavy metal barrier shell (ZnSe/ZnS); surface coating with an in-organic shell such as silica shell; embedding

the synthesized QDs in polymer matrices and encapsulation in lipid or polymer-based delivery system such as liposomes or chitosan [9-10, 21].

The use of a metal barrier shell to passivate the surface of a nanoparticle has assisted to produce material with high florescence intensity, long-term photo stability and to reduce toxicity effects [2, 5, 29- 30]. This approach is usually known as core-shell nanoparticles and it involves the epitaxial growth of the semi-conductor material (with a larger band gap) on another core with a lower band gap.

The synthesis of core-shell nanoparticles using CdTe core as the basic material has been reported in literature. These nanoparticles show excellent optical properties and find use as bio sensors and bio-imaging in various biological applications [31- 38].

It was Yang *et al in* 2010 who reportedly synthesized CdTe/CdSe core-shell by passivating the surface of the CdTe core with CdSe shell for improved optical properties and stability. The synthesized material was subsequently used as fluorescence probe for the determination of ascorbic acid in aqueous solution [33]. Also, He *et al* in 2012 synthesized CdTe/CdSe QDs coated with carboxyl methyl chitosan-coated CdTe/CdS using a microwave irradiation method. The synthesized QDs were used as fluorescent probe for imaging live Madin-Darby canine kidney (MDCK) cells. Preliminary studies demonstrated that the modified QDs possessed good biocompatibility and were promising candidates for bio-labeling and imaging applications [39].

Also, in 2009 Ruosheng and colleagues showed in their study that CdTe/CdSe core-shell QDs could be used as florescent probe in the labelling of tumor cell. The synthesized CdTe core-shell QDs were reported to show good optical stability compared to CdTe QDs [16].

Chen and co-workers also prepared near infrared emitting glutathione-capped CdTe/CdSe core-shell nanoparticle in aqueous solutions and used these for cellular imaging of human melanoma cancer A375 cells [34]. Furthermore, aqueous synthesis of highly stable CdTe/ZnS Core/Shell QDs by Saikai *et al* have found application in bioimaging of E. coli cells. These synthesized core-shell QDs were reported to show higher photoluminescence quantum yield (PLQY) approaching 50% compared to those of CdTe QDs only with nearly 12% PLQY. It was also observed that the synthesized CdTe core-shell showed better bio-compatibility compared with CdTe QDs during imaging studies with E. coli cells [40]

It should be noted that most of the CdTe core-shell discussed in various literature sources are passivated by CdSe or CdS shell. Therefore, the toxic Cd ion in CdSe or CdS shell need to be prevented from direct contact with cells/tissue during application involving in-vitro or in-vivo studies. The technique to mitigate this might be performed by coating the surface of the CdSe or CdS shell with another outer layer of ZnSe or ZnS. The passivation achieved by ZnSe or ZnS shell on the surface of the core-shell allows the synthesized CdTe/CdSe/ZnS or ZnSe multi-core-shell to produce even higher florescence intensity, show longer photo-stability and lower cytotoxicity [40- 42]. The confinement of the excitons within the CdTe/CdSe interface by the substantially wider band gap of ZnSe/ZnS shell usually accounts for the enhanced optical property displayed by CdTe multi-core-shell QDs [40]. The synthesis of CdTe multi core-shell QDs has also been reported in connection with applications involving deep tissue imaging. This is ascribed to its ability to emit light towards the NIR region of the spectrum [40- 41].

### 1.4. Thiol ligands

The surfaces of synthesized CdTe QDs are mostly stabilized by thiol ligands. Thiol-capped QDs are widely successful colloidal QDs in aqueous solutions [12, 17], they exhibit ease of processability leading to a variety of composite materials that serve as building blocks for higher order structures [21, 42]. Thiol capped QDs are responsible for about 40-80% of PLQY because of their good surface functionality in aqueous solutions [17].

Thiol capped CdTe QDs are commonly synthesized in aqueous solution though a precipitation reaction between a metal and a chalcogenide, this reaction takes place in the presence of a short chain thiol ligand in aqueous media [43- 44]. The metal-thiol complex is formed at the initial stage then the chalcogenide is injected into the reaction mixture which reacts together over time to form a thiol capped metal chalcogenide [17]. The CdTe nanoparticle that is formed in this case is surrounded by the thiol Ligand. The role of sulfur from the mercapto (thiol) is to passivate the surface to enhances the colloidal stability and the chemical functionality of the nanoparticles [12, 21]. In recent years, mercapto acids, specifically mercaptopropionoic acid (MPA) and thioglycolic acid (TGA) have been used to synthesize CdTe QDs because they impart a negative charge to the surface of the nanoparticles and allow formation of strongly emitting colloids that are stable for months and years [12]. There have also been other types of thiol ligands used extensively by various researchers in the past; however, the four main types of thiol ligands that have consistently demonstrated outstanding results when used to passivate the surface of CdTe QDs are MPA, TGA, L-cysteine and glutathione (GSH).

In the sketch which follows, we show the structural formulas for some of the thiol ligands.

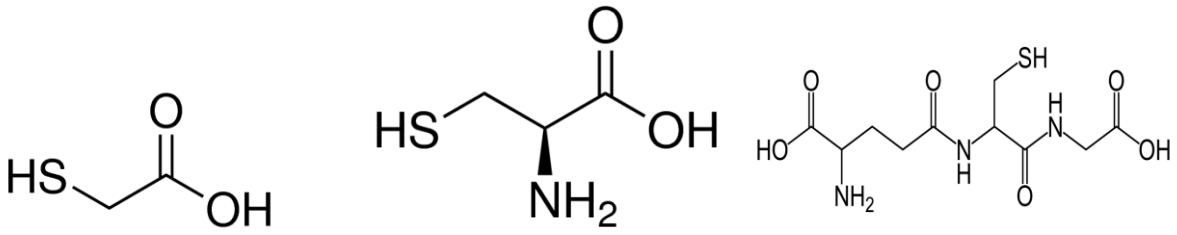


(a) Thioglycolic acid (b) L-cysteine (c) Glutathione

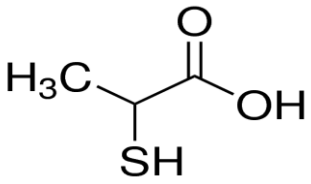


(d) 2-Mercaptopropionoic acid.

**Figure 1**. The structures of common thiol capping ligands employed in the aqueous synthesis of CdTe QDs [17].

In previous works, it was shown that the use of MPA and TGA as capping agent has led to the production of highly optically stable CdTe QDs [17].

In addition, MPA, GSH, TGA and L-Cysteine as capping agents have been used by various workers to stabilize the surface of CdTe core-shell and multi-core-shell QDs. In 2019, Khadem and colleagues embedded CdTeS/CdSe core-shell in a polymer matrix for the selective sensing of dopamine. The alloy core-shell was stabilized with Mercaptopropionoic acid (MPA) [31]. Wang and co-workers in 2015 also used microwave method to prepare high quality CdTe/CdS/ZnS-$SiO_2$ composite for sensing and imaging of $Hg^{+}$ in milk powder and Hela cells [32]. This hybrid system was prepared using *N*-acetly-L-cysteine as the capping agent. Yang *et al* (2010) synthesized CdTe/CdSe core-shell nanoparticle using TGA as the stabilizing agent. The synthesized material was used as a pH sensitive florescence probe for determination of

ascorbic acid [33]. In 2015, Chen and co-workers synthesized type II CdTe/CdSe core shell nanoparticles which were used in the imaging of cell stain studies. Glutathione was used as the surface ligand to stabilize the surface of the QDs [34]. In 2011 Zhang and co-workers synthesized CdTe/CdS core-shell nanoparticles in aqueous solution using L-Cysteine as stabilizing agent, these were used for labeling of Hela cells [35]. Aqueous synthesis of colloidal nanocrystal heterostructures consisting of CdTe core encapsulated by CdS/ZnS or CdSe/ZnS shells were synthesized by Samanta *et al in* 2012 using glutathione (GSH) to stabilize the surface of the nanocrystal. The synthesized type II CdTe/CdS/ZnS and CdTe/CdSe/ZnSe QDs showed high quantum yield up to 45% with emission ranging from visible to NIR wavelengths (500–730 nm) [36].

**1.5. Thiol dual capped CdTe QDs.**

Furthermore, in order to improve the chemical functionality and the surface chemistry of synthesized CdTe QDs, some work was conducted using two different thiol ligands to co-stabilize the surface of the fluorophore thereby enhancing the optical property and stability of the QDs. There are a few studies demonstrating the use of two different thiol- ligands related to the fabrication of CdTe cores and CdTe core-shells [44- 45]. The importance of using more than one thiol ligand is to further improve the surface chemistry of synthesized nanoparticles. Examples in this regard include Yu and co-worker in 2012 who used a combination of thiol-glycolic acid (TGA) and glutathione (GSH) to produce highly luminescent nano-crystals for labeling of colorectal cancer cell [44]. After optimizing the reaction condition, dual capped GSH-TGA-CdTe QDs was found to demonstrate higher florescence intensity and long-term stability compared to single capped GSH-CdTe QDs and MPA-CdTe QDs. In addition, Adegoke and Nyokong in 2013 used the combination of GSH-TGA to synthesize a highly fluorescent

CdTe/ZnS core-shell which could be used as nano-sensor for the sensitive and selective luminescent detection of peroxynitrite in aqueous solution [45]. Wang *et al* in 2012 in this report about electrochemiluminescence (ECL) behavior of the CdTe QDs pointed out that the addition of TGA as a co- stabilizing agent increased the sensitivity of the synthesized CdTe QDs towards the selective detection of $Pb^{2+}$ in aqueous media [14]. In 2017, we reported the synthesis of dual capped GSH-L-cysteine-CdTe core-shell system and evaluated their optical and structural morphology [18]. More recently, we reported pH-florescence dependent studies of synthesized CdTe QDs using five different dual stabilizing thiol ligands; MPA-TGA, MPA-L-cysteine, GSH-TGA, L-cysteine-TGA and GSH- MPA [4].

It is pertinent to point out that a limited number of studies involve the use of two different thiol dual capping agent to stabilize the surface of CdTe QDs, and to the best of our knowledge there has been no report on the synthesis of CdTe multi core-shell QDs involving the use of two different thiol ligands as dual stabilizing agents.

### 1.6. CdTe multi-core-shells QDs.

It was pointed out earlier that transformation of CdTe core to multicore-shell using ZnS or ZnSe as the outer shell improved the bio-compatibility of synthesized fluorophore by preventing the toxic Cd ion from having direct contact with cells. This chemical intervention allows the synthesized QDs to be used as optical probes in various imaging studies including deep-tissue cellular imaging applications [41].

As an example, in 2011 water soluble, near infrared emitting CdTe/CdSe/ZnSe quantum dots were synthesized in a simple one-pot procedure by Taniguchi and co-workers. The emission wavelength of synthesized QDs was found to be tuned from 530 nm (original CdTe core) to 670

nm (for the multi-core-shell) and the particle size was determined by TEM measurement. The resulting QDs were used in subcutaneous deep tissue monitoring of Wister rats' studies [42]

In addition, arginine functionalized CdTe/CdSe/ZnSe nanoparticles were synthesized under ambient conditions in the absence of an inert environment. The work was reported by Vuyelwa *et al* in 2017 and it was established that the synthesized fluorophore demonstrated high fluorescent intensity with enhanced cell viability for cellular imaging compared to the bare QDs. It has also been established that functionalized nanoparticle displayed reduced cyto-toxicity when investigated on KM-Luc/GFP cell line. The florescent images in this study revealed that the synthesized nanoparticles were taken up by the cell [46].

Water-dispersible CdTe/CdS/ZnS QDs was prepared by Zhang *et al* in 2012 by simply injecting $Zn^{2+}$ ions into an aqueous colloidal solution of CdTe/CdS core–shell QDs (with an average diameter of 3.8 nm) in the presence of MPA as the stabilizing agent. The optical properties of CdTe/CdS/ZnS QDs were controlled by adjusting reaction time, reaction temperature and concentration of $Zn^{2+}$ ions. The band-gap energy of CdTe/CdS/ZnS core–shell–shell QDs decreases gradually from 2.25 to 2.07 eV as the reaction time were varied from 0 to 720 min. The photoluminescence quantum yield (PLQY) of the aqueous solution of CdTe/CdS/ZnS core–shell–shell QDs was found to be 15 % compared to that of CdTe/CdS core–shell QDs that was observed to be 4 %. This indicated enhanced optical property by CdTe multi-core QDs over CdTe/CdS core-shell QDs [47].

In 2009, Green and co-worker also passivated the surface of CdTe/CdS core-shell with ZnS shell using simple successive injections of precursors in a one-pot reaction to produce CdTe/CdS/ZnS multi-core-shell nanocrystal. The synthesized QDs demonstrated a type II behaviour (QDs with

broad emission wavelength close to the infra-red) and were successfully used in imaging Hela cell with reduced cyto-toxicity compared to the bare CdTe/CdS core-shell [41].

More recently, eco-friendly synthesis of GSH-CdTe/CdSe/ZnSe double shell QDs were reported by Monaheng and co-workers in 2019. In this study, cytotoxicity and genotoxicity effects of these heterostructures were evaluated on Chinese hamster ovary cells. The synthesized QDs demonstrated good optical properties and produced an average particle diameter of 5.9 ± 1.13 nm. During the intracellular uptake study, the QDs were observed to show no sign of cytotoxicity to Chinese Hamster Ovary cells up to a concentration of about 25 ug $ml^{-1}$ but they were observed to demonstrate huge toxicity at higher concentrations (50 and 100 ug $ml^{-1}$). These particles were also reported to be genotoxic at all concentrations, it was therefore concluded that more experimental work is still needed to substantiate this observation [48].

### 1.7. Silica coated CdTe QDs.

The literature discussed this far involved the coating of ZnSe or ZnS shell in order to protect the Cd metal from leaching out of the compartment into the solution. However, there have also been other approaches that were reported to improve the bio-compatibility of CdTe QDs towards their use in various biological evaluations.

Passivating the surface of CdTe QDs with non-toxic inorganic silica shell has also been shown from literature to prevent contamination of Cd with immediate environment. One of the examples on the successful coating of silica shell on the surface CdTe QDs was reported by Wang *et al* in 2014. The study was conducted on a controlled thickness of silica coating on CdTe QDs using reverse microemulsion method better known for its application in the growth of rice. In this study, water-soluble thioglycolic acid (TGA) stabilized CdTe quantum dots were

synthesized, and the surface modification was conducted. The coating of the surface of CdTe QDs with silica as inert material was observed to improve the chemical properties of synthesized nanoparticles, the thickness of the silica shell could be varied from 40 to 400 nm. The silica coated CdTe QDs (40 nm) were observed to have good effects on the growth of rice root with reduced toxicity. This was the first time that silica coated CdTe QDs were observed to assist in the growth of rice [49]. Furthermore, growth of silica shells on CdTe quantum dots was evaluated with time by Modlitbová *et al* (2018). The study focused on optimization of thicknesses of silica shell at the surface of CdTe QDs for purpose of practical applications. The coating procedure involved the use silane primer (3-mercaptopropyltrimethoxysilane) so as to make the surface of the quantum dots (QDs) vitreophilic. In the study, the total size of the QDs was reported to be dependent on both the duration of silica shell growth in the presence of both sodium silicate and ethanol during the growth period. It was observed that in the presence of ethanol, the size of CdTe/$SiO_2$ QDs increased more prominently up to 115 nm (DLS data) and up to 83 nm (SEM data) [50].

Ruan *et al* (2011), reported the biocompatibility of silica coated-CdTe QDs-$Fe_3O_4$ nanoparticle (FMNPs) using human embryonic kidney 293 (HEK293) cells and mice. Silica coated-CdTe QDs-$Fe_3O_4$ nanoparticle (FMNPs) of about 150 nm in diameter were prepared and characterized by high-resolution transmission electron microscopy and photoluminescence (PL) spectra and magnetometer. It was reported that HEK293 cells were cultured with different doses of FMNPs (20, 50, and 100μ g/ml) for 1-4 days. Mice (30) were divided into three groups, the groups were injected via tail vein with 20, 60, and 100 μ g/ ml FMNPs respectively with continuous observation for 1, 7, and 30 days. It was concluded from this study that FMNPs exhibit good

biocompatibility to human kidney cells for a dose of less than 50 μg/ml, and to mice for a dose lower than 2mg/kg body weight [51].

In 2006, silica coated CdTe QDs were conjugated to anti-body proteins using polyethylene glycol and thiols terminated bio linkers. The work was reported by Walcot and co-workers in which a highly florescent water-soluble silica capped CdTe QD was synthesized. The coating of the silica shell at the surface of the QDs in this study was believed to prevent the leakage of toxic $Cd^{2+}$ and provide a surface for easy conjugation with biomolecules such as proteins. In the study, the presence of a silica shell of 2−5 nm in thickness was confirmed by transmission electron microscopy and atomic force microscopy measurements. It was also reported that the bioactivity and conjugation specificity of the thiolated QDs were confirmed by streptavidin−maleimide and biotinylated polystyrene microbeads. It was concluded that the synthesized silica-shell coated CdTe QDs demonstrated enhanced bio-compatibility and could be recommended for a number of applications in biolabeling and imaging [52].

### 1.8. Lipid and Polymer based system for the encapsulation of CdTe QDs.

Apart from covering the surface of CdTe QDs with Zn chalcogenides or silica shells, it has also been reported that the biocompatibility of CdTe QDs can be improved by encapsulating the QDs in lipid and polymer-based medium allowing them to be used as diagnostic tools in cellular imaging. The main delivery vehicles that have been explored in the successful application of CdTe QDs for cellular imaging are liposomes (lipid) and chitosan (biopolymer) [7- 11]. The loading of CdTe QDs in these two delivery systems have produced satisfactory results in various drug delivery and imaging studies found in literature. These compounds are non-toxic, environmentally friendly and highly bio-compatible [8-10].

### 1.8.1. Liposome loaded CdTe QDs, preparations and properties.

Liposomes are self-enclosed bilayer of lipids forming a sphere with an enclosed aqueous core. Because of the presence of an aqueous core and a lipid bilayer, liposomes can incorporate hydrophilic as well as lipophilic molecules [53]. Liposomes are composed of naturally occurring or synthetic phospholipids such as phosphatidylcholine (PC), phosphatidylethanolamine (PE), phosphatidylserine, and phosphatidylglycerol. There are various types of liposomes and these depend on size and lamellarity [53]. Lamellarity is a measure of the number of lipid bilayer present within the structure. There are small unilamelar (SUV, 20- 100 nm), long unilamelar (LUV, > 100 nm), giant uni-lamelar (GUV, > 1000 nm) and multi lamelar (MLV, > 5000 nm) vesicle liposomes [54- 56]. The illustration in figure 2 shows the image of various types of liposomes and their corresponding lamellarity.

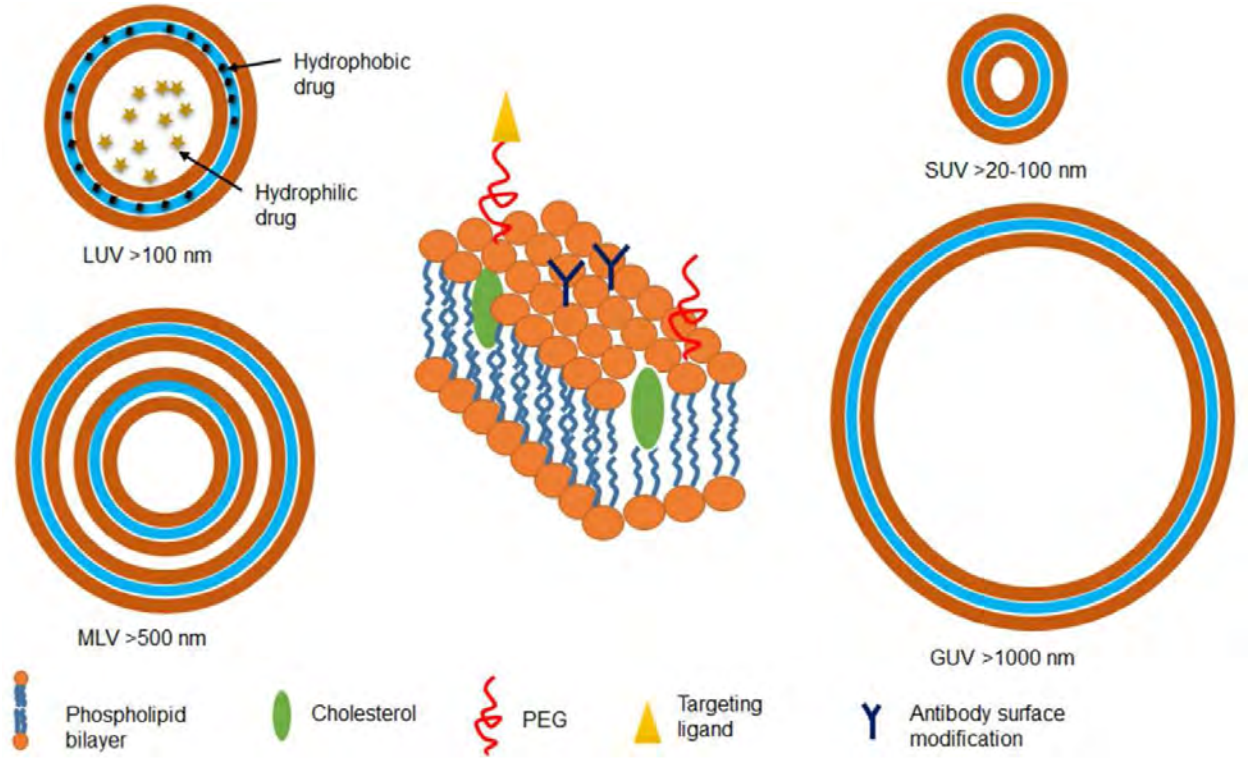

**Figure 2.** Different liposome types based on size and lamellarity. Also shown is a portion of a typical lipid bilayer with multifunctional surface modifications [53].

### 1.8.2. Lecithin.

Soybean lecithin is an example of a phospholipid source that has been reported in some studies for the preparation of liposomes loaded with CdTe QDs [56]. Lecithin is a generic name used to describe any group of yellow brownish fatty substances that can be found in animal and plant tissues [11]. They can attract both water and fatty substances which makes them possess both hydrophilic and lipophilic properties. Lecithin can be used as emulsifying agents, smoothing food textures and homogenizing liquid mixtures [11, 56]. Figure 3 demonstrate the image of lecithin which can be found in soybean.

**Figure 3.** An image of crude Soybean lecithin [11].

The main phospholipids in lecithin from soy and sunflower are phosphatidyl choline, phosphatidyl inositol, phosphatidyl ethanolamine, phosphatidylserine and phosphatidyl acid [10-11].

Phosphatidyl choline is one of examples of phospholipids found in lecithin and its chemical structure is shown in figure 4.

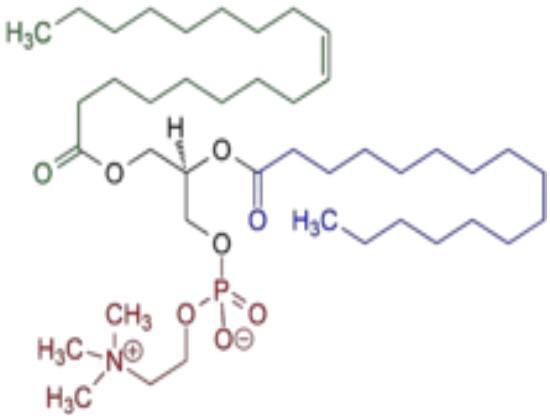

**Figure 4.** The chemical structure of phosphatidyl choline. Shown in red is choline and phosphate group while the black color represents the glycerol group. The green and blue color are the monounsaturated and saturated fatty acids [11].

Phosphatidyl choline is known to have an excellent solubility in ethanol compared to other phospholipids found in lecithin, this allows its easy extraction from crude lecithin components by evaporating the ethanol during the fractionating process [7, 11].

The preparation of liposomes using conventional methods has been reported in a number of works. Thin film hydration, solvent injection, reverse phase evaporation and detergent dialysis are some examples of conventional methods used in liposome preparation. The use of thin film hydration results in the production of SUV liposomes, the method involves the hydration of thin lipid films followed by either physical extrusion or sonication [8-11, 52- 53]. A commonly employed method in liposome preparation is the reverse phase evaporation technique. This technique consists of the initial formation of inverted micelles or water-in-oil emulsions where the aqueous phase carries the drug or QDs of interest and the organic phase consist of the lipids for the liposome bilayer formation [51]. However, it is worth to point out that all these methods have been used to generate different types of liposomes with excellent results. The method of choice eventually selected depends on the intended application of the liposomes. In addition, the

encapsulation of CdTe QDs in liposomes using these methods has been reported to show enhanced biocompatibility in a number of studies [52- 53].

The studies of liposome loaded with CdTe and CdHgTe QDs, fluorescence resonance energy transfer studies and near-infrared in-vivo imaging of mouse tissue were reported by Ye *et al* in 2012 using thin film hydration method. In this study, hydrophilic CdTe QDs and near-infrared (NIR) QDs of type CdHgTe were incorporated into liposomes by transferring the QDs from an aqueous solution into chloroform using cetyltrammonium bromide (CTAB) as the surfactant. It was reported that the QD encapsulated in liposomes displayed bright fluorescence enabling enhanced storage stability and reduced sensitivity to UV irradiation. In addition, the liposomes containing the QD were used to label human breast cancer cell (MCF 7) and in the in-vivo imaging of mouse tissue using a confocal laser scanning microscope. In the same study, it was also reported that florescence energy transfer (FRET) was observed between CdTe QDs (donor) and CdHgTe QDs (acceptor) both encapsulated in the liposome. During the imaging studies, it was reported that the QD-liposome vesicles (LVs) showed no cytotoxic effects following 120 min of incubation with living cells and no morphological change of the cells was observed during this incubation period. In the light of these findings, it was concluded that the QD-LVs are biocompatible with living cells, and capable of cellular uptake as well as intracellular trafficking [54].

The enhanced intra-cellular delivery of CdTe QDs was studied by Wang and colleagues in 2010 using a cationic liposome complex called with about 95 % encapsulation efficiency. The cellular uptakes studies of unencapsulated QDs and QD loaded in liposome vesicles were comparatively studied in three cell lines (human osteosarcoma cell line (U2OS); human cervical carcinoma cell line (HeLa) and human embryonic kidney cell line (293 T). These were analyzed using a laser

scanning confocal microscope. The encapsulation of QDs in liposome was conducted by mixing a cationic liposome complex with QDs in aqueous solution at various molar ratios ranging from 0.45:1 to 0.1:1 for duration of 10 min each. The liposome vesicles were formed in these mixtures by agglomeration, the mixtures were centrifuged for 10 min at 15000 rpm to harvest the QD loaded liposome vesicles (QD-LVs) in supernatants. The difference in cellular uptakes for QD-LVs and free QDs was evaluated using the flow cytometric analysis. The flow cytometric measurements further showed that the enhanced ratios of encapsulation of QDs are some 4– 8 times in 293 T and Hela cells than in other cells. Therefore, it was concluded that the cationic liposome encapsulation is an effective modality to enhance the intracellular delivery of CdTe QDs [55].

Liposome coated CdTe QDs for the targeting of sentinel lymph node (SLN) was reported by Chu and co-workers in 2010. In their study, liposome coated QDs demonstrated core–shell characterization, and after being continuously excited by a xenon lamp source (150 W) at 488 nm at 37 $^{0}$C for 1 h, their fluorescence emission did not decrease but slightly increased over this duration. They reported that the liposome coated CdTe QDs stored at 4$^{o}$ C in the dark for more than one and half years still retained their spherical structure with a large amount of QDs still present. It was also discovered that the intradermal injection of liposome-coated QDs with average size of 55.43 nm into the paw of a mouse (SLN) demonstrated strong fluorescence within only a few seconds of injection time and visualized easily in real time and lasted for about 24 h. It was also found that more QDs migrated into the SLN when the liposome-coated QDs with average size of 55.43 nm was injected compared with liposome-coated QDs with a larger average size (100.3 and 153.6 nm). In addition, after dialyzing against neutral water for 12 h, about 2.0% $Cd^{2+}$ ions were found to have been released from the uncoated QDs, whereas about

1.2% $Cd^{2+}$ ions were released from the liposome-coated QDs (average size: 55.43 nm). This observation indicated that liposomes provided enough coating in CdTe QDs so as to protect the toxic $Cd^{2+}$ toxic ions from leaching out into nearby environment compared to uncoated CdTe QDs. Hence the protocol described made significant contribution to the improvement of the biocompatibility of CdTe QDs and the delivery capacity of liposome encapsulated QDs into the SLN targets [56].

Muthu and co-worker in 2012 also reported the encapsulation of CdTe QDs and docetaxel in liposomes coated with D-alpha-tocopheryl polyethylene glycol succinate mono-ester (TPGS) for cancer imaging and therapy. The study included the preparation of non-targeting and folate receptor targeting TPGS coated theranostic liposomes prepared by the solvent injection method and characterized for particle size, polydispersity, zeta potential, surface chemistry and drug encapsulation efficiency. In their study MCF-7 breast cancer cells of folate receptor overexpression were employed as an in vitro model to assess cellular uptake and cytotoxicity of the drug and QDs loaded liposomes. It was revealed that the mean particle size of the non-targeting and the targeting liposomes was found to be 202 and 210 nm, respectively. The qualitative internalization of multifunctional liposomes by MCF-7 cells was visualized by confocal laser scanning microscopy (CLSM). The calculated $IC_{50}$ value which correspond to the sample concentration needed to kill 50% cells in a designated time period, was determined to be $9.54 \pm 0.76$, $1.56 \pm 0.19$ and $0.23 \pm 0.05$ mg/ml for the commercial Taxotere, non-targeting and targeting liposomes, respectively after 24 h culture with MCF-7 cells. Hence it was concluded that the targeting multi-functional liposomes showed greater efficacy than the non-targeting liposomes and possess great potential to improve the cancer imaging and therapy [7].

### 1.9. Chitosan loaded with CdTe QDs.

As mentioned in the foregoing section, the in-corporation of CdTe QDs in chitosan has been shown to improve the biocompatibility of the nanoparticle by preventing direct contact of toxic $Cd^{2+}$ ion with living cells during cellular imaging studies [57]. The loading of CdTe QDs in chitosan has been demonstrated in contemporary nano chemistry literature with promising results. Chitosan is a natural, biodegradable, biocompatible glucosamine polysaccharide obtained by the deacetylation of crustacean or fungal chitin [58]. It is composed of *β*-(1–4)-linked D-glucosamine and *N*-acetyl-D-glucosamine randomly distributed within the polymer [59]. Deacetylation refers to the process of removal of acetyl groups from chitin and substitution of reactive amino groups (single bond $NH_2$). The degree of deacetylation (DDA) determines the content of free amino groups present in the structure [59]. The degree of deacetylation can be used to differentiate between chitosan and chitin.

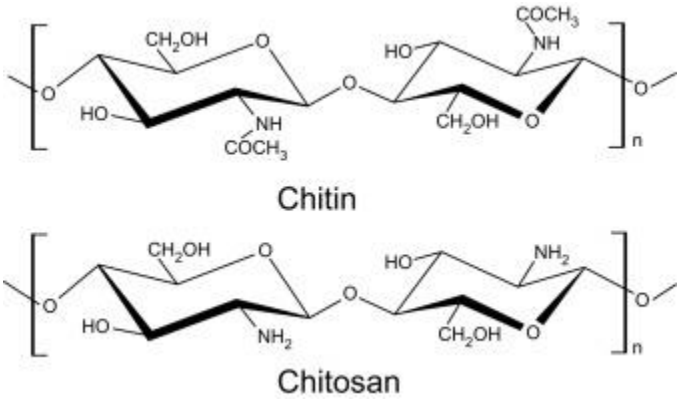


**Figure 5.** Chemical structure of chitin and chitosan [60].

The degree of deacetylation (DDA) is considered an important property in chitosan as it reflects the physicochemical and biological properties such as acid base and electrostatic characteristics,

biodegradability, self-aggregation, absorption properties, and the ability to chelate metal ions [61- 62]. The chemical advantages of chitosan over chitin in many solution-based reactions is its solubility in a moderate solvent such as diluted acetic acid and availability of several free amine groups as active sites in its structure [59]. The DDA of chitosan depends on the sources, species, preparation methods and varies from 56% to 99%. Chitin with a %DDA = 75 or above is known as chitosan [63]. Chitosan is also considered non-toxic, biocompatible, and environmentally friendly material with numerous chemical properties [64- 67]. The cationic nature of chitosan allows the formation of stable ionic complexes with ions or polymers of opposite charge [57]. Nanoparticles synthesized using chitosan which are usually referred to as Chitosan nanoparticle (CNP) are known to have enhanced membrane binding capacity and cellular uptake than polymeric chitosan, this is attributed to the size and charge of polymeric nanoparticles [58]. Chitosan also has the ability to gel upon contact with special polyanions, a process referred as `ionotropic' gelation [68- 71]. This gelation process involves the formation of cross-linking between/within polymer chains, mediated by the polyanions. One of the most widely used methods to obtain chitosan-based-hydro gel nanoparticle is based on the ionotropic gelation of chitosan with sodium tripolyphosphate (TPP). Furthermore, chitosan nanoparticles (CNPs) are widely used in delivery of insulin, peptides, and cancer drugs due to favorable biological properties and high loading efficiencies [58]. It seems expedient to embed QDs in a biocompatible vehicle to provide the advantage of biological safety to toxic QDs (CdTe) while imparting fluorescence characteristics to polymeric nanoparticles.

Furthermore, chitosan is known to exhibit poor solubility at pH above 6.5 due to the loss of its cationic nature. Hence, its antimicrobial activity and other applications are limited to acidic conditions. In order to resolve this problem, various derivatives of chitosan have been prepared

with goals to dissolve them in water over the entire pH range and thereby broadening its applicability [59]. The most common chitosan derivatives that have been reported in some literature for the loading of CdTe QDs is carboxyl methyl chitosan. This derivative is prepared by carboxymethylation process in which some of the OH groups of chitosan are substituted by acidic methyl groups [72]. Carboxymethyl chitosan has good solubility in organic solvents and exhibits unique chemical, physical, and biological properties [73]. It's an efficient means to convert chitosan into a water-soluble material. However, preparation of carboxymethyl chitosan is not cost effective and its availability is rare compared to chitosan which is readily available and eco-friendly. Notwithstanding these problems, the use of chitosan and carboxymethyl chitosan to enhance the bio-compatibility of CdTe QDs has been demonstrated in a number of literature sources.

In 2013 for example, Qiang and colleagues synthesized novel carboxymethyl chitosan–CdTe QDs for sensing of $Zn^{2+}$ ion in prostate cancer cells. This was achieved though the electrostatic interaction between amino groups in the carboxymethyl chitosan polymeric chains and carboxyl groups of the CdTe QDs. Carboxymethyl chitosan (CMC) on the surface of CdTe QDs was said to have strong binding affinity for $Zn^{2+}$, resulting in the enhancement of the photoluminescence of CdTe QDs. It was further established that the photoluminescence intensity of CMC–CdTe QDs probe was proportional to the concentration of $Zn^{2+}$ in the concentration range of $5.0 \times 10^{-6}$ to $5.0 \times 10^{-3}$ mol $l^{-1}$ with the limit of detection as $4.5 \times 10^{6}$ mol $l^{-1}$. It was concluded from this study that the CMC–CdTe QDs possess favorable cell compatibility, good sensitivity and selectivity for intracellular ions sensing, and this makes them promising candidates for cellular imaging and sensing in prostate cancer cells [74].

The use of chitosan to enhance the biocompatibility of CdTe QDs was also reported by Ghormade *et al* who embedded green fluorescent CdTe QDs in biocompatible CNPs. It was revealed that the electrostatic interactions between thiol-capped QDs (4 nm, −57 mV) and CNPs (~300 nm, +38 mV) generated CdTe QDs-embedded CNPs that were stable up to three months. The cytotoxicity of QDs-embedded chitosan nanoparticles was evaluated using $NIH_3T_3$ mouse embryonic fibroblast cell lines for 24 and 48 h respectively. Cell viability was observed after treatment with bare CNPs, bare CdTe QDs, and QDs-embedded chitosan nanoparticles at concentration ranges of 0.01, 0.1, 1 and 10 ug/ml. It was reported that CdTe QDs-embedded chitosan nanoparticles demonstrated no cytotoxicity at the lower concentrations (0.01, 0.1 μg/ml) at 24 and 48 h. It was also highlighted that at 10 μg/ml, QDs-embedded chitosan nanoparticles showed 34 and 39% increased viability at 24 and 48 h, respectively, as compared to the bare QDs. These results suggested that embedding CdTe QDs in CNPs increased their biocompatibility significantly and that CNPs do not release the QDs up to 48 h and do not cause extended toxicity [58].

In 2012 Parani *et al* reported the encapsulation of bio-polymer stabilized- CdTe QDs in folic acid conjugated chitosan. Alginate biopolymer stabilized CdTe quantum dot (QD) was prepared and subsequently encapsulated with folic acid conjugated chitosan for controlled drug delivery of anticancer drug 6 mercaptopurine (6-MP). Results from the UV–vis absorption and florescence spectra confirmed the loading of CdTe QDs and 6-MP in chitosan. Furthermore, alginate was found to bind to the drug leading to enhanced loading efficiency of the resulting drug carrier. The drug release profile of the carrier was investigated using in-vivo studies. It was concluded from this study that chitosan is an effective drug carrier for application involving drug delivery. These observations enable chitosan as an important candidate for cancer therapy [75].

An innovative drug delivery system based on magnetic and fluorescent multifunctional chitosan nanoparticles was developed by Li and colleague in 2007. In their study, a combination of magnetic targeting, fluorescent imaging and stimulus-responsive drug release properties of the QDs were incorporated into one drug delivery system. Water-soluble superparamagnetic $Fe_3O_4$ nanoparticles, CdTe quantum dots (QDs) and pharmaceutical drugs were simultaneously incorporated into chitosan nanoparticles. The composite particles were cross-linked with glutaraldehyde which determined their size, morphology, surface properties and drug release behaviors. In this study, it was reported that the system showed superparamagnetic and strong fluorescent properties, and was used as a controlled drug release vehicle, whose prolonged drug releasing properties were tied to pH. Hence it was concluded that the composite magnetic and fluorescent chitosan nanoparticles were potential candidates for smart drug delivery system [76].

In 2013, Kumar *et al* described the synthesis of water-soluble L-cysteine-functionalized CdTe quantum dots (QDs) with size tunable emission at different time intervals. Various characterization techniques such as Fourier transform infrared (FTIR) spectroscopy, X-ray diffraction (XRD), differential scanning calorimetry (DSC), thermo gravimetric analysis (TGA) and scanning electron microscope (SEM) were used to elucidate the structure of the synthesized CdTe QDs–chitosan film. UV–vis and photo-luminescence (PL) spectroscopy were used to analyze the optical properties of the composite system and its antibacterial activity was screened for Gram positive (*Staphylococcus aureus*) as well as Gram negative (*Pseudomonas aurigionasa* and *Escherichia coli*) bacteria by disc diffusion method. The loss of tunable light emission effect of QDs as well as the positive result obtained from the antibacterial study reveal that the synthesized QDs based chitosan film is a promising candidate for a wide range of biomedical applications [77].

It is clear that most of the literature mentioned above focus on enhancing the bio-compatibility of CdTe QDs for the purpose of in-vivo or in-vitro studies. However, the loading or encapsulation of CdTe multi-core-shell in liposome or chitosan to improve their bio-compatibility has not yet been reported in the literature. Admittedly, as reported in some studies, the coating of ZnSe or ZnS shell at the surface of CdSe shell in heterostructure such as CdTe/CdSe/ZnSe or ZnS is sufficient to reduce the toxicity of these nano-particle during their use in cellular imaging or drug delivery system [41- 42, 46]. Nevertheless, Monaheng and co-worker in their study slightly disagree with the general belief that the passivation of ZnSe or ZnS shell at the surface of CdSe shell is enough to protect the toxic $Cd^{2+}$ from leaching out into the nearby solution to cause damage to cells during their use in imaging application. It was discovered in this study that the synthesized CdTe/CdSe/ZnSe multi-core-shell QD were cyto-toxic to Chinese Hamster Ovary cells at a particular concentration and they were geno-toxic to these cells at all concentration [48]. The foregoing report established that there is further need to protect the synthesized CdTe multi-core-shell QDs from leaching out, without destroying their bio-compatibility and environmental safety so that these can be used effectively used as florescence probes in drug delivery applications. Therefore, encapsulating these compounds in liposome or chitosan for enhanced bio-compatibility may be more ideal to further reduce the toxicity of $Cd^{2+}$ to living cells.

Furthermore, it has been reported by various researchers that the synthesis of CdTe multi-core shells QDs usually takes longer reaction time to reach the highest emission maxima. For examples, in 2012 Zhang and co-workers spent about 720 min (12 h) to complete the synthesis of CdTe/CdS/ZnS with the highest emission wavelength located around 610 nm [47]. Similar reaction time was also reported by Taniguchi *et al* in 2011 where the synthesis of

CdTe/CdSe/ZnSe multi-core shell took some 16 hours to reach the highest emission maxima [42]. In 2009, the fabrication of CdTe/CdSe/ZnSe multicore-shell reported by Green *et al* also took 24 hours to reach emission maximum of 660 nm [41]. In 2017, Arginine functionalized CdTe/CdSe/ZnSe nanoparticles were also reported by Vuyelwa *et al* to have taken around 7 h to reach the highest emission wavelength of about 610 nm [46]. This long reaction route implies that lots of resources and energy have to be expanded to effectively synthesize and size tune the hetero-structured compound to reach the desired emission wavelength without complete loss of intensity.

More recently, in our study, we reported the rapid synthesis of CdTe multi core-shells QDs over 35 mins reaction time with the highest emission maxima located at 625 nm. The surface of the synthesized CdTe multi-core-shell QDs was dual stabilized using different thiol ligand; MPA-TGA, GSH-TGA, GSH-MPA, L-cysteine-MPA and L-cysteine-TGA leading to five different dual surfaces.

In addition, the synthesis of CdTe multi-core reported in the said study firstly was initiated by constructing their corresponding cores which were later upgraded to core-shells. In a recent report we highlighted pH-florescence dependent studies, optical properties and structural morphology of these cores [3].

Based on the foregoing observations in previous reports, it is necessary to further improve the bio-compatibility of synthesized multi core-shell QDs. As such in this current study, the synthesized CdTe multi-shell QDs which was reported by our group was encapsulated in chitosan nano-particles (CNP) and liposome respectively using modified protocols [56, 58]. The cytotoxicity measurement and cellular internalization studies of the QDs-liposome and QDs-

CNP composite were investigated using Vero and HeLa cells. In this study, we also investigated the best environment that could improve the bio-compatibility of CdTe multi-core-shells QDs towards cellular imaging studies. The encapsulation of CdTe multi-core-shell QDs in liposomes and CNP led to some 14 and 12 different experimental trails to determine optimal condition for encapsulation. The QDs loading efficiency in liposome and CNP was evaluated following a procedure reported by Wang *et al* in 2011 [55].

The UV-Vis and Photoluminescence spectroscopies (PL) were used for optical properties measurement while Transmission electron microscope (TEM) was used to estimate the morphology of the various compounds. X-ray diffraction microscopy (XRD), Energy dispersive x-ray spectroscopy (EDX), Thermo gravimetric analysis (TGA), Dynamic light scattering (DLS) and Fourier transform infra-red spectroscopy (FTIR) were all used to determine the respective physio chemical properties.

The high positive and negative zeta potential values obtained for both QD-CNP and QD-liposome vesicles (LVs) indicates that the synthesized nano-composite systems are highly stable. The characterization of their optical properties at various formulations affirms the interaction between the QDs with CNP and QD with liposome vesicles (LVs) which results with good florescence at various QDs loading contents. The photo-stability studies of the unencapsulated QDs and the nanocomposite was also evaluated under UV illumination. As a following to preliminary findings and investigations so far undertaken by various workers including our own laboratory findings, we hereby report the rapid synthesis of thiol-co-capped CdTe/CdSe/ZnSe multi-core-shell QDs and its encapsulation into liposomes and chitosan nanoparticle; comparative bio-compatibility studies using HeLa and Vero cells.

### 1.9.1. Objective and scope of the study.

(i) To show that CdTe/CdSe/ZnSe multi-core-shell QDs can synthesized within a short reaction time. This can be initiated through the synthesis of CdTe cores via the construction CdTe/CdSe core-shell nanoparticles.

(ii) To study the optical properties and structural morphology of synthesized CdTe cores, core-shell and multi-core-shell nanoparticles.

(iii) To encapsulate the synthesized CdTe multi core-shell QDs in a biocompatible environment such liposomes and chitosan nanoparticles. This is necessary to improve the bio compatibility of synthesized CdTe muti-core-shell QDs.

(iv) To study the optical properties, structural morphology and physicochemical properties of synthesized CdTe multi-core-shell nanocomposites.

(v) To conduct a cell viability and florescence imaging studies of synthesized CdTe multi core-shell nanocomposites using Hela and Vero cells.

# CHAPTER 2.

As stated in Chapter 1, there is a need to further improve the bio-compatibility of CdTe multi-core-shells QDs in order to use them effectively as diagnosis tool in applications like drug deliveries. The preparation and characterization processes of CdTe multi-core-shells QDs starting from the synthesis of the cores and their remaining counterpart are hereby highlighted in this section.

## 2. Materials and Chemicals.

Cadmium acetate [Cd $(CH_3COO)_2$], zinc sulphate ($ZnSO_4$), potassium tellurite ($K_2TeO_3$), glutathione (GSH), mercaptopropionoic acid (MPA), thioglycolic acid (TGA), L-cysteine, sodium borohydride ($NaBH_4$), sodium sulphite, selenium powder, acetic acid, hydrochloric acid, sodium phosphate (monobasic), sodium phosphate (dibasic), sodium citrate and citric acid were all purchased from Sigma-Aldrich (Germany). Chitosan low molecular weight (85% deacetylation) for the synthesis of CNP was also obtained from Sigma-Aldrich (Germany). Cholesterol used was from Carlo Erba/Divisione Chimica (Italy) while soybean lecithin granules used in this study were sourced from Health Connection Wholefoods (USA). Chloroform was purchased from BM Scientific/Parow Industrial (South Africa). Tripoly-phosphate (TPP) was purchased from Sigma-Aldrich (Germany). All the chemicals were used without further purification, unless otherwise indicated.

### 2.1. Instrumentation

**2.1.1. Optical properties:** The Ultraviolent (UV) and photoluminescence (PL) spectrophotometer measures the amount of energy (photon) absorbed or emitted by the nanoparticles. This usually corresponds to a specific wavelength of light within a particular

excitation or emission window of ultraviolent-visible-infra red region of the electromagnetic spectrum [2]. These techniques can be typically be used to determine the optical properties of the synthesized nanoparticles including QDs [2, 10]. Hence, the absorption spectra of the dual capped CdTe core, core-shell and multi-core-shell were run on a Perkin Elmer Lambda 25 ultraviolet- visible spectrophotometer in the wavelength range 200-1200 nm. A Perkin Elmer LS 55 photoluminescence (PL) spectrophotometer was used to record the florescence of CdTe QDs (cores, cores-shell and multi-core-shell) (Perkin Elmer South Africa), CNP and liposomes coated CdTe/CdSe/ZnSe multi-core-shell at an excitation wavelength of 400 nm (Perkin Elmer, South Africa). The measurements were conducted at room temperature using 10 mm path length quartz cells at an excitation wavelength of 400 nm. The exposure of the QDs to UV irradiation was performed at an excitation wavelength of 314 nm with 130 W UV lamp from Lasec South African (Pty) limited. The photoluminescence quantum yield (PLQY) of the CdTe core-shell and CdTe-core-shell-shell was measured according to the method described by Crosby and Demas (1971). Rhodamine 6G was chosen as a reference standard (QY = 95%, in ethanol), The standard and samples were both diluted to an absorbance of 0.05 at their corresponding excitation wavelength and the same solution was used to measure their florescence. The expression to calculate quantum yield is provided as following:

$$Y_u = Y_s \times \frac{F_u \times A_s}{F_s \times A_u} \times \left(\frac{n_u}{n_s}\right)^2 \quad \text{..... (1)}$$

In Eq. (1), the subscripts s and u denote standard (rhodamine 6G) and test samples respectively, Y is quantum yield, F is the integrated emission peak area, A is the absorbance at excitation wavelength and n represent the solvent refractive index. [10].

**2.1.2. Morphology:** Transmission electron microscope (TEM) is usually employed to determine the shape, size and monodispersity of synthesized nanoparticles. This allows us to have an idea of the structural properties of the materials being synthesized [2, 21]. Therefore, the shape, particle size of bare QDs, empty liposomes and CNP, QDs composites and encapsulation of CdTe core-shell-shell in CNP and liposome was verified using transmission electron microscopy (Zeiss Libra 120kV, Germany). For each sample, a solution in methanol or suitable solvent was sonicated, then a drop was deposited on holey-carbon copper grids and the solvent in excess was absorbed using a piece of filter paper. The prepared TEM samples were allowed to dry over 48 h at room temperature. The mean particle size and size distribution of corresponding TEM images of the particles was performed using image J soft-ware.

### 2.1.3. Physicochemical characterizations

**2.1.3.1. Thermogravimetric analysis (TGA).** Thermogravimetric analysis measures the thermal behavior of the synthesized nanoparticles which are usually analyzed at temperature ranges between 30 – 600 ºC [10, 54]. The thermal behavior of freeze-dried bare liposomes and liposome embedded with CdTe core-shell-shell, bare CNP and CNP embedded with CdTe core-shell-shell were demonstrated using thermogravimetric analysis. The instrument was also used to investigate any physicochemical interactions between CdTe core-shell-shell QDs and lipid components or CNP. The samples were heated in nitrogen saturated atmosphere using PerkinElmer TGA-4000 instrument (South Africa). The heat range was 30 to 800º C at a flow rate of 10º C/ min. The inert nitrogen gas flow was set at 20 ml/min. TGA thermograms with

respective mass loss curves were recorded and data were analyzed using the software TGA Pyris series.

**2.1.3.2. Fourier transform infrared spectroscopy (FTIR).** The Fourier transform infrared spectroscopy can be used to determine the vibrational modes of different functional groups present at the surface of synthesized nanoparticles. The various modes such as bending and stretching vibrations can be used to determine which organic functional group is present at the surface of the synthesized nanoparticles. Hence, this can be used to confirm the synthesis of such materials [3 – 5]. The presence of QDs in CNP was investigated by Fourier transform infrared (FT-IR) spectroscopy. The IR spectra were recorded by the attenuated total reflection method using PerkinElmer Spectrum 1 FT-IR Spectrometer (South Africa) and each experiment was performed in the frequency range of 4000–650 $cm^{-1}$.

**2.1.3.3. Energy dispersive X- ray spectroscopy (EDX).** The energy dispersive X-ray spectrophotometer helps to show the elemental composition of the material synthesized. This can be used to confirm if the actual nanoparticle has been synthesized [2, 10]. Therefore, the elemental composition of multi-core-shell QD, empty liposomes and CNP, QDs- LVs, QDs-CNP were measured using Vegan Tescan EDX spectrometer (Oxford Instruments, Germany).

**2.1.3.4. X-Ray diffraction (XRD):** The X-Ray diffraction spectrophotometer helps to determine the crystalline state of the synthesized nanoparticle. They can also be used to estimate the particle size of the materials synthesized [2 – 3, 10]. The crystalline state of QDs and the nano-composites were conducted using Cu-Kα radiation set at 1.5404 Å with a nickel filter, on Bruker D8 Discover instrument equipped with a Lynx Eye detector (Germany). The freeze-dried

samples were placed on a glass sample holder and the diffraction patterns were recorded in the range of 2θ from 10 to 60$^{o}$ with a step size of 1$^{o}$/min and a slit width of 6.0 mm.

**2.1.3.5. Zeta Potential determination:** The zeta potential analyzes the charges present at the of the synthesized nanoparticles which is usually carried out using a Zetasizer [2, 52 – 58]. The surface of the Freeze-dried samples of CdTe css, bare liposomes and CNP, liposome and CNP-loaded with CdTe css were analyzed for zeta potential using Zetasizer nano (Malvern Instruments, Germany). The samples were gently dispersed in distilled water at room temperature. The measurements were performed at the scattering angle of 173$^{o}$ C using either an ordinary cuvette or a capillary one in accordance with the determination of Zeta Potential, respectively

**2.1.3.6. Loading efficiency and weight of QDs embedded in liposome and CNP.**

The loading efficiency and weight of QD encapsulated in liposome and CNP was determined following the protocols reported by Wang *et al* and Ghormade *et al* in 2011 and 2014 respectively [55, 58].

For loading efficiency, an indirect estimation from their corresponding florescence intensities can be used to calculate the amount of QDs encapsulated in the liposome vesicles. The PL emission intensity of the nanocomposite can be compared with that of the original QD solution at the concentration of 13.3 mg/ ml which was just the concentration used in liposome encapsulation. It was explained by Wang *et al* that the florescence obtained from the QD-LVs totally came from the loaded QDs so that the comparison of florescence intensities between the QD-LVs solution and the unencapsulated QD solution could estimate the loading content of QDs in QD-LVs [55].

Therefore, this means that;

$$\text{Loading efficiency (\%)} = \frac{\text{QD-LVs}}{\text{bare QDs}} \times 100$$

The same procedure was also used to determine the loading efficiency of QDs embedded CNP. In a study reported by Ghormade *et al* in 2014, the weight of QDs embedded in CNP can be obtained by taking the difference between the initial and final weight of freeze-dried QDs, CNP and CNP loaded with QDs [58]. Hence, we therefore used this procedure to determine the weight concentration of QDs encapsulated in both CNP and liposome. The loading efficiency of all formulations corresponding to QD-LVs and QD-CNP were estimated from the same QDs solution at concentration of 13.3 mg/ ml and all formulation were done in triplicate.

**2.2. Cytotoxicity and florescence imaging studies.**

The cytotoxicity study of QDs-LVs and QD-CNP were accessed using two different cell lines which are HeLa (cancer cells) and Vero cells (normal cells). In order to carry out the cytotoxicity study, three formulations were randomly selected from the list of prepared liposome and chitosan composite. The total number of samples used for this study are ten, namely: bare liposomes, bare chitosan nanoparticles, MPA-TGA-CdTe/CdSe core-shell (CS), MPA-TGA-CdTe/CdSe/ZnSe core-shell-shell (CSS), QD-LVs-F1, QD-LVs- F4, QD-LVs- F12, QD-CNP-F3, QD-CNP-F4 and QD-CNP-F9. Paclitaxel is an anti-cancer drug that was used as a control for the experiment.

Similarly, the florescence imaging studies of the corresponding liposome and chitosan nanoparticles composites was also investigated with HeLa cells using three compounds which are: QD-LV-F9, QD-CNP-F12 and bare QDs (CSS).

## 2.3. Routine culture of mammalian cell lines

HeLa and Vero cell lines were used to test the chemosensitivity of the 10 samples. The HeLa cell line was purchased from American Tissue Culture Collection (ATCC) while the Vero cell line was from CELLONEX South Africa. Both were cultured in DMEM (Life Technologies/Gibco) containing FBS (10 % [v/v], Life Technologies/Gibco) and PSA (penicillin [100 U/ml], streptomycin [100 µg/ml], amphotericin [12.5 µg/ml], Life Technologies/Gibco). Cells were incubated at 37 °C and 9 % $CO_2$. Sub-culturing was carried out by removing the media, washing with phosphate buffered saline (PBS, 10 mM $Na_2HPO_4$, 1.8 mM $KH_2PO_4$, 2.7 mM KCl, 140 mM NaCl, pH 7.4) and lifting the cells using a trypsin (1% [v/v]) in ethelenediaminetetra-acetic acid (EDTA, 0.3 % [w/v]) solution. Cell counting for plating a given number of cells was done by mixing equal volumes of trypan blue and cell suspension, counting the number of stained cells using a haemocytometer (cells x [2 x $10^4$] x volume re-suspended in [ml]) and calculating the volume of media to re-suspend the pellet. Cells were confirmed to be mycoplasma free by staining with Hoechst 33342 (1 µg/ml).

## 2.4. Cytotoxicity assays for analysis of the chemosensitivity/$IC_{50}$ determination of 10 samples on two cell lines

The chemosensitivity of the cell lines to the 10 samples was tested using the MTT assay. For each sample 5 x $10^3$ cells/well were seeded in the inner wells of a 96 well plate while the outer wells

contain PBS. The cells were allowed to sit overnight before being treated in triplicate with a range of concentrations (0.5 mg/ml – $2.56^{-7}$ mg/ml) of the samples. The plates were incubated at 37 °C and 9 % $CO_2$ for 72 h. All the media was removed and MTT reagent (1 mM) was added to each well after the 72 h incubation. The plates were incubated at 37 °C for 4 hours to allow crystal formation after which 100 µl solubilization solution (10 % [W/V] SDS and 0.01 M HCL) was added and the plates incubated overnight. The absorbance at 595 nm was read and the half maximum effective concentration ($IC_{50}$) was calculated by non-linear regression using GraphPad Prism version 4.0.

### 2.5. Immunofluorescence staining and confocal microscopy analysis

HeLa cells were seeded at 1 x $10^5$ onto coverslips in a 24 well plate and allowed to adhere overnight at 37 °C in the $CO_2$ incubator. Cells were treated with selected compounds (0.5 mg/ml) for 24 h. Cells were washed with PBS and fixed with 4 % (w/v) paraformaldehyde for 15 minutes at room temperature followed by 3 x 10 minutes washes in PBS. Cells were mounted in DAKO mounting media. Images were captured using the Olympus BX43 Fluorescence Microscope (Olympus Life Science Microscopes, USA) and were analyzed by Olympus cellSens Entry 2009 (Olympus Life Science, USA).

## 2.6. Synthesis of thiol dual capped- CdTe core, CdTe/CdSe core-shell, CdTe/CdSe/ZnSe core-shell-shell.

The synthesis of CdTe multi core-shell or core-shell-shell QDs in this study as reported earlier began firstly by constructing CdTe cores dual stabilized by five different thiol ligands.

After investigating the optical properties and structural morphology of these cores, a pH-florescence dependent studies were also conducted in order to examine the sensitivity of QDs at different pH media. The result obtained from these studies have recently been reported [3].

### 2.6.1. Synthesis of thiol dual capped CdTe QDs

The synthesis of five dual capped CdTe QDs was performed using a method previously reported in 2017 [18]. Briefly, Cd $(CH_3COO)_2$. $2H_2O$ (0.053 g, 0.2 mmol) was dissolved in deionized water (50 ml). Subsequently, each of the corresponding stabilizing agent (0.2 mmol) described in Table 1 was added to the resultant solution. The pH of the obtained mixture was then adjusted to a desired level using NaOH solution (1 M). Thereafter, the mixture was stirred for 5 min and $K_2TeO_3$ (0.04 mmol) was added to the reaction medium followed by $NaBH_4$ (2 mmol) and the reaction was allowed to proceed for another 5 min. The solution was quickly transferred to a three-necked flask attached to a condenser and refluxed at 100 °C under open-air condition. The growth of the CdTe QDs was monitored using UV-vis and PL spectra at different reflux times of 15 min, 30 min, 1h, 3 h, and 7 h. The mole ratio of Cd:Te: QD: $NaBH_4$ was 1:0.2:1:10.

**Table 1. QDs stabilizing agents and synthetic media pH of CdTe**

| Code | Thiol stabilizing agent | Synthetic medium pH |
|---|---|---|
| G-M | GSH/MPA | 11.0 |
| G-T | GSH/TGA | 9.0 |
| L-T | L-Cysteine/TGA | 12.0 |
| M-T | MPA/TGA | 9.0 |
| L-M | L-Cysteine/MPA | 10.0 |

### 2.6.2. pH sensitivity study

Solutions of citrate and phosphate buffers were prepared using a known method with slight modifications (http://ksemt.kr/down/buffer.htm: Accessed on 14/08/2016).

For citrate buffers, citric acid (2.1 g) was weighed and dissolved in distilled water (100 ml) to give citric acid solution (0.1 M) (A) ranging from 0.95- 3.3 ml. This was followed by separately weighing sodium citrate (2.9 g) into a separate beaker to produce sodium citrate solution (0.1 M) (B) ranging from 1.7- 4.15 ml. Solution A (X ml) was mixed together with solution B (Y ml) diluted to a total of 10 ml with distilled water. The resulting solution was used to prepare buffer 4, 5 and 6 according to Table 2:

**Table 2. Preparation of Buffer 4, 5, and 6**

| Solution A (ml) | Solution B (ml) | pH |
|---|---|---|
| 3.3 | 1.7 | 4.0 |
| 2.05 | 2.95 | 5.0 |
| 0.95 | 4.15 | 6.0 |

For sodium phosphate buffer, sodium phosphate mono basic (1.2 g) was measured and dissolved in de-ionized water (10 ml) to produce sodium phosphate mono basic solution (1 M). This was followed by separately weighing sodium phosphate dibasic (1.42 g) into another separate beaker containing 10 ml distilled water to produce sodium dibasic solution (1 M). From these solutions, sodium monobasic (0.577 ml) was mixed with sodium dibasic solution (0.423 ml) to produce a buffer solution of pH 7.0. Similarly, sodium monobasic (0.932 ml) was mixed with sodium dibasic solution (0.68 ml) to produce another buffer solution with pH 8.

To prepare buffer solution of pH 7.4, sodium mono basic (0.31 g) is measured and dissolved in 100 ml distilled water, followed by the addition of sodium dibasic (1.09 g). The mixture was stirred together to produce buffer solution of pH 7.4.

Citrate and phosphate buffers were used for QDs dilution in pH range 4–6 and 7–8, respectively by mixing 2, 950 ml of each of the buffers (pH 4 – 8) with 0.05 ml of QDs solution. The emission properties of QDs were monitored in order to evaluate any effect of pH on the photo-physics of QDs. At the same time, buffer pH 7.4 (4.917 ml) was used to dilute QDs sample (0.083 ml) for titration experiments with HCl (0.1 M) and using distilled water as a control for dilution effects. The luminescence properties of QDs were continuously measured throughout

titration experiments. It must be noted that all the pH- florescence dependent studies were conducted in duplicates under similar reaction conditions.

### 2.6.3. Synthesis of dual capped- CdTe/CdSe core-shells.

The synthesis of CdTe core-shells were achieved from their corresponding cores according to a method we reported in 2017 [18].

### 2.6.4. Selenium reduction.

For the reduction of selenium, sodium sulphite ($Na_2SO_3$); (0.5 g, 3.9 mmol) was added to deionized water (50 ml) that contained selenium powder (0.1574 g, 1.99 mmol). The reaction was allowed to proceed for 6 h with stirring at 70 °C to form sodium seleno-sulphite ($Na_2SeSO_3$). The formation of a clear brownish solution indicate that the reduction reaction has been successfully completed.

### 2.6.5. Synthesis of dual capped- CdTe/CdSe core-shells.

Following 3 h of reflux time of corresponding cores of each dual capped CdTe QDs, reduced selenium solution (5 ml) was added drop-wisely to coat the surface of respective CdTe cores. The addition of the selenium changed the colour of the solution gradually from green to red within a few seconds (s). Aliquots were taken at regular intervals to monitor the growth of the shell on the surface of the core. The surface property of the synthesized material was then modified using volumes of reduced selenium solution to give a mole ratio of Te: Se, 1: 0.2 (v/v, 1 ml of selenium solution), 1: 0.4 (v/v, 2 ml of selenium solution), 1: 0.6 (v/v, 3 ml of selenium solution). 1: 0.8 (v/v, 4 ml of selenium solution) and 1: 1 (v/v, 5 ml of selenium solution) respectively. It must be noted that as the volume of Se ions injected into the solution increases,

the injection time also increases. Injection at 1 – 5 ml of Se ions was monitored from 10 - 50 s approximately.

Note: The synthesis of the core-shell nanoparticles was conducted at 3 h for cores (section 2.6.5) while the 3 hours core-shell was used to build a multi-core-shell in order to size tune the corresponding synthesized material towards the near infra-red (NIR) for imaging purposes and high emission intensities (section 2.6.6).

**2.6.6. Synthesis of dual capped-CdTe/CdSe/ZnSe multi-core-shells or core-shell-shell QDs.**

The corresponding CdTe core-shells also reported above were promoted to their multi-core-shells following a method reported by Zhang *et al* in 2009 but with substantial modification. [24]. An example of such modification includes the use of different selenium sources and type of QDs formed after the injection of selenide ions into the solutions.

**2.6.7. Formation of Zn complex ions**

Zn sulphate (0.28 g, 1 mmol) was weighed and dissolved in 50 ml of deionized water. In separate reactions, MPA (49 ul, 1 mmol), TGA (30 ul, 1 mmol), L-Cysteine (0.121 g, 1 mmol), and Glutathione (0.15 g, 1mmol) were added into the reacting media producing M-T, L- T, L-M, G-T and G-M dual caps. The pH of the solution was adjusted to 10.8 using 1M NaOH with continued stirring leading to the formation of five different thiol dual capped -Zn complex ions.

### 2.6.8 Formation of ZnSe shell on the surface of CdTe/CdSe core-shells.

During the construction of CdTe/CdSe core shells, equal volumes of Zn and Se ions (1ml) were gradually injected seven times at intervals of 5 min into the reacting vessels following 3 h of CdTe/CdSe reflux time. This led to a total of 7 ml per each of Zn and Se ions that were injected into the solutions over 35 min. Aliquots were taken at 5 min intervals following the injection to monitor the photo-physics of the core-shells. However, aliquots at the 3 hours mark following reflux were taken prior to the first injection of the Zn/Se solutions in order to monitor any wave-length shift following injection of the first set of solutions at 5 min. The color of the reaction was observed to be continuously changing as the volumes of Zn and Se ion (1–7 ml) increased signifying a change in material composition of the system. The condition of the reaction was further optimized by separately increasing the volumes of the Se and Zn ions from 1 ml to 2 ml, making a total of 14 ml (2 ml at every 5 min) in one experiment and subsequently changing the volume to 3 ml in the final experiment to make a total of 21 ml (3 ml at every 5 min) of Zn and Se ions in the reacting vessels, in an attempt to improve the photo-physical properties of synthesized materials.

Following the synthesis of the five-thiol dual cap CdTe cores, CdTe/CdSe core-shell and CdTe/CdSe/ZnSe core-shell-shell described in the text, the estimated particle sizes derived from corresponding UV-Vis excitonic peaks are provided in Table 3- 4 according to equation 2

$$D = (9.8127 \times 10^{-7})\,\lambda^3 - (1.7147 \times 10^{-3})\,\lambda^2 + 1.0064\,\lambda - 194.84 \quad \ldots\ldots\ldots \quad (2)$$

Where λ represent excitation wavelength [18].

**Table 3: Estimated particle size of CdTe cores (3h) and CdTe/CdSe core-shell (50 s- 7 h) for M-T at 1: 1, Te/Se and (10 s- 7 h) for G-M, G-T, L-T and L-M at 1: 0.2, Te/Se).**

| Reaction time | M-T (nm) | Reaction time | G-M (nm) | G-T (nm) | L-T (nm) | L-M (nm) |
|---|---|---|---|---|---|---|
| 3 h core | 2.7 (λ= 517) | 3 h core | 3.26 (λ= 552) | 1.9 (λ= 487) | 2.6 (λ= 512) | 2.7(λ= 517) |
| 50 s | 2.9 (λ= 526) | 10 s | 3.27 (λ= 553) | 2.1 (λ= 492) | 2.7 (λ= 518) | 2.9 (λ= 526) |
| 30 min cs[1] | 3.1 (λ= 541) | 30 min | 3.31 (λ= 557) | 2.2 (λ= 498) | 3.1 (λ= 541) | 3 (λ= 530) |
| 1 h cs | 3.2 (λ= 546) | 1 h cs | 3.33 (λ= 567) | 2.3 (λ= 502) | 3.2 (λ= 546) | 3.1(λ= 542) |
| 3 h cs | 3.4 (λ= 568) | 3 h cs | 3.34 (λ= 566) | 2.6 (λ= 512) | 3.3 (λ= 550) | 3.2(λ= 545) |
| 7 h cs | 3.5 (λ= 581) | 7 h cs | 3.35 (λ= 568) | 3.3 (λ= 560) | 3.4 (λ= 565) | 3.6 (λ= 586) |

[1]core-shell

**Table 4: Estimated particle size of CdTe cs (3 h) and CdTe/CdSe/ZnSe core-shell-shell (5 min- 35 min) for M-T, G-M, G-T, L-T and L-M dual caps at injections of 7 ml each of Zn and Se ions.**

| Reaction time | M-T (nm) | G-M (nm) | G-T (nm) | L-T (nm) | L-M (nm) |
|---|---|---|---|---|---|
| 3 h cs | 2.9 (λ= 526) | 3.5 (λ= 583) | 2.4 (λ= 503) | 2.4 (λ= 502) | 2.5 (λ= 504) |
| 5 min css[1] | 3.12 (λ= 541) | 3.5 (λ= 583) | 2.4 (λ= 503) | 2.5 (λ= 505) | 2.6 (λ= 512) |
| 10 min css | 3.14 (λ= 542) | 3.5 (λ= 583) | 2.4 (λ= 503) | 2.6 (λ= 512) | 2.7 (λ= 517) |
| 15 min css | 3.16 (λ= 543) | 3.5 (λ= 583) | 2.4 (λ= 503) | 2.7 (λ= 517) | 2.9 (λ= 526) |
| 20 min css | 3.19 (λ= 545) | 3.5 (λ= 583) | 2.4 (λ= 503) | 2.8 (λ= 519) | 3.1 (λ= 541) |
| 25 min css | 3.22 (λ= 548) | 3.5 (λ= 583) | 2.4 (λ= 503) | 2.9 (λ= 526) | 3.3 (λ= 550) |
| 30 min css | 3.24 (λ= 550) | 3.5 (λ= 583) | 2.4 (λ= 503) | 3 (λ= 530) | 3.5 (λ= 583) |
| 35 min css | 3.25 (λ= 551) | 3.6 (λ= 586) | 2.5 (λ= 506) | 3.2 (λ= 546) | 3.6 (λ= 586) |

[1]core-shell-shell

**Table 5: Estimated particle size of CdTe cs (3 h) and CdTe/CdSe/ZnSe core-shell-shell (5 min- 35 min) for M-T, G-M, G-T, L-T and L-M dual caps at injections of 14 ml each of Zn and Se ions.**

| Reaction time | M-T (nm) | G-M (nm) | G-T (nm) | L-T (nm) | L-M (nm) |
|---|---|---|---|---|---|
| 3 h cs | 3.2 (λ= 546) | 3.43 (λ=571) | 2 (λ= 488) | 2.3 (λ= 502) | 2 (λ= 489) |
| 5 min css | 3.3 (λ= 549) | 3.43 (λ= 571) | 2.1 (λ= 490) | 2.6 (λ= 512) | 2.1 (λ= 490) |
| 10 min css | 3.32 (λ= 554) | 3.44 (λ= 572) | 2.13 (λ= 491) | 2.8 (λ= 514) | 2.13 (λ= 491) |
| 15 min css | 3.34 (λ= 560) | 3.45 (λ= 573) | 2.14 (λ= 492) | 2.9 (λ= 515) | 2.15(λ= 492) |
| 20 min css | 3.37 (λ= 562) | 3.46 (λ= 574) | 2.16 (λ= 494) | 3.0 (λ= 520) | 2.17(λ= 494) |
| 25 min css | 3.4 (λ= 564) | 3.48 (λ= 577) | 2.17 (λ= 495) | 3.2 (λ= 540) | 2.2 (λ= 497) |
| 30 min css | 3.44 (λ= 565) | 3.5 (λ= 579) | 2.18 (λ= 496) | 3.3 (λ= 548) | 2.25(λ= 500) |
| 35 min css | 3.47 (λ= 568) | 3.55 (λ= 586) | 2.2 (λ= 498) | 3.4 (λ= 560) | 2.28(λ= 501) |

**Table 6: Estimated particle size of CdTe cs (3 h) and CdTe/CdSe/ZnSe core-shell-shell (5 min- 35 min) for M-T, G-M, G-T, L-T and L-M dual caps at injections of 21 ml each of Zn and Se ions.**

| Reaction time | M-T (nm) | G-M (nm) | G-T (nm) | L-T (nm) | L-M (nm) |
|---|---|---|---|---|---|
| 3 h cs[1] | 3.3 (λ= 557) | 2.44 (λ= 504) | 2.19 (λ= 497) | 2.6 (λ= 513) | 2.3 (λ= 501) |
| 5 min css[2] | 3.33 (λ= 559) | 2.46 (λ= 506) | 2.19 (λ= 497) | 2.8 (λ= 515) | 2.4 (λ= 503) |
| 10 min css | 3.35 (λ= 561) | 2.47 (λ= 507) | 2.2 (λ= 499) | 3.0 (λ= 517) | 2.6 (λ= 513) |
| 15 min css | 3.37 (λ= 566) | 2.48 (λ= 508) | 2.24 (λ= 500) | 3.1 (λ= 518) | 2.8 (λ= 515) |
| 20 min css | 3.38 (λ=568) | 2.5 (λ= 510) | 2.26 (λ= 502) | 3.2 (λ= 519) | 3.0 (λ= 518) |
| 25 min css | 3.39 (λ=571) | 2.56 (λ= 512) | 2.27 (λ= 503) | 3.3 (λ= 520) | 3.3 (λ= 555) |
| 30 min css | 3.47(λ= 576) | 2.62 (λ= 515) | 2.29 (λ= 505) | 3.4 (λ= 521) | 3.4 (λ= 574) |
| 35 min css | 3.48(λ= 580) | 2.7 (λ= 520) | 2.3 (λ= 506) | 3.5 (λ= 522) | 3.42 (λ= 576) |

The encapsulation of CdTe multi-core-shells QDs in liposome and chitosan nanoparticles (CNP was demonstrated with MPA-TGA dual caps using a total of 21 ml injection of Zn and Se ions at 5 min reaction time. The reason for choosing this particular dual cap is that (apart from the fact that they demonstrated the longest emission maxima at 35 min) its highest PLQY (89 %) can be found at 5 min reaction time compared to other dual caps for similar reaction times. The synthesis of CNP and the embedding of MPA-TGA dual- capped-CdTe/CdSe/ZnSe multi-core-shell nanoparticles in CNP was conducted following Ghormade *et al* method with slights modifications [58]. In their studies they reported the encapsulation of CdTe cores in CNP while we reported the loading of CdTe multi-core-shell QDs in CNP.

### 2.7. Synthesis of Chitosan Nanoparticles (CNP).

Chitosan was sterilized overnight at 100 ºC in an Oven. CNP was prepared by weighing chitosan (0.01, 0.015 and 0.02 g) in separate reaction flasks and dissolving them in 10 ml of 0.1 M acetic acid. The mixture was stirred vigorously (650 rpm) over-night in order to allow the polymer to completely dissolve in the acetic acid media. Tri-poly phosphate (TPP) (0.003, 0.005 and 0.006 g) was dissolved in 2 ml of distilled water and added under stirring to chitosan solution above in separate reaction flasks. The formation of an opalescent colloidal solution due to CNP was observed immediately and centrifuged for 15 min. The CNP formed was washed thrice and re-suspended in 3 ml of 0.1 M acetic acid.

#### 2.7.1. Encapsulation of MPA-TGA CdTe multi-core-shell QDs in CNP.

The solutions of CNP (3 ml) from above was sonicated with QDs at various volumes (6 ml, 9 ml, 12 ml and 15 ml) (at a concentration of 4.2 mg/ml). Sonicated solutions of CNP were thereby incubated with QDs at various volumes for 30 min at room temperature to allow incorporation of

QDs in the CNPs in one simple step. The resultant CdTe/CdSe/ZnSe- QDs-embedded CNPs were centrifuged and washed thrice to remove any unattached QDs. QDs–CNPs settle down during centrifugation at 4500 rpm (15 min) while unattached QDs remain suspended. The unencapsulated QD was thereby removed and the QD-CNP was re-suspended in various volumes of 0.1 M acetic acid (6 ml, 9 ml, 12 ml, and 15 ml).

In order to optimize the reaction conditions, the interaction between CNP and QDs led to the generation of some 12 formulations (F1- F12) which can be observed according to the table 7.

**Table 7. Formulation table corresponding to the interaction between different amount chitosan nanoparticles (CNP) and various volumes of QDs.**

| Formulations | Chitosan (g) | QDs (ml) (4.2 mg/ml) |
|---|---|---|
| F1 | 0.01 | 6 |
| F2 | 0.015 | 6 |
| F3 | 0.02 | 6 |
| F4 | 0.01 | 9 |
| F5 | 0.015 | 9 |
| F6 | 0.02 | 9 |
| F7 | 0.01 | 12 |
| F8 | 0.0 15 | 12 |
| F9 | 0.02 | 12 |
| F10 | 0.01 | 15 |
| F11 | 0.015 | 15 |

| | | |
|---|---|---|
| F12 | 0.0 2 | 15 |

**2.8. Encapsulation of CdTe/CdSe/ZnSe multi-core-shell QDs in liposome.**

Liposomes loaded with QDs was prepared using thin hydration following a protocol reported by Chu and co-workers in 2010 with slight modifications [56]. Some of the modification performed in our studies was the encapsulation of CdTe multi-core-shell QDs in liposomes. In our studies we also reported the use of dilute HCl to adjust the pH of the QDs solution.

Typically, soy-bean lecithin (50, 100, 150 mg) and cholesterol (16.7, 33.3, 50 mg) in separate reactions flasks were dissolved in chloroform (1 ml) in a round bottomed flask and dried via rotary evaporation to make a thin film. An aqueous solution (3 ml, 4.2 mg/ml) of CdTe/CdSe/ZnSe QDs was added to the flask to hydrate the dry lipid film after adjusting the pH of the QDs solution to 7.2 with 0.015 M dilute HCl in a separate reaction. The contents were stirred vigorously at 400 rpm to obtain multi lamellar vesicle (MLV) liposomes at various stirring time of 15, 30 and 45 min. This was followed by sonicating the MLV liposomes in a water bath sonicator in order to break down the multi lamellar to small unilamellar vesicles (SUV) liposomes. The QD-LVs solution was further centrifuged at 4500 rpm for 90 min in order to separate unencapsulated QDs from the encapsulated ones. The unencapsulated QDs at the - The QD-liposome vesicles (LVs) were washed 3 times using distilled water and finally resuspended in distilled water before emission analysis.

It must however be noted that the preparation of liposome loaded with QDs for formulation 10-14 follows the same procedure as above except that 100 mg of lecithin interacted with various

volumes of QDs (1.5 ml, 6 ml, 9 ml, 12 ml and 15 ml) and stirred for 45 min. The formulation table for various amount of lecithin interacting with QDs for different stirring time is shown in Table 8 below.

**Table 8. Formulation table for various amount of lecithin interacting with QDs at different stirring time.**

| Formulations | Lecithin (mg) | Vol of QDs (ml) (4.2 mg/ml) | Stirring time (min) |
|---|---|---|---|
| F1 | 50 | 3 | 15 |
| F2 | 50 | 3 | 30 |
| F3 | 50 | 3 | 45 |
| F4 | 100 | 3 | 15 |
| F5 | 100 | 3 | 30 |
| F6 | 100 | 3 | 45 |
| F7 | 150 | 3 | 15 |
| F8 | 150 | 3 | 30 |
| F9 | 150 | 3 | 45 |
| F10 | 100 | 1.5 | 45 |
| F11 | 100 | 6 | 45 |
| F12 | 100 | 9 | 45 |
| F13 | 100 | 12 | 45 |
| F14 | 100 | 15 | 45 |

# CHAPTER 3.

## 3. Optical properties and structural morphology of thiol dual capped-CdTe cores.

It was previously emphasized in Chapter two (section 2.6) that the synthesis of thiol-dual capped-CdTe/CdSe/ZnSe multi-core-shell QDs began firstly by synthesizing CdTe cores which later led to the synthesis of CdTe/CdSe core-shell and finally CdTe/CdSe/ZnSe core-shell-shell. The optical properties and structural morphology of synthesized thiol dual-capped-CdTe cores are hereby discussed in this chapter. The changes in florescence intensities of the five thiol-dual caps (G-M, G-T, L-T, M-T and L-M) in various pH buffer media (4- 8) were also investigated.

It should be noted that all the result and discussions in this chapter has already been published in the journal of florescence [3].

### 3.1. UV-Vis and Fluorescence spectra of G-M, G-T, L-T, M-T and L-M- dual cap CdTe cores.

The fluorescence spectra of all synthesized dual capped CdTe QDs can be found in figure 6 and 7. The UV-vis including fluorescence spectra of GSH-MPA-CdTe QDs is also found in figure 6. The absorption spectra of the synthesized materials demonstrated a shift in excitonic peak from 464 to 540 nm while a shift in the emission band was observed from 502 to 512 nm (figure 6b). The corresponding increase in excitonic and emission wavelength peaks with reaction time indicates increase in growth of the nano-particles as bigger particles are formed at higher wavelength. The change in emission intensity may be due to Oswald ripening mechanism where

smaller particles dissolve to give bigger particle size [18, 46]. Each of the materials were also observed to be blue shifted from the bulk material (867 nm) confirming the process of quantum confinement [20, 34, 41]. It must be recalled that a bulk material usually has their sizes above 100 nm in all dimensions while nanomaterials have their sizes in 1 – 100 nm range in at least in one dimension [20, 24].

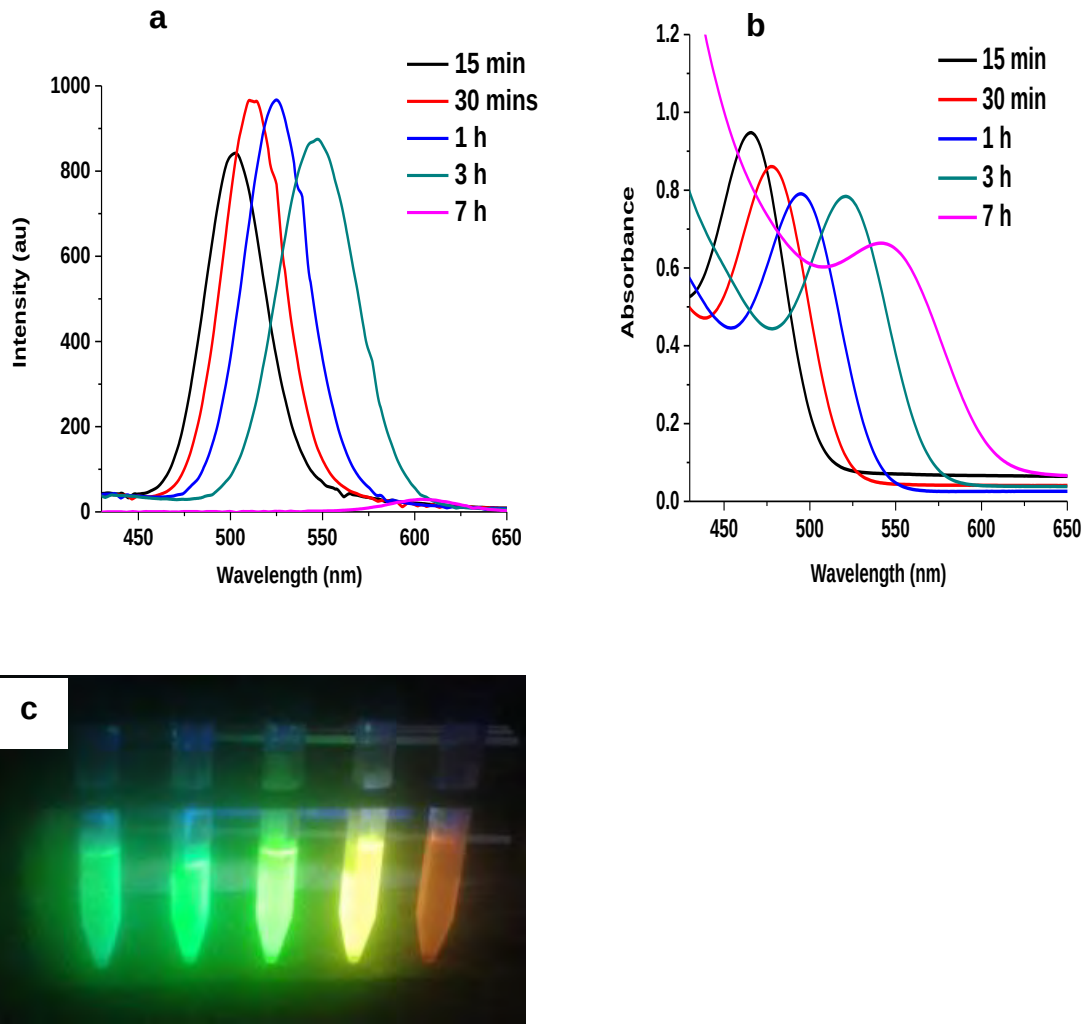

**Figure 6.** Typical UV-vis (a) and fluorescence spectra (b) of GSH-MPA capped CdTe obtained after refluxing for 15 min, 30 min, 1 h, 3 h and 7 h respectively. Image c shows various emission colours (green for 15 min– orange for 7 h) of the QDs upon UV illumination.

The increase in emission intensity at 30 min and 1 h reveals an increase in surface passivation of the synthesized material due to reduced non-radiative recombination sites while a drastic decrease in intensity at 7 h may be due to formation of material with bigger particle sizes [20, 21, 38]. The increase in surface passivation may be due to good surface interactions caused by the dual stabilizing agents located on the surface of the CdTe QDs, which led to formation of strong GSH-MPA-$Cd^{2+}$ bond. The use of higher mole ratio of $NaBH_4$ might have reduced all the Te to the extent that there are no excess Te left in the solution. The greenish to orange colours observed in figure 6c reveal emission colours of the nanoparticles prepared at 15 min–7 h reaction time, suggesting an increase in particle sizes of the synthesised materials [1, 12, 18].

The photoluminescence spectra of G-T, L-T, M-T and L-M- CdTe QDs are further presented in figure 7 (a- d), here too we observe that all synthesized dual capped QDs demonstrated good optical behaviours. The florescence properties of G-M (figure 6a) and G-T (figure 7a) seem to resemble each other. This is due to the formation of higher fluorescent intensities at 30 min and 1 h reaction time compared to the other remaining dual caps. The presence of more capping group in glutathione may also contribute to higher florescnce intensities observed at these reflux time [13, 35].

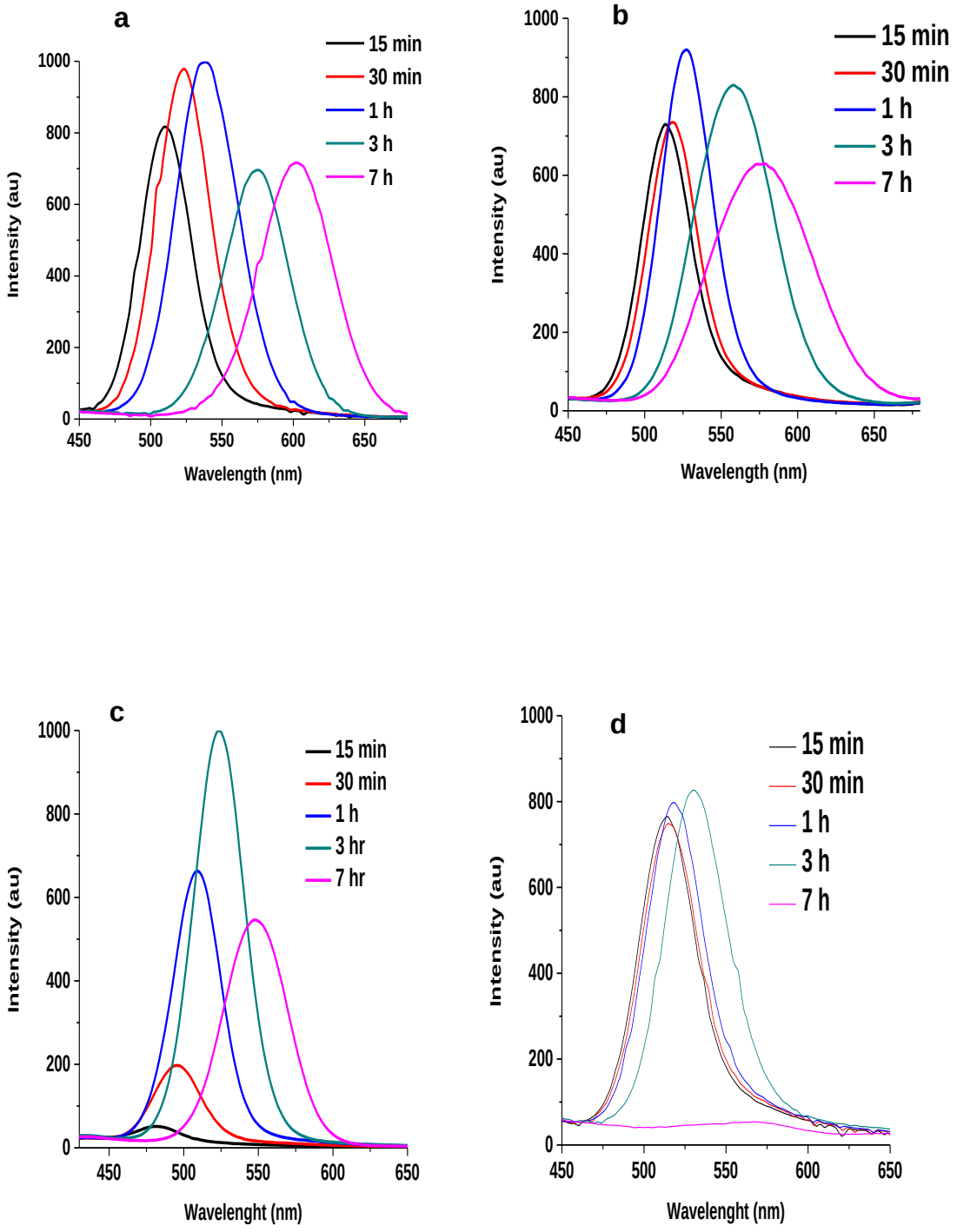


**Figure 7.** The PL evolution spectra of GSH-TGA (a), L-cysteine-TGA (b), MPA-TGA (c) and L-Cysteine- MPA (d) dual capped CdTe QDs following refluxing for 15 min, 30 min, 1 h, 3 h and 7 h in each case respectively.

Significant decrease in emission intensity can be observed at 15 min, 30 min and 1 h for MPA-TGA-CdTe QDs compared to other QDs at similar reaction time. The functionalization of the two thiol ligands (MPA and TGA) in passivating the surface of synthesized QDs might be responsible for this. Although this result is unusual given that MPA and TGA are usually known as some of the best thiol ligands used to synthesize CdTe QDs with tremendous photo-physical properties [17]. An example discussed earlier is the use of CdTe QDs and CdTe/ZnS core-shell nanoparticle by Adegoke and Nyokong in 2014 for selective luminescent detection of peroxy-nitrite in solutions [45]. These QDs were stabilized by both MPA and TGA. In addition, MPA and TGA have also been used on several occasions as single stabilizers in the synthesis of CdTe QDs with high fluorescence intensities. This property has allowed them to be applied in optical imaging for cell labelling [20, 21, 30, 38, 44, 46]. Despite this result it is clear that the best fluorescence intensity is found at 3 h reaction time compared to the remaining dual cap for similar reaction times.

The UV-vis spectra (not shown) for G-M, G-T, L-T and M-T were all observed to demonstrate sharp absorption band edges with the exception of L-M which demonstrated weak absorbance (figure 8). This could be due to the formation of tertiary co-ordination sites between the amine group on L-cysteine and the metal ion ($Cd^{2+}$) in addition to the primary and secondary co-ordination sites formed by the mercapto and carboxylic acid groups. The coordination with the amine polar group might have restricted the normal growth process by reducing the electrostatic repulsion within $Cd^{2+}$ -L-cysteine-MPA, leading to uncontrollable growth process [78]. This may be the reason for the formation of weak absorption band edges observed at 7 hours reaction time in figure 8.

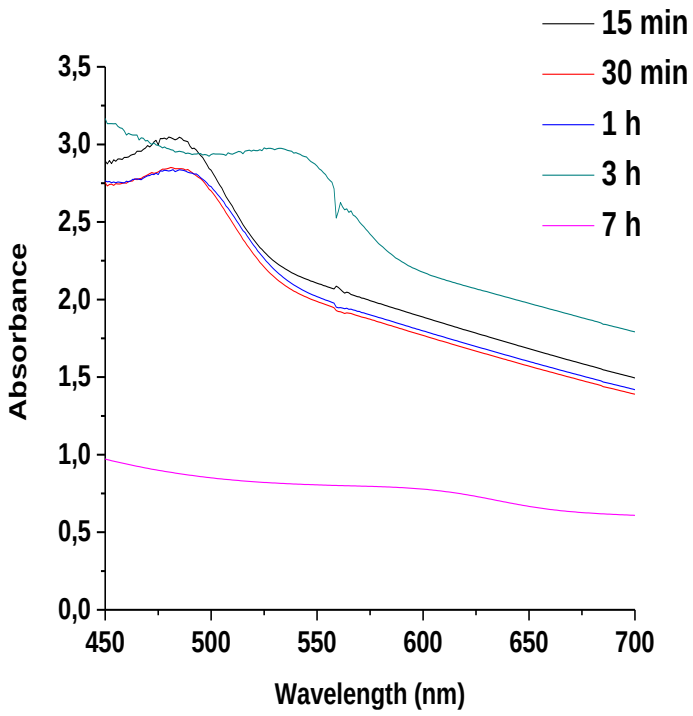


**Figure 8.** UV spectra for L-M dual-capped CdTe QDs obtained after refluxing for 15 min, 30 min, 1 h, 3 h and 7 h respectively.

### 3.2. Particle morphology

Figure 9a and c illustrates the TEM micrographs for G-M and L-T- CdTe QDs along side their corresponding size distribution curves. The individual TEM images signify that the synthesized nanoparticles are quantum dots with an average size distribution of 8.74 ± 2.72 and 9.73 ± 2.33 for G-M (9b) and L-T (9d) dual cap respectively, indicating that the syntheiszed materials fall within the nanosize ranges [1]. During the synthesis of these materials, their desired size was achieved by controlling the reflux time and balancing the mole ratio at which each chemical precussors interacts with each other.

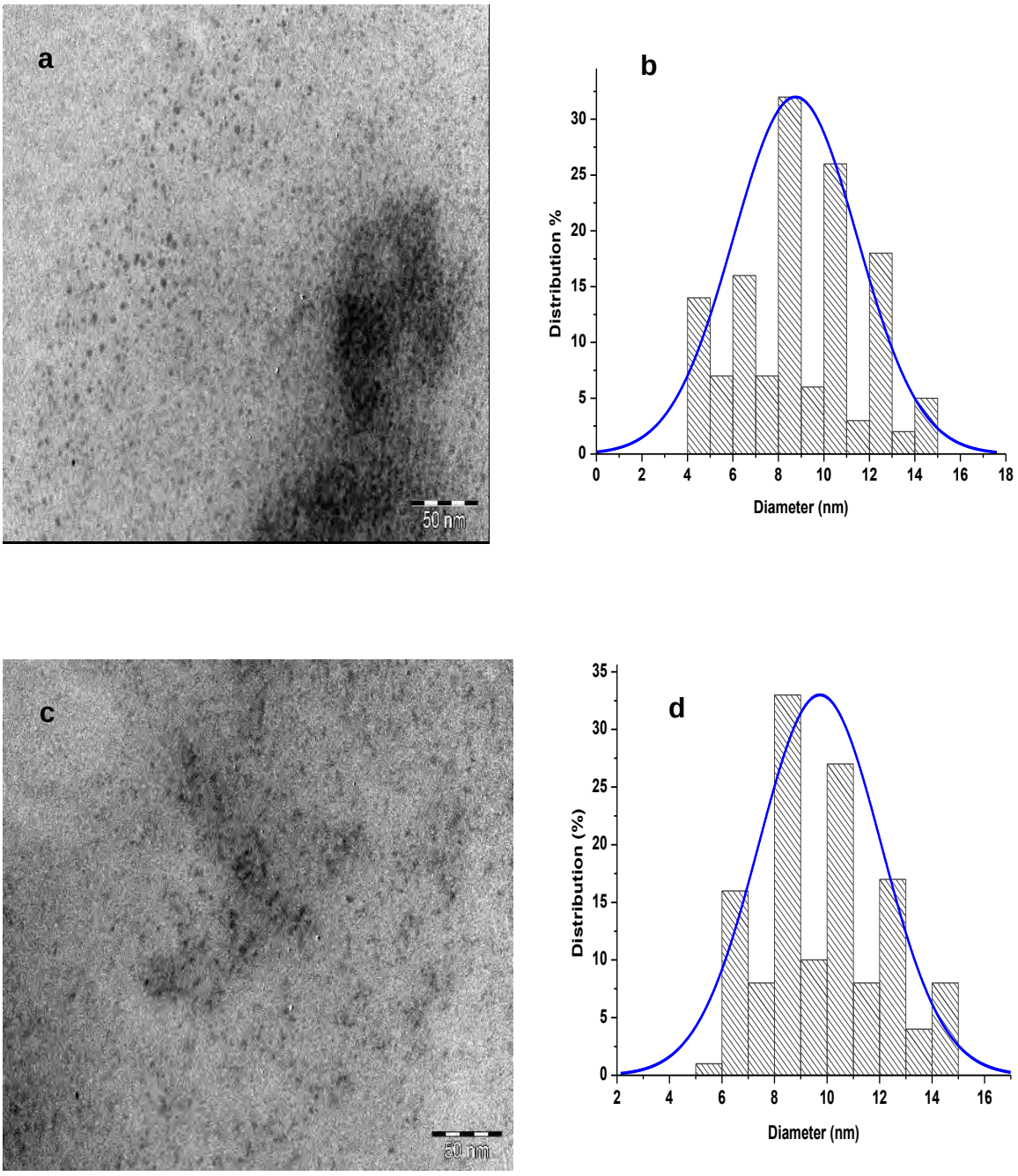


**Figure 9.** Typical TEM images of G-M (a) and L-T (c) CdTe QDs.

### 3.3. FTIR analysis of the synthesized materials.

Figure 10 a and b present the FTIR spectra of G-M and L-T-CdTe QDs in comparison with their corresponding starting materials. The main bands for N-H stretch, alcoholic and carboxylic acid O–H stretching vibrations were found at 3064-3330 $cm^{-1}$, while the C=O stretch is located at around 1737 $cm^{-1}$. The bands at 700-1400 $cm^{-1}$ belong to alkane and alkene (C-H bend) groups and also to phenol, acyl and alkoxy C-O. It can be observed that the S-H vibrations at 2500 $cm^{-1}$ on GSH, MPA, L-cysteine and TGA were suppressed on the GSH-MPA- CdTe QDs and L-Cysteine-TGA-CdTe QDs indicating successful capping on the surface of QDs [2, 18, 20, 34].

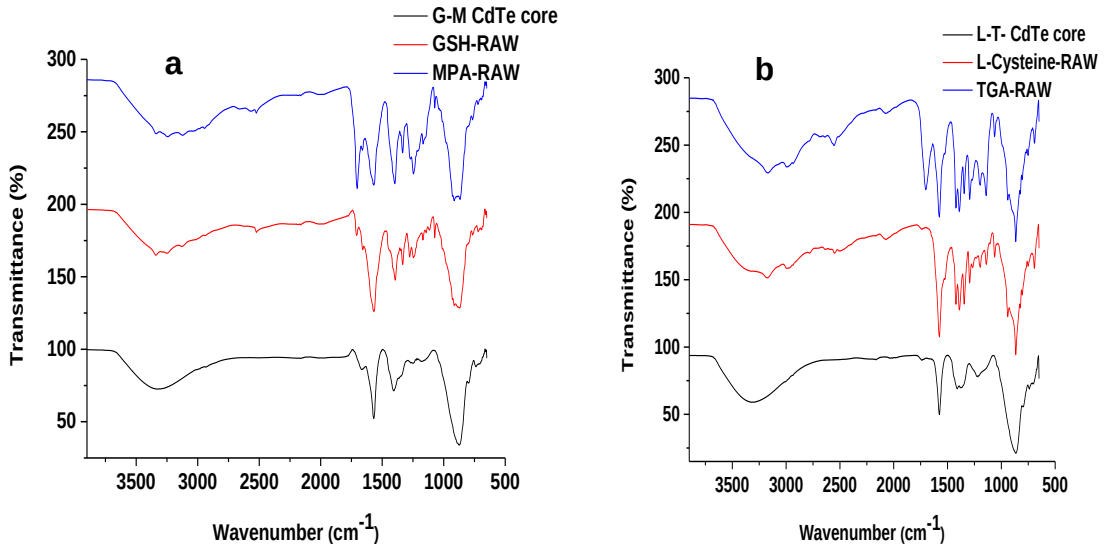


**Figure 10.** FTIR spectra of G-M (a) and L-T (b) CdTe QDs with their corresponding individual capping agent.

### 3.4. Effects of pH changes on QDs fluorescence intensities.

A pH variation study was conducted using citrate and phosphate buffers in the pH range: 4–6 and pH 7–8 respectively. These pH ranges were deemed to be suitable for investigating the potential biological applications of the QDs based on some medical and clinical reports [79], which highlighted the average pH environment for most cancerous cells as lying between 6.0 – 7.4 which is slightly acidic [79]. The QDs have been shown to be excellent fluorescent materials, as it turns out, the instability of photoluminescence intensity upon pH changes could be useful for development of multifunctional biological nanodevices. Figure 11 presents the graphs showing the effect of pH media on the fluorescence intensity of G-M, G-T, L-T and M-T- dual cap CdTe QDs. Surprisingly, all the QDs exhibited remarkable variations in emission intensities depending on the acidity of buffer used.

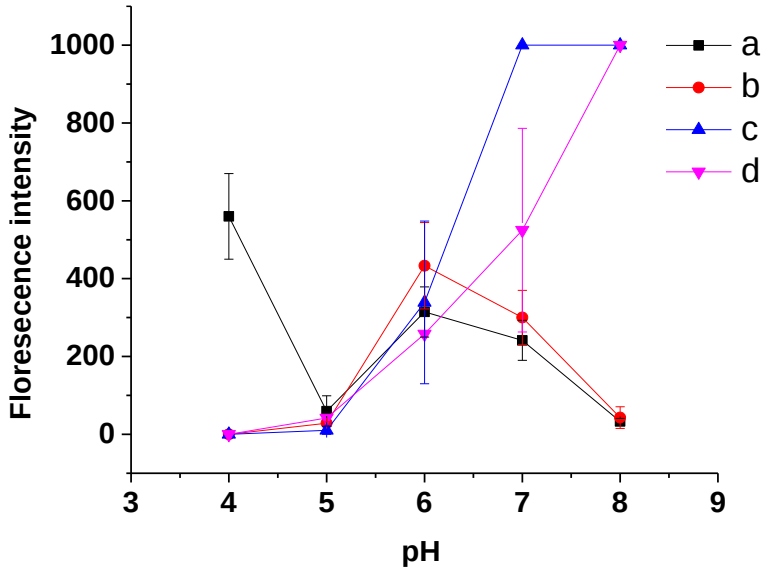


**Figure 11.** Fluorescence intensities of G-M (a), G-T (b), L-T (c) and M-T (d) dual cap- CdTe QDs as a function of pH.

Of particular interest, L-T and M-T dual caps were observed to maintain high luminescence in pH 7 and 8 ranges while drastic quenching was observed in acidic media. Unlike L-T and M-T dual caps, irregular correlation was found between the pH of the media and the luminescence intensity of G-M and G-T dual caps. L-T and M-T dual caps can be considered as pH-responsive materials due to a gradual decrease in luminescence intensity from alkaline to neutral media and to acidic environment. This reason for this behavior might be due to the fact that the combination of MPA and TGA with themselves or L-Cysteine allows enough negative charges to be supplied to the surface of synthesized CdTe nanoparticles thus maintaining a high repulsion forces between each nanoparticle at pH 7 and 8 [17]. This may not be the case when GSH is combine with either MPA or TGA because GSH carries more co-ordination sites in its chemical structure compares to L-cysteine. This may have caused an in-balance to the reaction equilibrium between GSH and MPA or TGA thereby leading to the irregularities in florescence intensities of the dual caps [2]. Furthermore, titration experiments were conducted using HCl (0.1 M) in order to further confirm the pH responsiveness of L-T and M-T dual caps (figure 12a and b).

The graphs shown in figure 12 reveal constant decrease in fluorescence intensity for L-T and M-T dual caps upon titration with HCl (0.1 M), while the dilution effect evaluated with distilled water was found to have a constant influence. This supports the data observed from pH studies using the buffers. This makes CdTe QDs dual capped with L-T and M-T thiol ligands potential candidates for further development of multifunctional pH-responsive nanomaterials that would be useful in medical applications such as theranostics, considering the acidity of cancer cell micro environments [79].

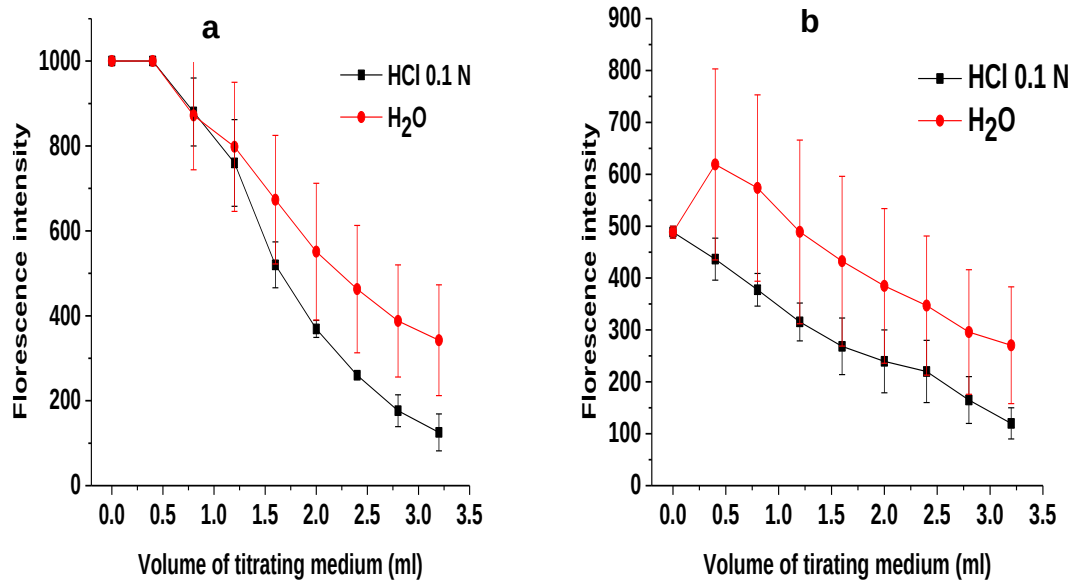


**Figure 12.** Titration of L-T (a) and M-T (b) dual cap CdTe QDs using 0.1 M HCL and distilled water.

Therefore, in conclusion, it can be established that all the synthesized QDs above demonstrated improved photo-physical properties depending on the reaction time. Hence, each of the synthesized thiol-dual capped CdTe QDs were promoted to their corresponding core-shell at 3 h reaction times and later to multi-core-shell QDs. This will follow in the next chapter subsequently.

# CHAPTER 4.

## 4. Photophysical Investigation of CdTe core shells.

The discussions in chapter three elucidate the optical properties and structural characterization of five different thiol-dual capped CdTe cores with their corresponding florescence- pH dependent studies. However, it has been established from various literature discussed in chapter one that the coating of the surface of CdTe QDs with ZnSe or ZnS prevents the toxic $Cd^{2+}$ from leaching out into the immediate environment during biological investigation. However, this does not only enhance their bio-compatibility but also improves their photo-physical properties such as stability and florescence. In this chapter, we report the conversion of this cores stabilized with five different thiol ligands into CdTe multi-core-shells. Preceding the synthesis of the multi-core-shells, the surfaces of each dual cap core were coated with CdSe shell, this contributed to the improvement of their photo-physical properties. During the synthesis of the core-shells, various volumes of selenide ions were injected into the reacting mixture containing CdTe cores at 3 h reaction time in order to optimize the QDs results in-terms of florescence intensities. As emphasized in the first chapter it is worth noting that the synthesis of CdTe multi-core-shells reported in this study took only 35 min reaction time to obtain the highest emission maxima, reported studies in the literature claim to have taken more than 6 hours. Optimization of various reaction conditions such as concentration and injection time of $Zn^{2+}$ and $Se^{2-}$ were applied in order to generate the QDs with optimal result. We discuss below the evaluation of the corresponding optical properties and structural morphology of synthesized five different thiol-dual cap-CdTe/CdSe core-shell and CdTe/CdSe/ZnSe core-shell-shell QDs. The procedures involved in the conversion of CdTe cores to CdTe/CdSe/ZnSe multi-core-shell via CdTe/CdSe core-shell

was discussed previously in chapter two. caps (G-M, G-T, L-T, M-T and L-M) in various pH buffer media (4- 8) were also investigated.

It must also be noted that all the result and discussions in this chapter has already been published in the nanomaterials [15].

### 4.1. UV and PL spectra of dual capped-CdTe/CdSe core-shells.

Results from the photo-emission spectra of M-T dual capped CdTe/CdSe core-shell QDs indicate that virtually all synthesized core-shell at various mole ratios demonstrated high florescence intensity at 3h reaction time (section 4.8, figure 27 a-e). However, the largest wavelength shifts between 3 h core and 50 s for the core-shell can be observed at 1:1 of Te/Se (section 4.8, figure 27e). This account for the reason why this mole ratio was used to improve the synthesized core shell to a multi-core shell. Hence it was further observed that the remaining four dual capped CdTe core-shell (G-M, G-T, L-T and L-M) showed their best results at 1: 0.2 of Te/Se for the 3 h core-shell compared to the other mole ratios at equal reaction time (section 4.8 figure 27- 31). Therefore, this reaction time and mole ratio was chosen as a starting condition to promote each of them to a multi-core-shell with the aim of maintaining their enhanced florescent property as they approach the red region of the spectrum.

### 4.1.2. UV and PL spectra of MPA-TGA-CdTe/CdSe core-shell QDs at 1:1 of Te/Se.

A significant shift in wavelength of 34 nm is observed for CdTe core (496 nm at 3h) and for the CdTe core-shell (530 nm at 50 s) (figure 13 a) indicating an increase in particle size within a

short reaction time due to the formation of CdSe shell at the surface of CdTe core. The construction of CdSe shell at the surface of the core is due to the reaction between reduced Se ions injected into the solution and Cd ions present inside the solution [46]. The concomitant increase in florescence intensity between 3 h CdTe core (PLQY 65 %), and 50 s CdTe core shell (PLQY 83 %), with increase in particle size indicates increase in surface passivation provided by the thin layer of CdSe shell at the surface of the core [18, 38]. The thickness of CdSe shell formed at the surface of CdTe core was estimated to be about 0.2 nm. The corresponding particle size of CdTe core at 3 h was calculated to be 2.7 nm and CdTe/CdSe core- shell at 50 s is calculated to be 2.9 nm

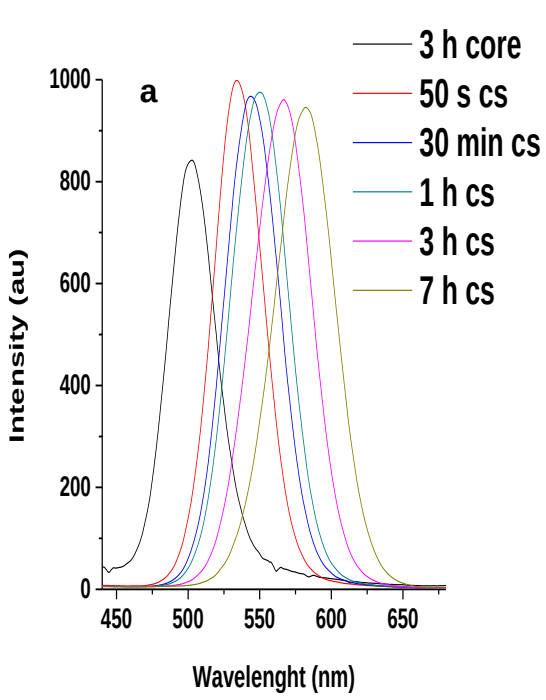


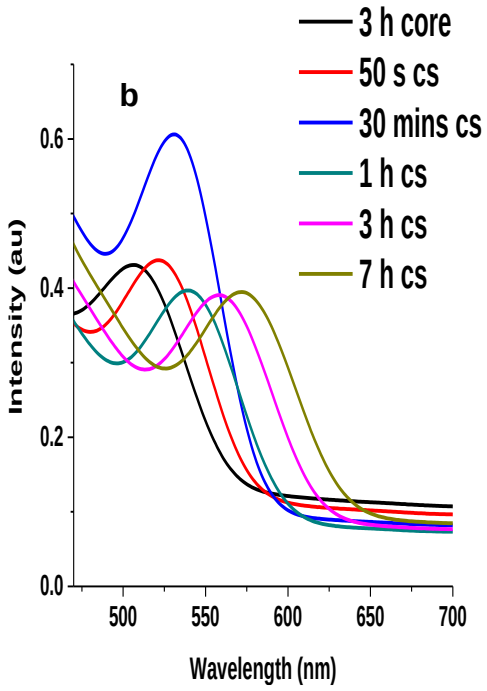


**Figure 13.** PL spectra (a) and UV spectra (b) of MPA-TGA-CdTe/CdSe core shell at 1:1 of Te/Se and emission colours (c) produced at 3 h CdTe core (green) – 7 h CdTe core-shell (orange). Note: cs represent core-shell.

Furthermore, the passivation provided by the CdSe shell at the surface of the CdTe core is thought to reduce the surface defect of synthesized material thereby leading to an increase in emission intensity of the resulting CdTe core-shell. The emission intensity of the core-shell however decreased at 3 and 7 hours of reaction time due to the formation of thicker CdSe shell. The estimated particle size according to Table 3 are 3.4 and 3.5 nm respectively, which would indicate an increase in shell growth compared to other reaction times [4, 18].

Result from the UV spectra (figure 13b) indicates a slight red shift in excitonic peak between 3 h for CdTe core and 50 s for CdTe core-shell due to the passivation of CdSe shell at the surface of CdTe core. It is observed that the Intensity of the absorbance at 30 min reaction time is higher compared to all others which might indicate enhanced surface reconstruction process under open air conditions as reaction time increases. However, the slight decrease in PL intensity after 50 s might be due to low surface recombination effects by the charge carriers. However, further investigation is required to clarify this observation. Figure 13 c indicates various emission colors produced by synthesized QDs under UV illumination. The green emission to the extreme left corresponds to 3 h for CdTe core which gradually changes to orange as one move from (L-R) due to the deposition of CdSe shell at the surface of CdTe core, to produce CdTe core-shell.

It will be observed in figure 27- 31 (section 4.8) at the end of this chapter that as the concentration of Se ion increases, significant shift in wavelength occurs at 3 h between the core and the core-shell corresponding to each of the mole ratio. The shift in wavelength seems to

follow the order: 1: 0.2 (4 nm), 1: 0.4 (8 nm), 1: 0.6 (16 nm), 1: 0.8 (18 nm), 1: 1 (36 nm) corresponding to the Te/Se ratios respectively. The reason for the increase in wavelength shift with increase in the relative amount of selenide ion is thought to be due to electro-static interaction between free Cd ions in the solution and reduced Se ions coming back into the solution. This would lead to formation of thicker CdSe shell thereby increasing the size of the heterostructure [4, 18].

### 4.1.3. PL spectra of CdTe/CdSe core-shell QDs at 1:0.2 dual capped with L-T, L-M, G-T and G-M.

It was mentioned earlier that CdTe core-shell dual capped with L-T, L-M, G-T and G-M indicate optimal fluorescence spectra for the Te/Se ratio at 1:0.2. This observation was ascribed to the optimal 3 h reaction time corresponding to this mole ratio.

All the dual capped core-shell in figure 14 (a- d) demonstrate slight shift in wavelength between 3 hours of their corresponding core to 10 s of their individual core-shell. Increase in emission intensity is also observed, because of the passivation provided by thin layer of CdSe shell at the surface of the CdTe core [21, 41- 42]. This passivation could also account for the slight increase in emission wavelength between the two reaction times. The PLQY for L-M dual capped was observed to increase from 68 % for the core at 3 h to 87 % for the core-shell at 10 s.

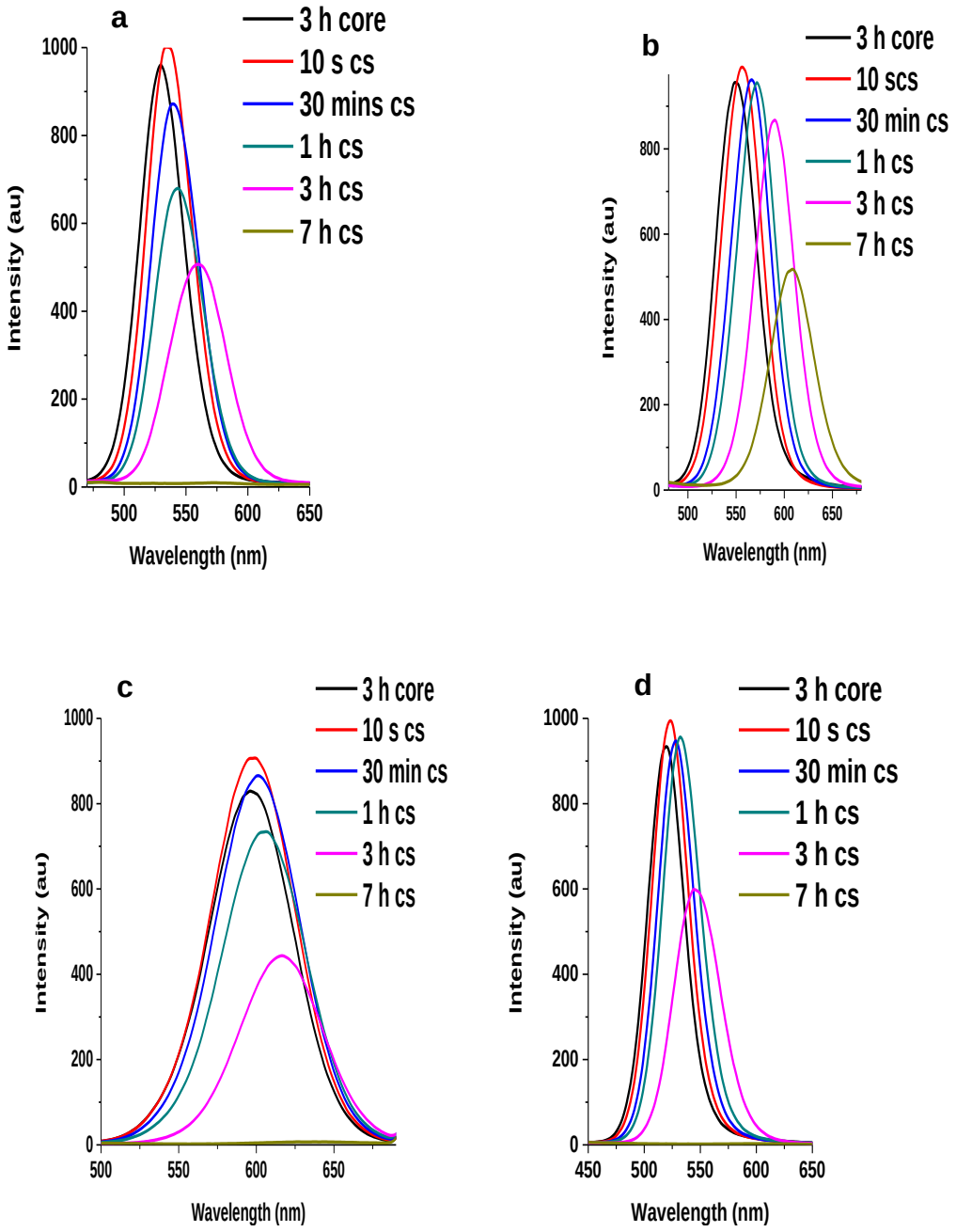


**Figure 14.** Typical PL spectra of L-T (a), L-M (b), G-M (c) and G-T (d) dual capped CdTe/CdSe core-shell nanoparticles at 1:0.2 mole ratio of Te/Se for various reflux time (3 h CdTe core- 7 h CdTe/CdSe core-shell). Note: cs represent core-shell.

Furthermore, gradual decrease in fluorescence intensities of CdTe core-shell is observed from 30 min of reaction time, this is thought to be due to the formation of larger particle sizes at higher

reaction time [1, 46]. It is highlighted here that CdTe core-shell dual capped with L-cysteine-thioglycolic acid (L-T) demonstrated highest intensity of fluorescence at 3 h (PLQY 67 %) and 7 h (PLQY 49 %) reaction times among the dual capped core-shells as shown in figure 14b. This observation is attributed to favorable surface chemistry interaction between L-cysteine and thioglycolic acid during the construction of the nanoparticle [3,14,17]. Hence, it is observed for all the spectra in figure 14 that the combination of Thio-glycolic acid (TGA) as dual stabilizing agents produces an improved surface passivation of synthesized CdTe core-shells. This is seen from the displayed intensities by G-T and L-T dual caps**.** The G-T dual capped showed higher fluorescence intensities at 30 min (69 %) and 1 h (70 %) compared to G-M dual capped for same reaction time. The reason for this type of behavior produced by TGA may be due to the presence of shorter carbon chain in its structure (2 carbon atoms) compared to MPA (3 carbon atoms) [14, 17]. This property gives rise to good photo-physical attributes as mentioned from the literature and allows QDs stabilized with TGA to be used as fluorescence probes in various imaging applications [17, 44].

However, as mentioned previously in section 4.1, the florescence properties of MPA-TGA (M-T) are still regarded as the best result, this is due to the observed high florescence intensity for all the mole ratios of Te/Se (1: 0.2 – 1: 1) for almost all reaction times compared to similar dual capped thiols (section 5 figure 27- 31). Figure 15 shows the uv-vis spectra of L-T dual capped; the sharp band edges are observed for all the reaction time indicating a sign of good photo-physical behavior.

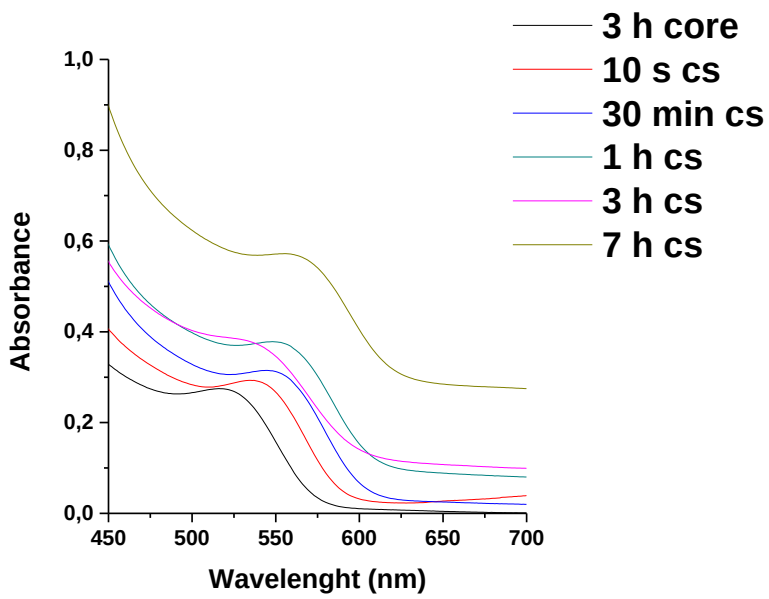


**Figure 15.** UV-vis spectra of L-T-dual capped CdTe core (3 h) and CdTe/CdSe core-shell (0 min- 7h). Note: cs represent core-shell.

### 4.2. TEM images of M-T-CdTe/CdSe core and core-shell at 3 h reaction time.

Figure 16 represents the TEM images of M-T-CdTe core and CdTe/CdSe core-shell. It is clear from the two TEM micrograph in figure 16a and 16c that there are individual particles separated and their corresponding spherical shapes resembles that of a QDs [2]. The calculated average particle size for the TEM images of CdTe core in figure 16b is 3.65 ± 1.31 nm while that of CdTe/CdSe core-shell in figure 16d is 4.92 ± 2.28 nm. The increase in average particle size from the core to the core-shell signifies that each of the core-shell particles are considerably bigger than their respective cores, this is interpreted as an extra coating of CdSe shell at the surface of CdTe core.

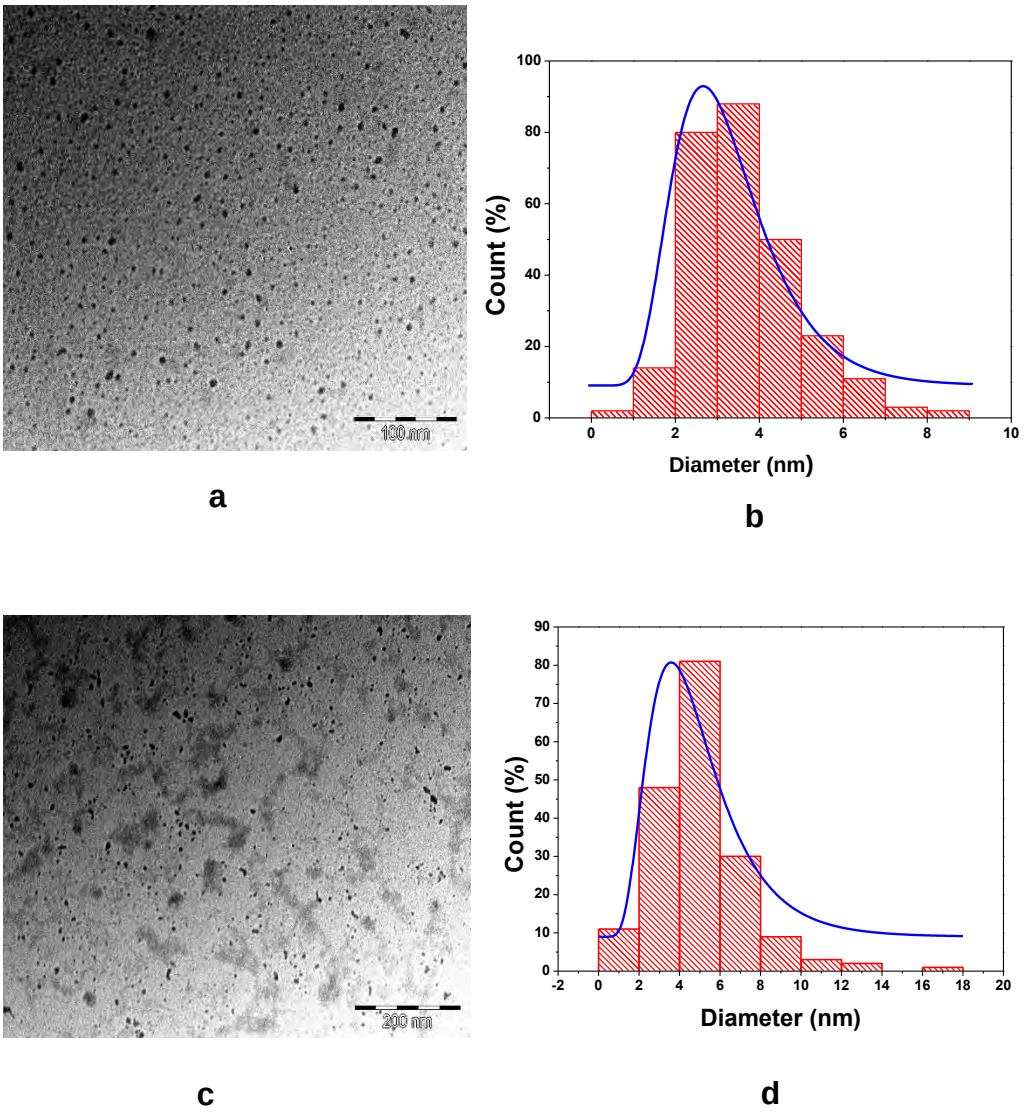


**Figure 16.** TEM image of M-T-CdTe core(a) and M-T-CdTe/CdSe core-shell(c) both at 3 h reaction time. Size distribution of CdTe core (b) and CdTe/CdSe core-shell (d).

### 4.3. FTIR spectra for L-T-CdTe/CdSe core-shell.

In figure 17, we show the FTIR spectrum of L-T-CdTe/CdSe core-shell alongside the corresponding starting materials. The main bands for N-H stretch, alcoholic and carboxylic acid O–H stretching vibrations were found at 3064-3330 $cm^{-1}$, while the C=O stretch is located at

around 1737 $cm^{-1}$. The bands at 700-1400 $cm^{-1}$ belong to alkane and alkene (C-H bend) groups and also to phenol, acyl and alkoxy C-O. It can be observed that the S-H vibrations at 2500 $cm^{-1}$ on MPA and TGA were suppressed indicating successful capping on the surface of QDs.

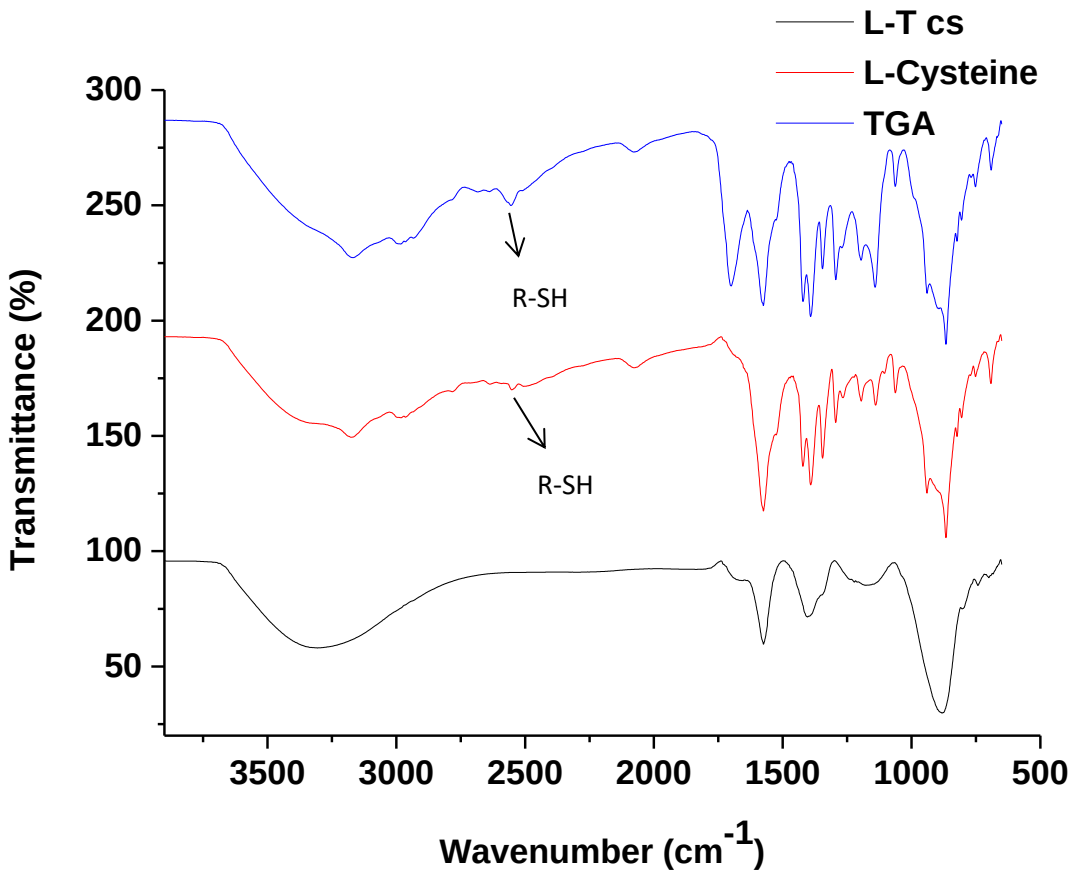


**Figure 17.** FTIR spectra of L-Cysteine-TGA-CdTe/CdSe core-shell (QD cs), raw L-Cysteine and TGA.

### 4.4. UV and PL spectra of MPA-TGA-CdTe/CdSe/ZnSe core-shell-shell QDs

The PL spectra in figure 18b demonstrate significant shift in wavelength and simultaneous increase in emission intensity at 3 h for the CdTe core shell and at 5 min for CdTe core-shell shell following injection of 1 ml each of Zn and Se ions, respectively. The shelling of ZnSe shell

at the surface of CdTe core-shell accounts for the increase in fluorescence intensity of the multi-core-shell. The ZnSe shell having a substantial wider band gap confines the exciton within the CdTe/CdSe interface and isolates it from the solution environment thus leading to increase in emission intensity of the heterostructure [41- 42, 46, 48].

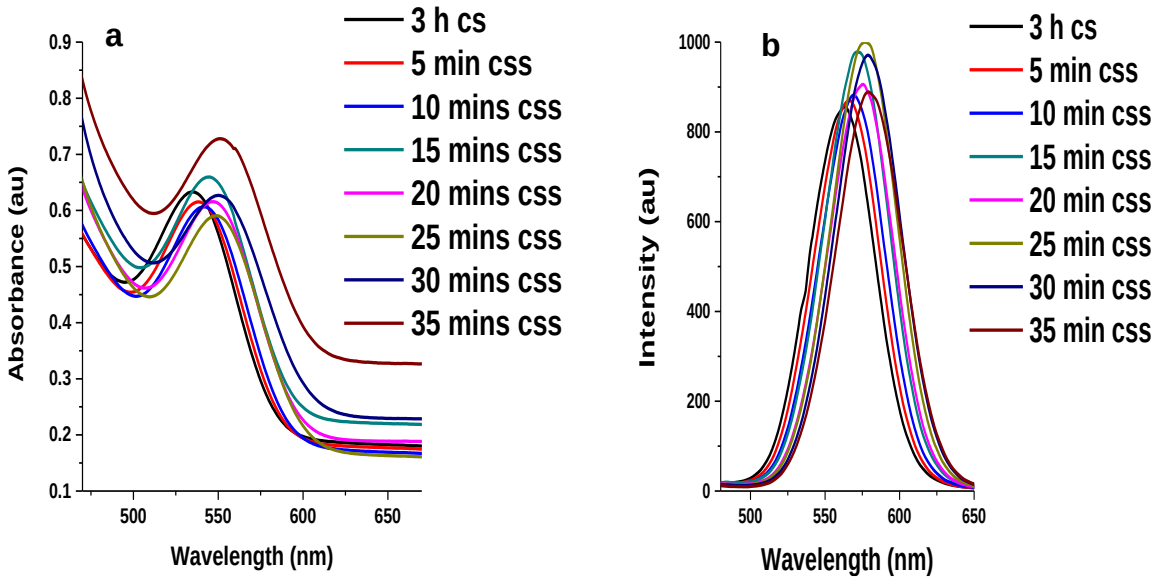


**Figure 18.** UV-vis (a) and PL spectra (b) of MPA-TGA-CdTe css. Note: cs and css represent core-shell and core-shell-shell.

The observation from the UV spectra also confirms the fabrication of CdTe multi core-shell which absorbs at longer wavelength (figure 18 a).

### 4.4.1. PL spectra of M-T- CdTe multi-core-shell at 14 and 21-ml injection of Zn and Se ions.

Optimization of the reaction condition was performed to improve the photo-physical properties. This was conducted by increasing the volume of Zn and Se ions to 14 and 21 ml respectively. Injection at these volumes led to wavelength shift of about 35 nm (14 ml) (figure 19a) and 39 nm (21 ml) (figure 19b) between 3 h for the CdTe core-shell and 35 min for the core-shell shell. The emission wavelength at 35 min (14 ml) is recorded at 616 nm (PLQY 30 %) while that for 21 ml is observed at 625 nm (PLQY 16 %). This indicates increase in particle size due to formation of thicker ZnSe shell as concentration of Zn and Se ions is increased. The significant quench in fluorescence intensity might be attributed to large lattice mismatch as a result of the increased thickness of ZnSe shell. This could lead to an interfacial strain at the surface of CdTe/CdSe shell and cause the trapping of photo-degenerated charge carriers. Similar observations were reported by Taniguchi *et al* in 2009 and Vuyelwa et in 2011 during the synthesis of CdTe/CdSe/ZnSe core-shell-shell QDs. [42, 46].

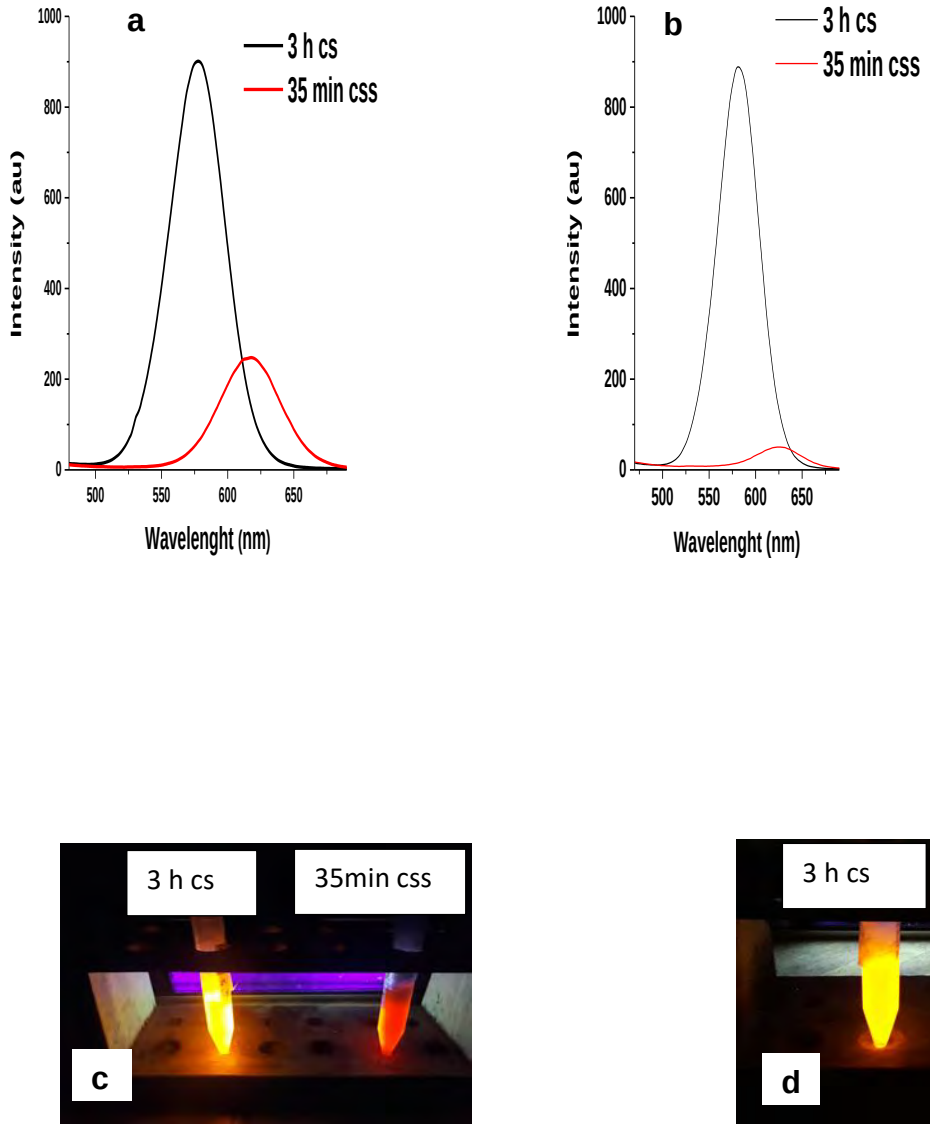


**Figure 19.** PL spectra of 3 h CdTe core-shell as compared to 35 min CdTe core-shell shell at 14 ml (a) and 21ml (b) stabilized by MPA and TGA. 'c' and 'd' represent corresponding emission colours under UV lamp for 14 ml and 21 ml injection of Zn and Se ions respectively Note: 'cs' represents core-shell while "css" represent core-shell-shell.

The differences in wavelength shifts can further be observed in images 19c and 19d where the CdTe multi-core-shell in image 19d showed a stronger red emission color compared to the multi-core-shell in image 19c.

### 4.4.2. PL spectra of M-T -CdTe multi-core-shell at injection intervals of 30 and 5 min.

The effect of time on the wavelength shifts of the multi core-shell was also investigated by injecting 1 ml of Zn and Se ion respectively at 30 min intervals (figure 20a) for over 210 min compared to the routine time intervals of 5 min discussed earlier. It was established that the wavelength shift corresponding to the 3h core-shell and the CdTe multi-core-shell in spectra of figure 20a remained the same (17 nm) as the wavelength shift for the CdTe multi core-shell in spectra of figure 20b.

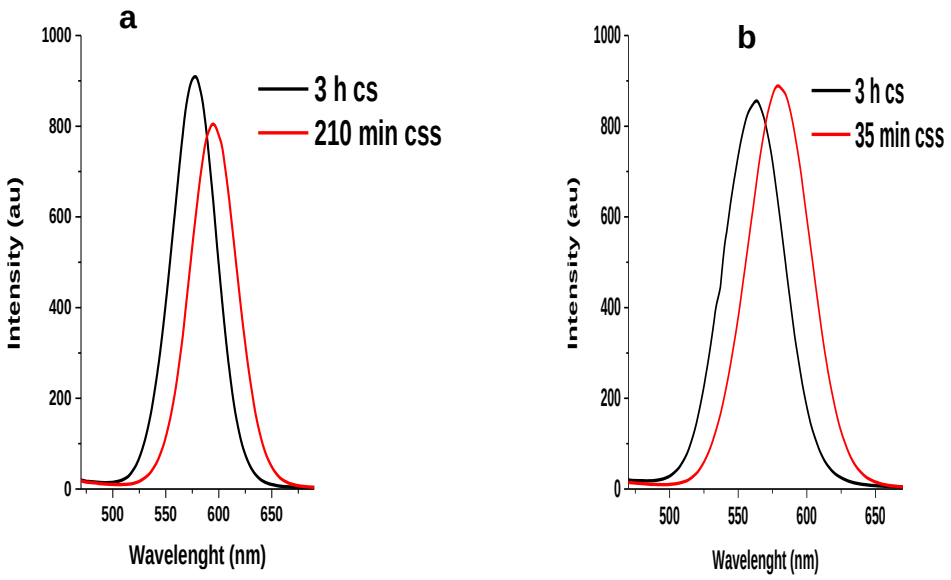

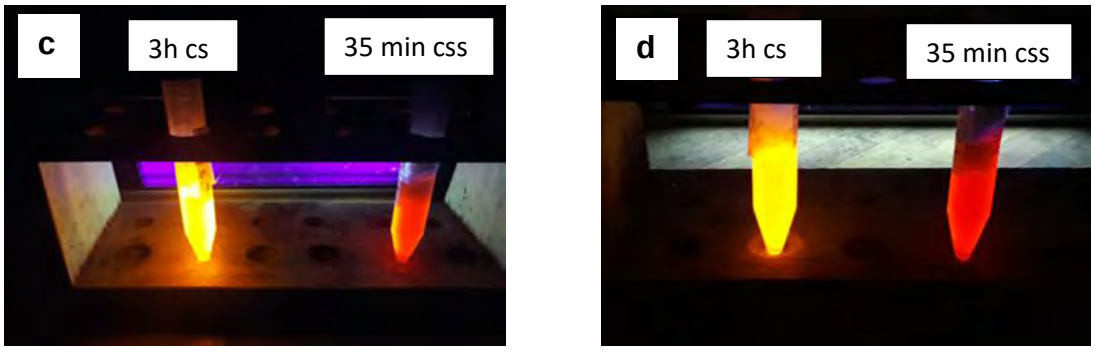


**Figure 20.** PL spectra of M-T -CdTe core-shell shell with injection of 7 ml of Zn and Se ions at 30 min (a) and 5 min interval (b). Note: cs and css represent core-shell and core-shell-shell.

This result indicates that even though the total reaction time for the fabrication of the multi core-shell in figure 20a is 210 min, the shift in wavelength at 3 h for CdTe core-shell and at 210 min for the CdTe core-shell shell remained the same as the shift at 3 hours for CdTe core-shell and the CdTe core-shell shell at 35 min as depicted in spectra of figure 20b. Thus, it can be concluded that the relative concentrations of Zn and Se ions played a larger role in shifting the wavelength of the QDs.

### 4.4.3. PL emission spectra of L-T and L-M dual caps compared to G-T and G-M at 7 ml injection of Zn and Se ions.

Following the same procedure used to synthesize M-T dual capped CdTe multi core-shell discussed earlier, the other four CdTe core-shells containing various thiol dual caps discussed in section 4.1.3 were also promoted to their corresponding multi-core-shells resulting in improved photo physical properties. However, it was observed that multi-core shells dual capped with L-M and L-T demonstrated similar fluorescent behaviors to M-T- CdTe core-shell-shell compared to G-T and G-M dual caps. The similarities of the fluorescence spectra for these three (M-T, L-T

and L-M duals caps) is mainly due to similarities of their corresponding wavelength shifts as a consequence of the formation of the ZnSe shell at the surface of CdTe/CdSe core-shell by addition of 7 ml of Zn and Se ions respectively, this behavior was absent for G-T and G-M dual caps. The corresponding spectra in figure 21 (a-d) illustrated this point by comparing the PL spectra of L-T and L-M-dual capped (figure 21a and 21c) to those for G-T and G-M dual capped (figure 21b and 21d). The lack of any wavelength shift in florescence wave-length of G-T and G-M dual cap can also be inferred from the calculated particle sizes in Table 4 compared to the particle size of M-T, L-T and L-M. The only change in G-M and G-T dual caps is a gradual enhancement of emission intensity during the formation of ZnSe shell indicating increment in surface passivation of the synthesized material

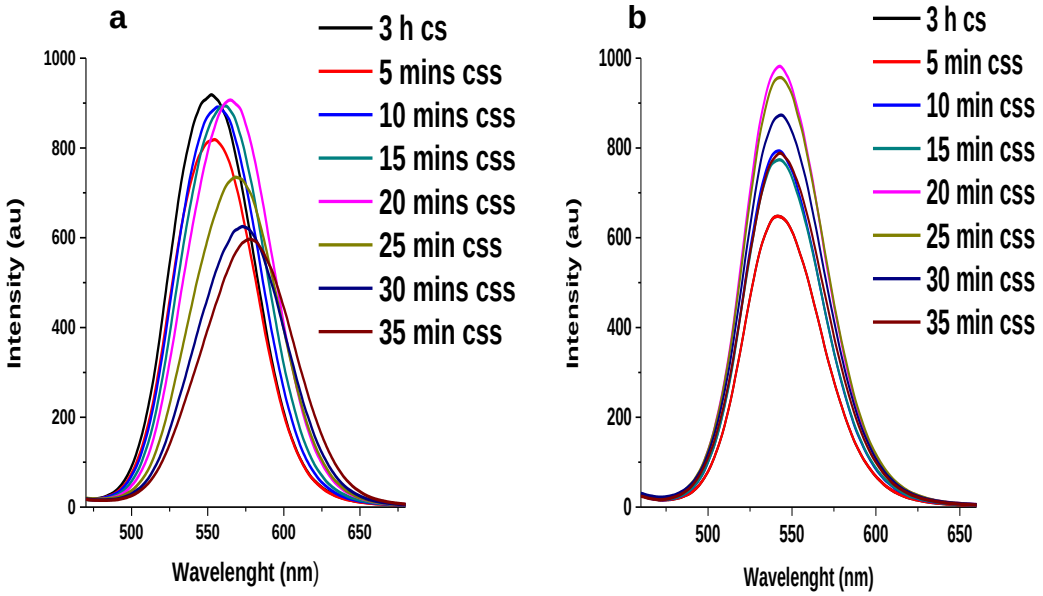

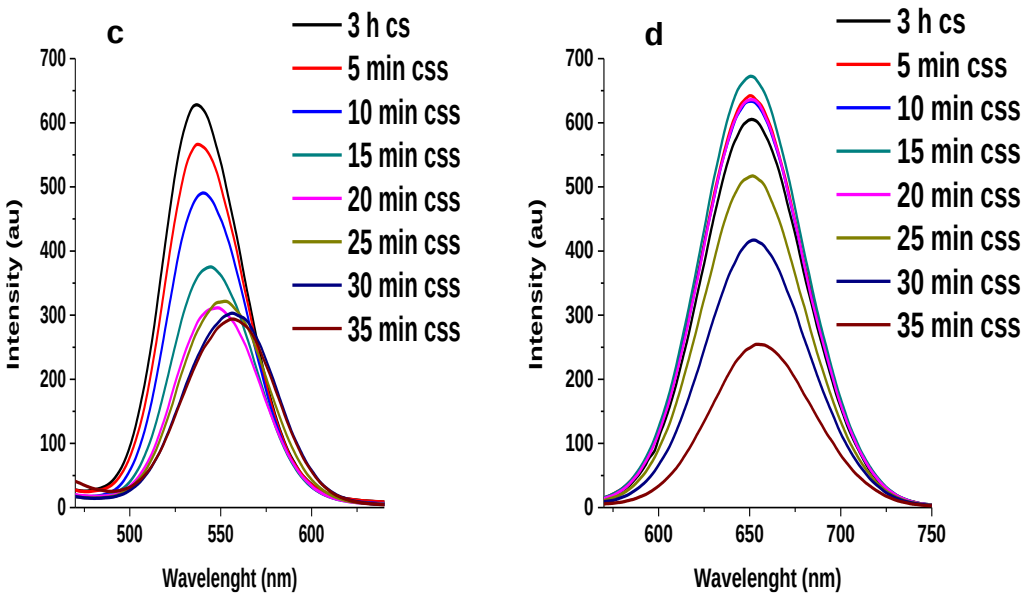


**Figure 21.** PL emission spectra of L-T (a) and L-M (c) dual caps compared to G-T (b) and G-M (d) using 7 ml of Zn and Se ions at 3 h cs – 35 min css. Note 'cs' means core-shell and 'css' means core-shell shell.

It is possible that, the presence of more capping groups (carboxylate and amino) in the structure of glutathione (GSH) might be responsible for the absence of shift in the emission wavelength of G-T and G-M dual cap following injection of 7 ml each of Zn and Se ions into the reacting mixture. The observation is further highlighted through figure 21b, that is, as the shell growth increases, the fluorescence intensity of G-T-CdTe css at 25 and 30 min seems to be higher than those of G-M-CdTe css at similar reaction times (figure 21d). Similar observation can be made with L-cysteine-TGA (figure 21a) compared to L-cysteine-MPA (figure 21c) at the same reaction times. These observations were also noticed during the course of the synthesis of their corresponding core-shells as previously discussed in figure 14. All these observations point towards the positive effects of using TGA as a dual stabilizing agent [3, 14, 17, 44- 45]. Moreover, when the reaction conditions for the two dual capped were changed to 14 and 21 ml

of Zn and Se ions respectively, some shift in emission wavelength was observed following 10 min of reaction time, this gradually increased as reaction approached 35 min (figure 22 a-d). It was further discovered from the study of the two dual caps that injection of 21 ml of Zn and Se ions gave the highest wavelength shift (13 nm for G-T and 30 nm for G-M) at 3 h for the core-shell and 35 min for the core-shell shell. Furthermore, the maxima for emission wavelengths at 35 min for both G-T and G-M dual caps can be found at 576 nm and 620 nm, respectively

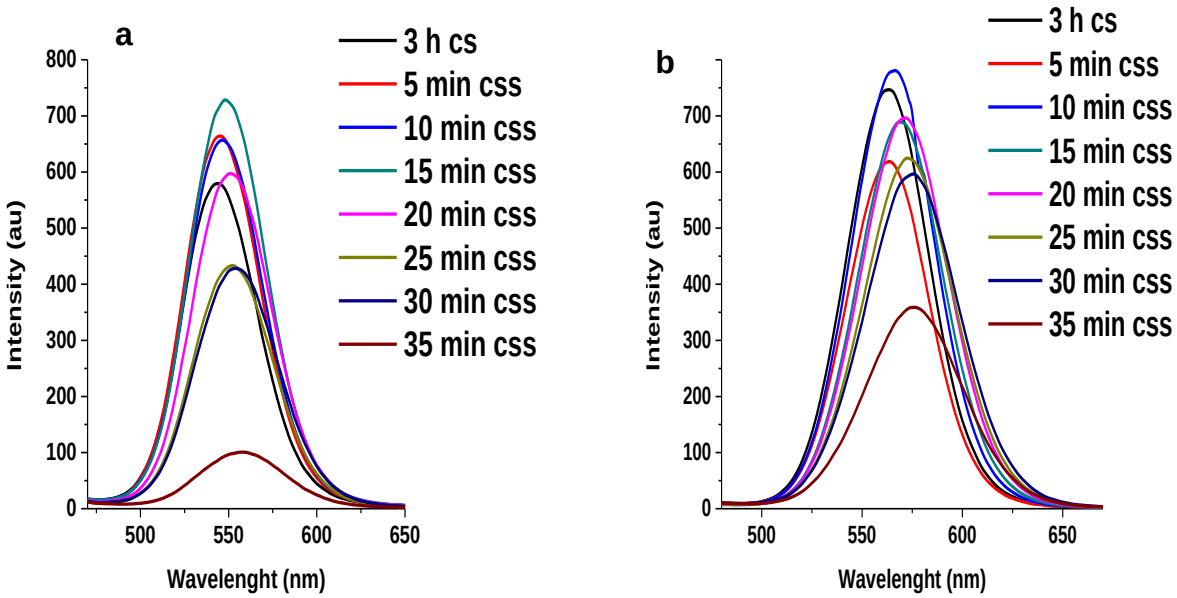

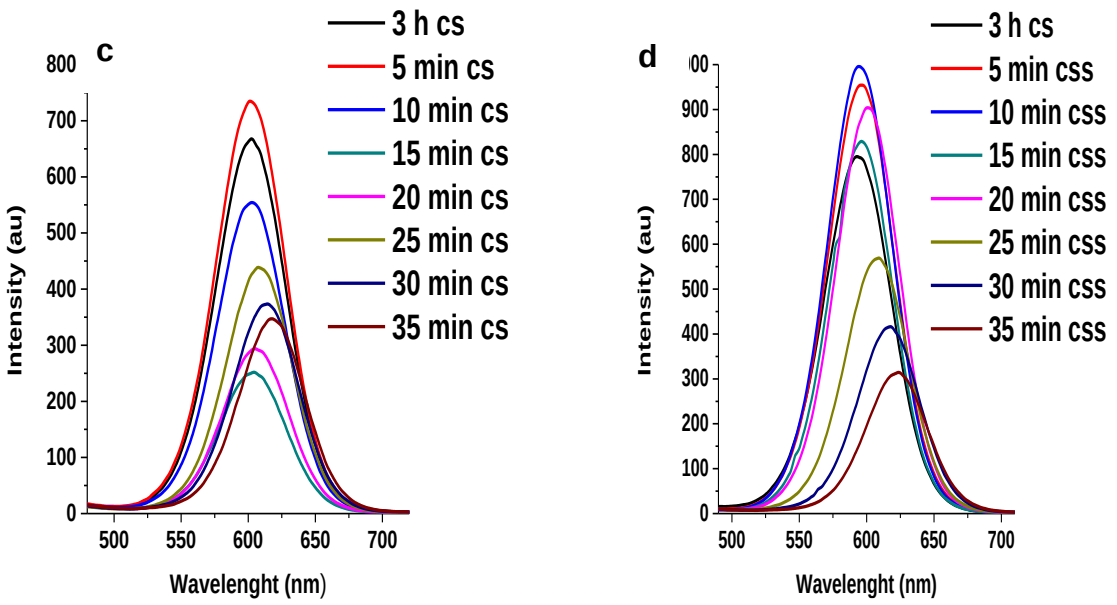


**Figure 22.** PL emission spectra of G-T (a and b) and G-M (c and d) dual capped CdTe css compared with 14 and 21 ml of Zn and Se ions at 3 h cs – 35 min css. Note 'cs' means core-shell and 'css' means core-shell shell.

In addition, in G-T dual capped PL spectra (14 ml) (figure 22a), the emission intensity increased slightly at 5 – 20 min for css compared to 3 h for cs. This indicates passivation provided by the ZnSe shell at the surface of CdTe/CdSe core-shell. Furthermore, the observed fluctuations in emission intensities observed for some reactions times may be a result of competition between stability and luminescence in aqueous media [2]. Nevertheless, the capping provided by most of the thiol stabilizing agents discussed here was significant with glutathione demonstrating enhanced capping functionality, this may be ascribed to the presence of more coordinating sites in its structure [2, 80].

The optimal reaction condition conducted for L-T and L-M dual capped using 21 ml of Zn and Se ion respectively is observed in figure 23 (a and b). The emission maxima at 35 min reaction time can be observed at 602 nm and 620 nm, respectively. These studies confirm that MPA-

TGA-CdTe css demonstrated the highest emission maxima of 625 nm at 35 min reaction time following the injection of 21 ml of Zn and Se ion, respectively.

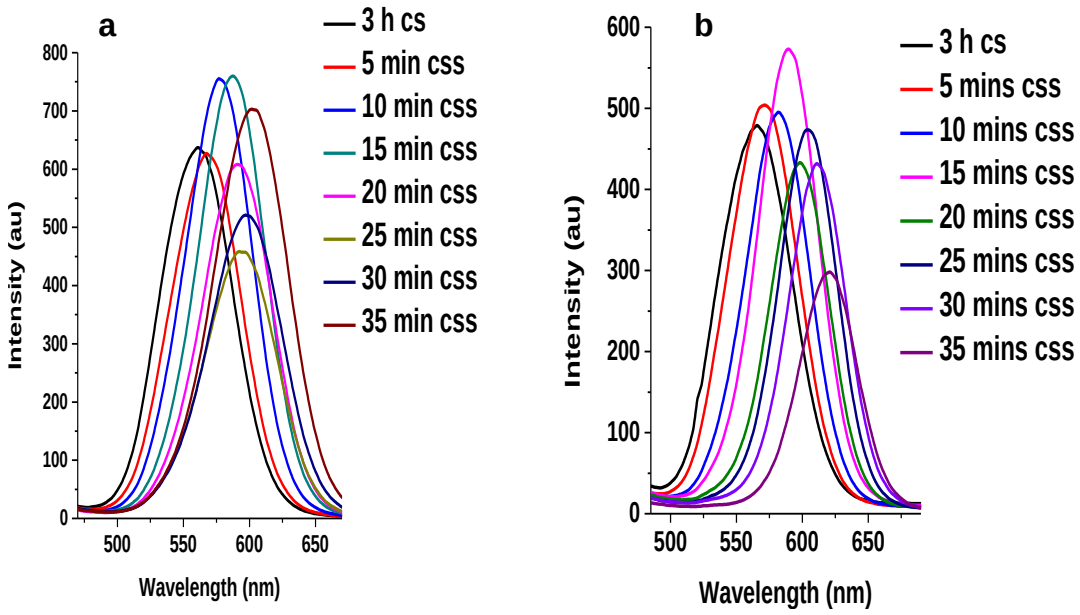


**Figure 23.** PL emission spectra of L-T (a) and L-M (b) dual capped CdTe css at 21 ml injection of Zn and Se ions at 3 h cs – 35 min css. Note 'cs' means core-shell and 'css' means core-shell shell.

**4.5. EDS analysis.**

The elemental composition of synthesized CdTe multi core-shell was further confirmed with the aid of electron disperse X-ray spectroscopy (EDS). The EDS result below confirm the presence of Zn and Se in M-T dual capped CdTe/CdSe/ZnSe multi core-shell.

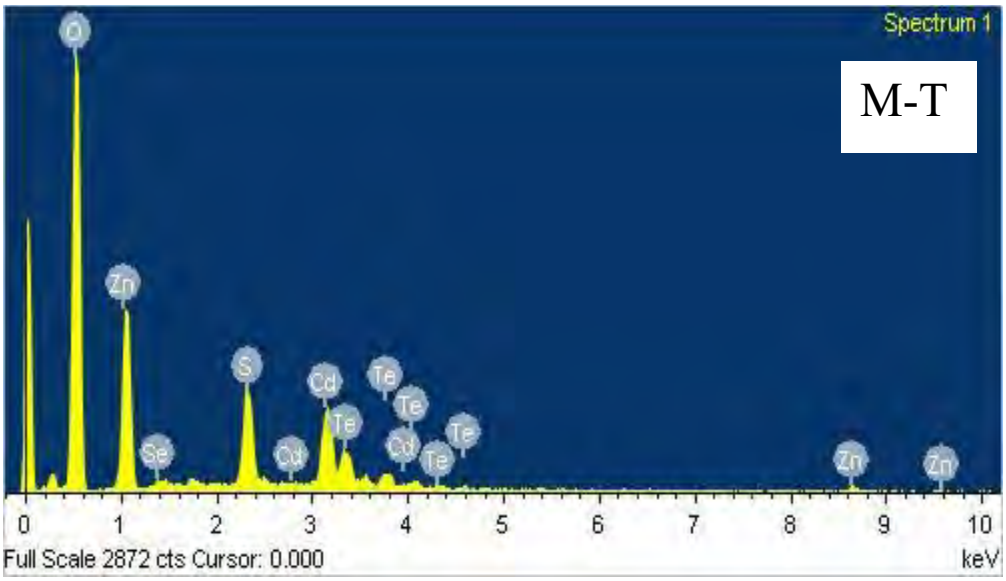


**Figure 24.** EDS analysis of M-T dual capped multi core-shell.

The presence of Zn and Se ions in the EDS spectrum of M-T dual caps double shell above indicates the likely presence of the ZnSe shell at the surface of CdTe/CdSe core-shell particles. Apart from these two elements, the presence of Cd and Te ions also signify the synthesis of CdTe cores which was passivated by CdSe shell. However, the signal observed for sulphur might be due to the large amount of stabilizing agent and reducing agents used during the preparation of Zn metal complex while the signal observed for oxygen may be due to the synthesis of the multi-core-shell under open air condition.

### 4.6. TEM Images of M-T-CdTe/CdSe/ZnSe core-shell-shell QDs.

The TEM morphology for M-T-CdTe core-shell-shell at 35 min reaction time (21 ml of Zn and Se ion injection) is represented in figure 25a. The formation of a spherical shape nanoparticle can be observed. This was also observed in the TEM image for their corresponding cores and core-shell displays in figure 16 (a and c). The average particle size from the TEM image is calculated to be 10.5 ± 3.16 which is bigger than those of the core-shell discussed earlier (figure 16 d). This reveals that each multi-core-shell particle is considerably bigger in size than its core-shell counterpart, this could be attributed to the formation of a thicker ZnSe shell at the surface of CdTe/CdSe core-shell. The injection of the top volume of 21 ml of Zn and Se ions might be a contributing factor for the larger particle size

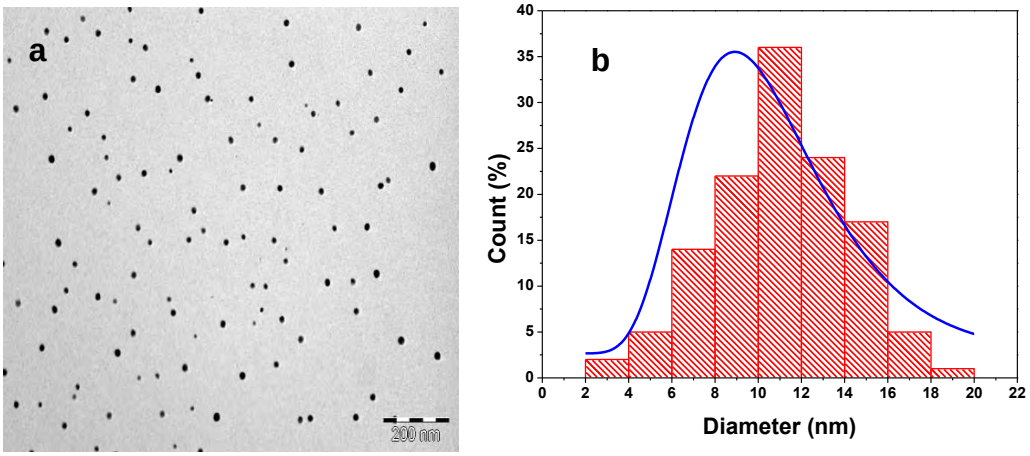


**Figure 25.** TEM image of -M-T-CdTe/CdSe/ZnSe multi-core-shell QDs (a) with its corresponding particle size distribution (b).

### 4.7. Exposure of M-T-CdTe/CdSe core-shell and multi-core-shell to UV illumination

Figure 26 illustrates the photostability investigation of CdTe/CdSe core-shell QDs at 3 h reaction time and CdTe/CdSe/ZnSe multi-core-shell at 35 min reaction time under continuous exposure to UV radiation for 18 h. It is clear that as the illumination time increases, the two QDs demonstrate enhancement in fluorescence with the core-shell having the highest fluorescence intensity at PLQY of 89 % corresponding to 6 h illumination time, while the multi-core-shell demonstrates its highest fluorescence intensity at PLQY of 23 % corresponding to 1.5 h illumination time. Therefore, the PLQY for the core-shell increased by 16 % from the initial values of 73 % while the multi-core-shell increased by 7% from the initial values of 16 %. Similar results that have been reported in some literature on the effects of UV light on QDs which reveals that the increase in fluorescence intensity could be due to photoetching effects and surface re-combination processes during exposure of UV radiation to QD surfaces [81- 83]. A similar study was also reported by Hosnedlova *et al* in 2020 during their study of physico-chemical changes of CdTe QDs following their exposure to environmental conditions [84]. Furthermore, it is observed that as the illumination time increases, the two QDs show some florescence quenching which leads to a significant decrease in their corresponding PLQY values.

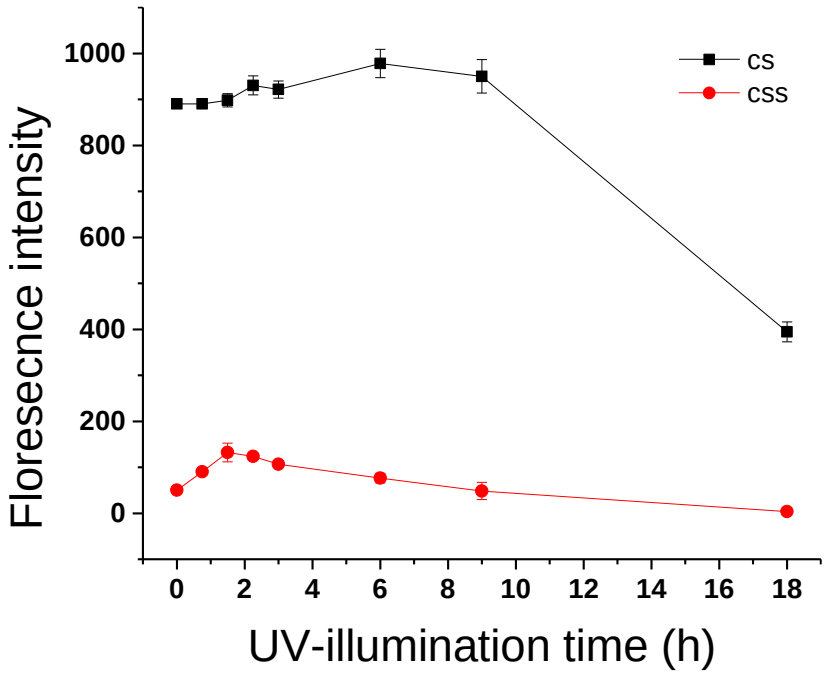


**Figure 26:** M-T-CdTe/CdSe core-shell (3 h) and CdTe/CdSe/ZnSe core-shell-shell (35 min) exposed to continuous UV irradiation for 18 h.

Gradual decreases in fluorescence for the multi-core-shell was observed from 2.25 h illumination time which proceeded to deteriorate drastically up to 18 h of exposure time to UV irradiation. The sharp decline in florescence of CdTe/CdSe core-shell was also observed from 9 h till 18 h of illumination time. As reported from previous studies, prolonged exposure of QDs to UV irradiation causes the release of metal atoms from the surface due to oxidation process. This observation was reported by Derfus *et al* during the exposure of CdSe QDs to UV radiation [85]. It was further explained by Hosnedlova *et al* that during this oxidation process, the $O_2$ molecules oxidize chalcogenide atoms located on the surface of the QDs to form oxides [84]. These oxide molecules desorb from the surface, leaving behind "dangling" reduced metallic atoms. Hence, in our case prolonged exposure of these QDs to an oxidative environment might have led to the

decomposition of their structure, thereby leading to desorption of $Cd^{2+}$ ions or $Zn^{2+}$ from the CdTe/CdSe or CdTe/CdSe/ZnSe complexes. Furthermore, we also assumed that the slight percentage increase in the PLQY of CdTe multi-core-shell QDs compared to its core-shell might be due to an increase in surface passivation provided by ZnSe shell on the surface of CdSe shell. However, the quick loss in fluorescence of the multi core-shell QDs upon further exposure to UV illumination might be due to a large lattice mismatch between the interface of CdSe and ZnSe shell. However, further studies are being contemplated to verify the role of some of these factors.

**4.8. Florescence spectra of MPA-TGA, GSH-MPA, GSH-TGA, L-Cysteine-MPA, L-Cysteine-TGA dual capped CdTe/CdSe core-shell QDs at various mole ratios of Te/ Se (1:0.2- 1:1).**

The florescence spectra below represent the optimization of the reaction condition of five different thiol dual cap-CdTe/CdSe core-shell QDs at various amounts of $Se^{2-}$ to $Te^{2-}$ present in the solution. These graphs can serve as points of reference for the explanations of the photophysical investigation of CdTe core shells in this chapter.

**M-T**

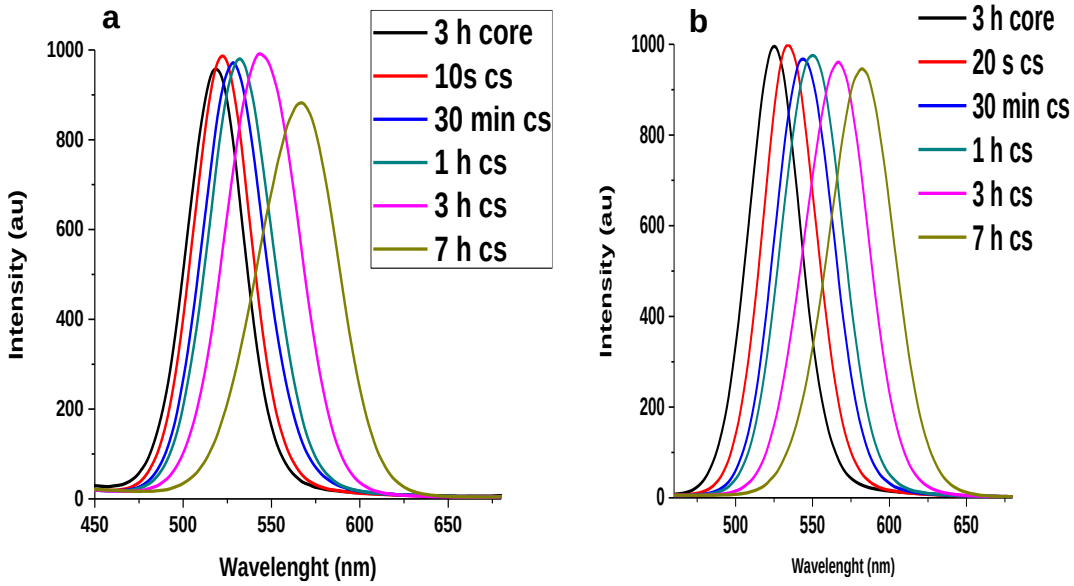

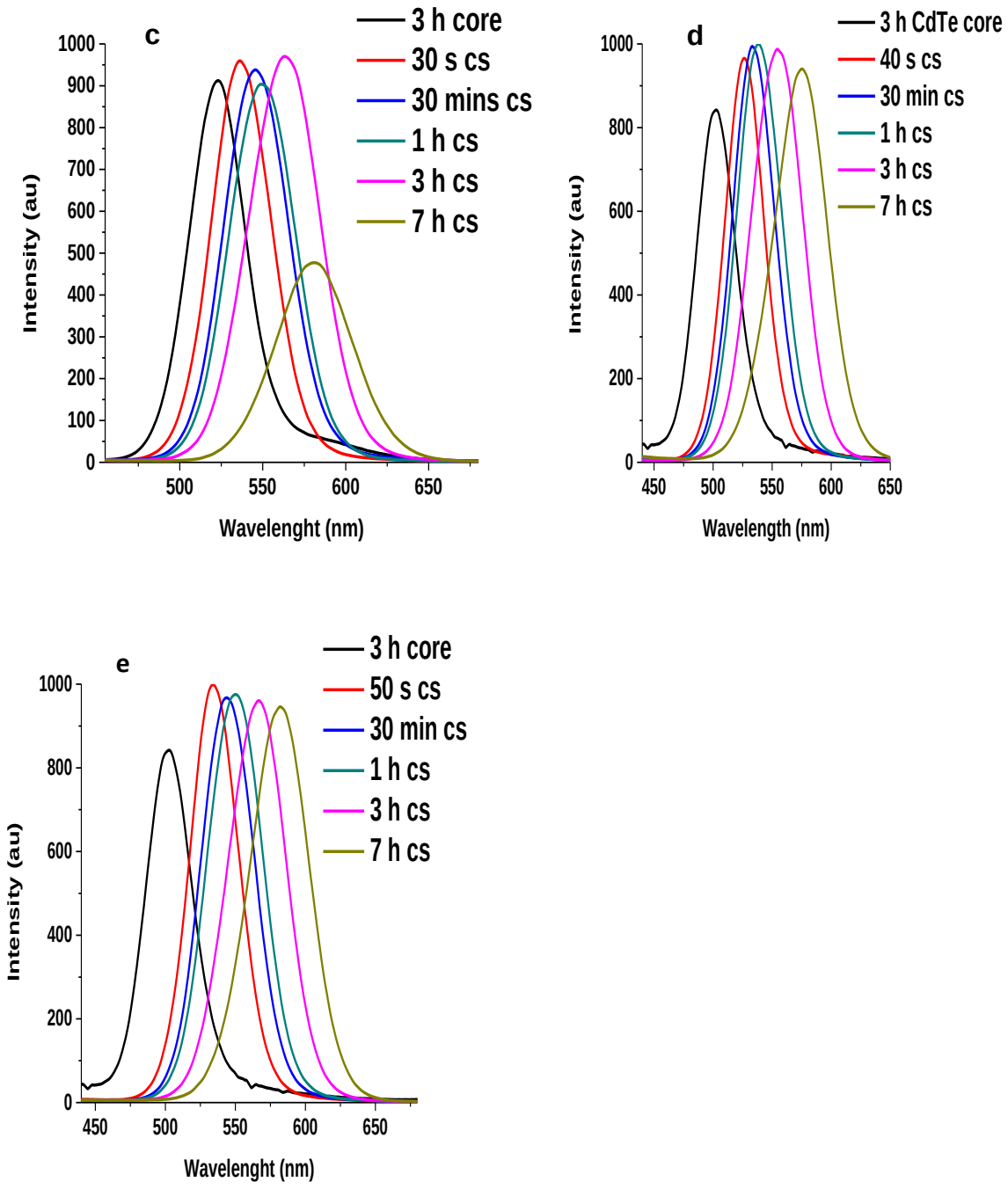


Figure 27. Emission spectra of M-T-CdTe/CdSe core shells at various mole ratios of Te/Se: a (1:0.2), b (1:0.4), c (1:0.6), d (1:0.8) and e (1:1). Note: cs represent core–shell

**G-M**

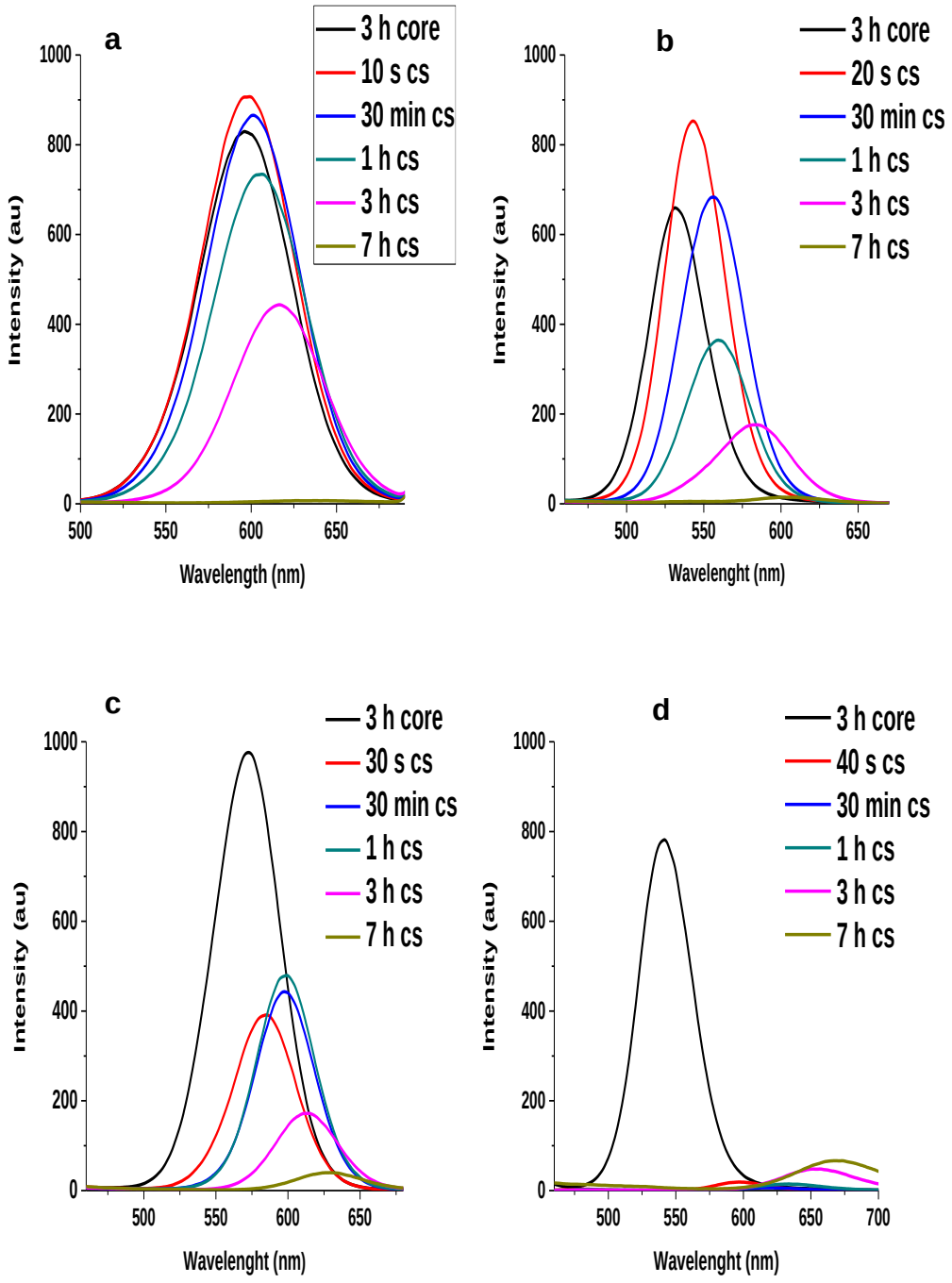
a
3 h core
10 s cs
30 min cs
1 h cs
3 h cs
7 h cs
Intensity (au)
Wavelength (nm)
b
3 h core
20 s cs
30 min cs
1 h cs
3 h cs
7 h cs
Intensity (au)
Wavelenght (nm)
c
3 h core
30 s cs
30 min cs
1 h cs
3 h cs
7 h cs
Intensity (au)
Wavelenght (nm)
d
3 h core
40 s cs
30 min cs
1 h cs
3 h cs
7 h cs
Intensity (au)
Wavelenght (nm)

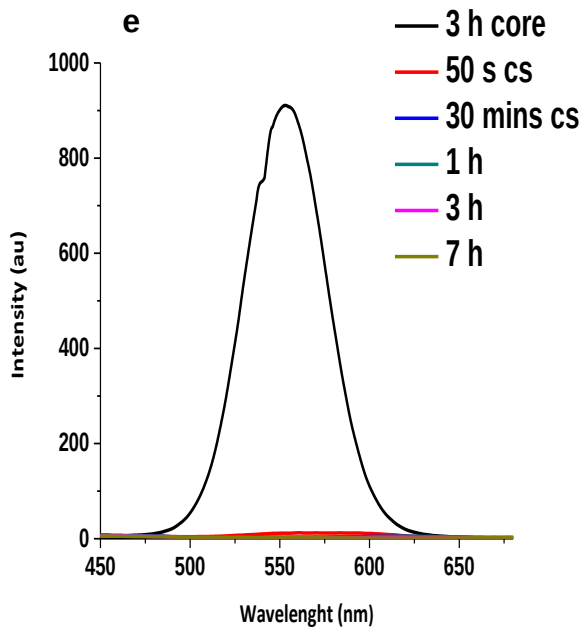


Figure 28. Emission spectra of G-M-CdTe/CdSe core shells at various mole ratios of Te/Se: a (1:0.2), b (1:0.4), c (1:0.6), d (1:0.8) and e (1:1). Note: cs represent core–shell.

**G-T**

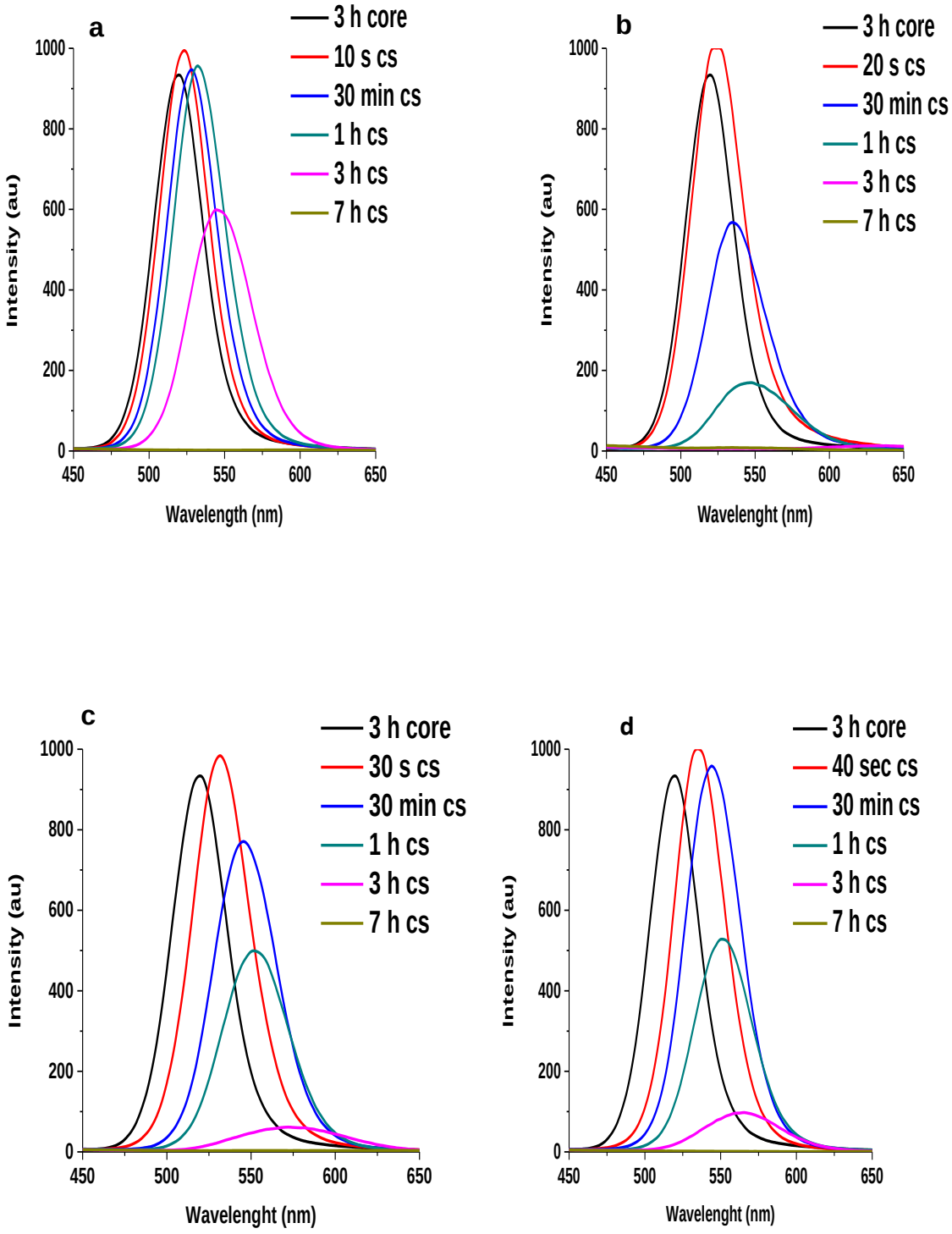
a
3 h core
10 s cs
30 min cs
1 h cs
3 h cs
7 h cs
Intensity (au)
Wavelength (nm)
b
3 h core
20 s cs
30 min cs
1 h cs
3 h cs
7 h cs
Intensity (au)
Wavelenght (nm)
c
3 h core
30 s cs
30 min cs
1 h cs
3 h cs
7 h cs
Intensity (au)
Wavelenght (nm)
d
3 h core
40 sec cs
30 min cs
1 h cs
3 h cs
7 h cs
Intensity (au)
Wavelenght (nm)

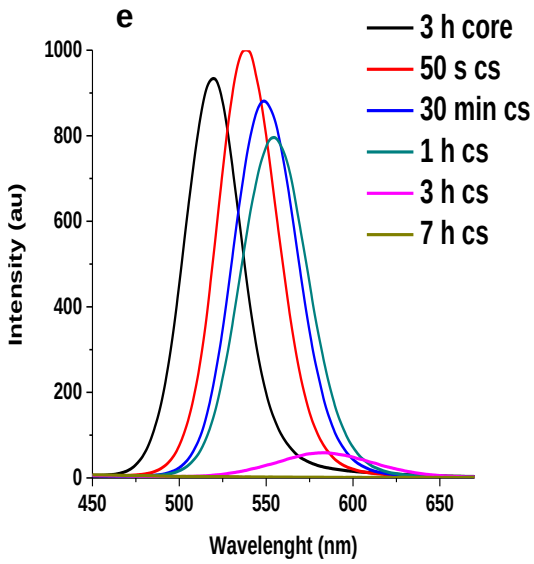


Figure 29. Emission spectra of G-T-CdTe/CdSe core shells at various mole ratios of Te/Se: a (1:0.2), b (1:0.4), c (1:0.6), d (1:0.8) and e (1:1). Note: cs represent core–shell.

**L-T**

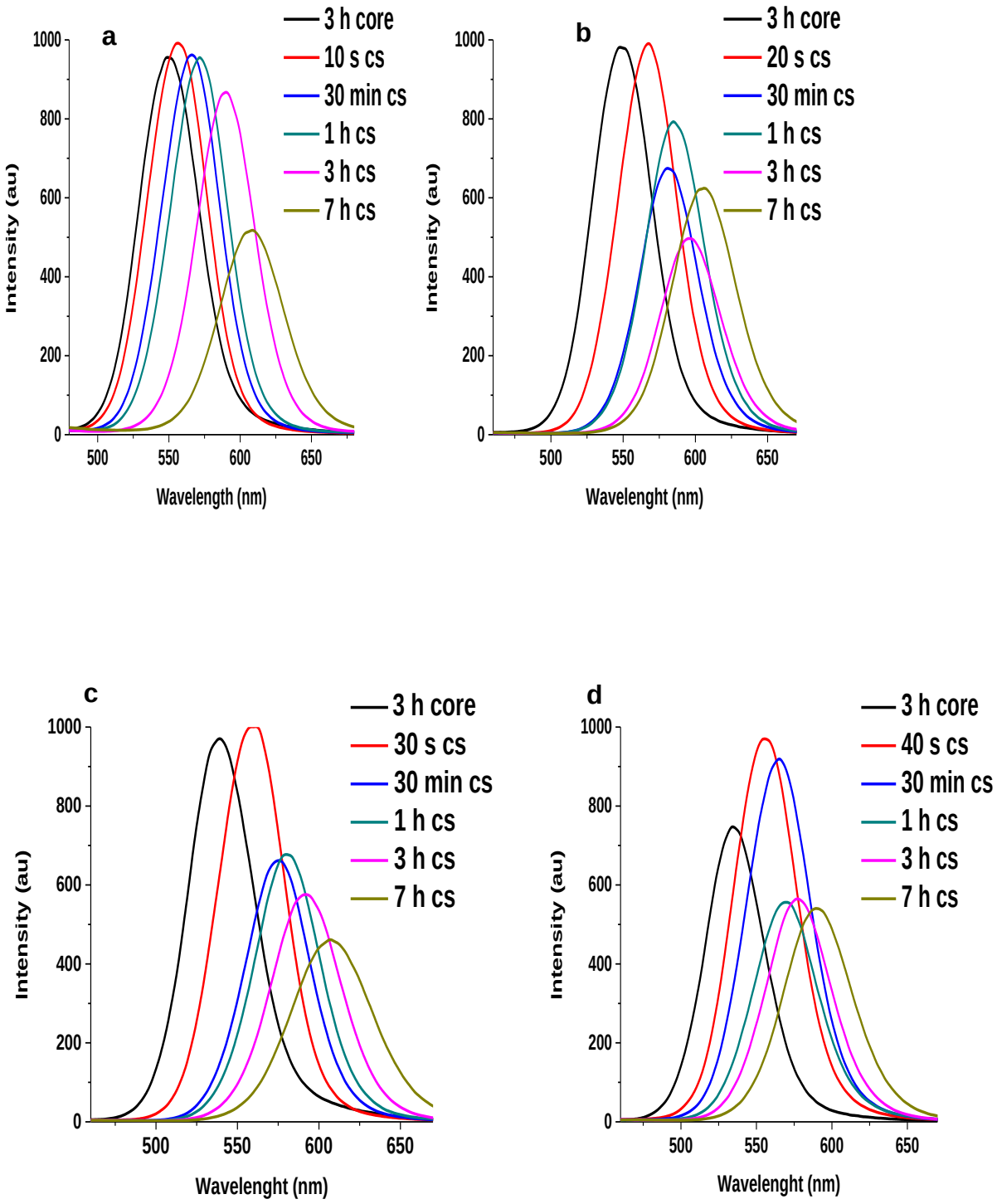
a
3 h core
10 s cs
30 min cs
1 h cs
3 h cs
7 h cs
Intensity (au)
Wavelength (nm)
b
3 h core
20 s cs
30 min cs
1 h cs
3 h cs
7 h cs
Intensity (au)
Wavelenght (nm)
c
3 h core
30 s cs
30 min cs
1 h cs
3 h cs
7 h cs
Intensity (au)
Wavelenght (nm)
d
3 h core
40 s cs
30 min cs
1 h cs
3 h cs
7 h cs
Intensity (au)
Wavelenght (nm)

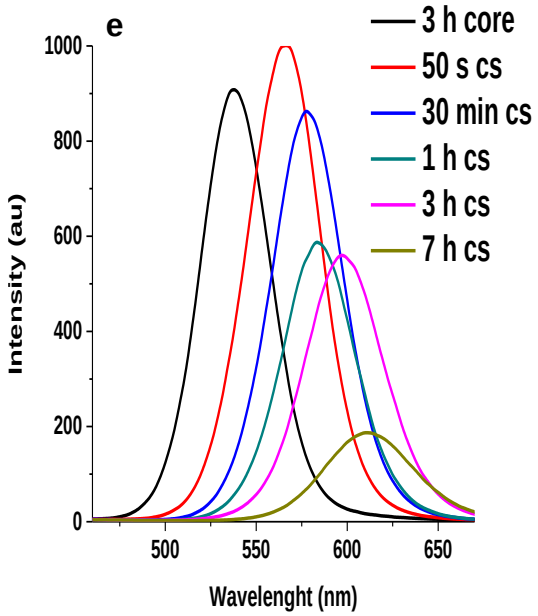


Figure 30: Emission spectra of L-T-CdTe/CdSe core shells at various mole ratios of Te/Se: a (1:0.2), b (1:0.4), c (1:0.6), d (1:0.8) and e (1:1). Note: cs represent core–shell.

**L-M**

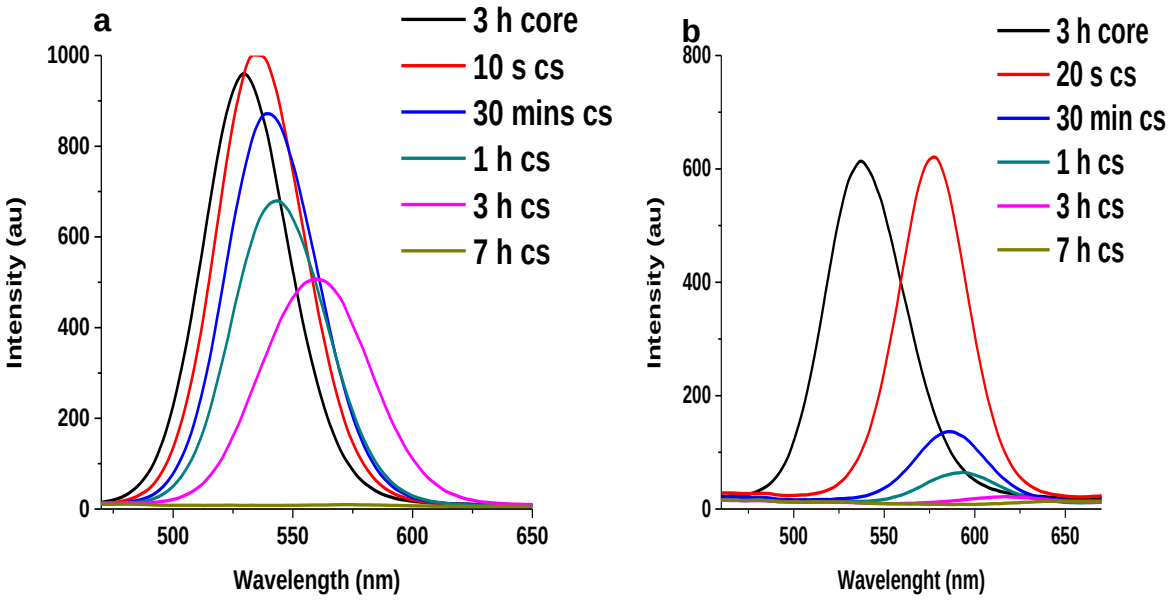
a
3 h core
10 s cs
30 mins cs
1 h cs
3 h cs
7 h cs
Intensity (au)
Wavelength (nm)
b
3 h core
20 s cs
30 min cs
1 h cs
3 h cs
7 h cs
Intensity (au)
Wavelenght (nm)

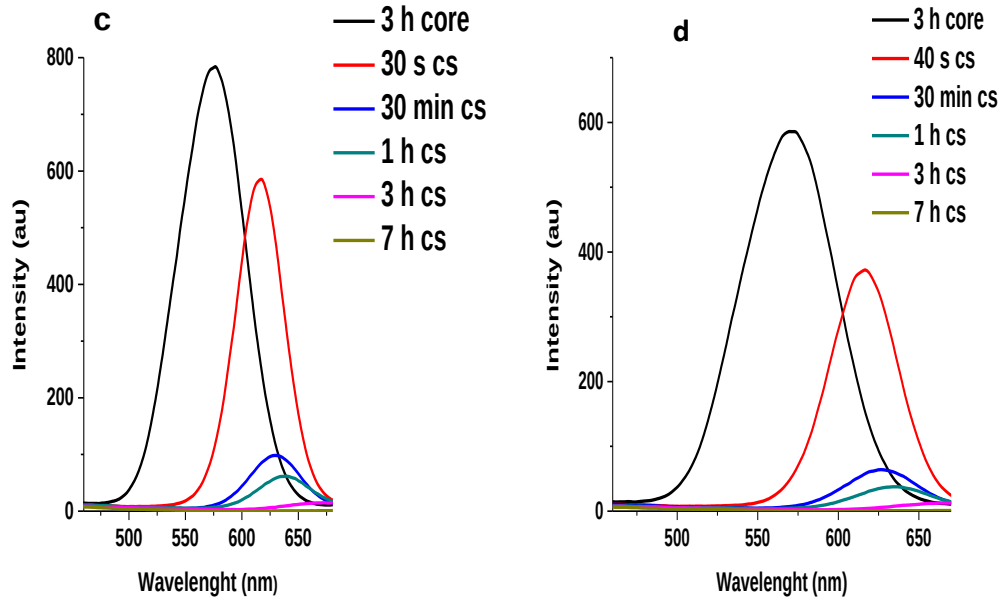
c
3 h core
30 s cs
30 min cs
1 h cs
3 h cs
7 h cs
Intensity (au)
Wavelenght (nm)
d
3 h core
40 s cs
30 min cs
1 h cs
3 h cs
7 h cs
Intensity (au)
Wavelenght (nm)

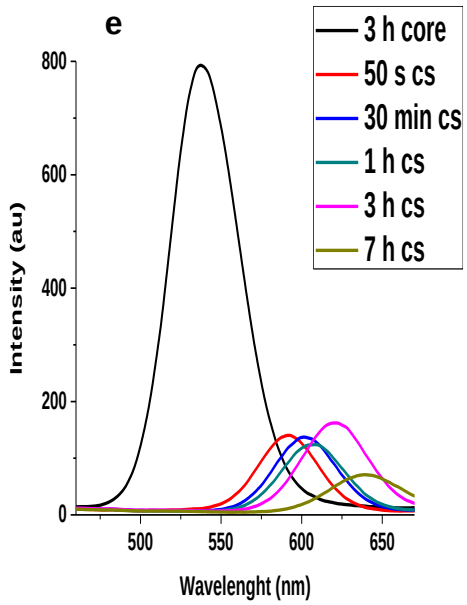


Figure 31: Emission spectra of L-M-CdTe/CdSe core shells at various mole ratios of Te/Se: a (1:0.2), b (1:0.4), c (1:0.6), d (1:0.8) and e (1:1). Note: cs represent core–shell.

# CHAPTER 5.

In this chapter, the encapsulation of CdTe/CdSe/ZnSe multi-core-shell QDs or core-shell-shell QDs in liposomes and chitosan nanoparticles are discussed. However, it should be pointed out that discussions on the rapid synthesis of CdTe multi-core-shell QDs demonstrated the highest emission maxima of around 625 nm (35 min) which correspond to MPA-TGA (M-T) dual cap-CdTe multi-core-shell QDs. Because of particle aggregation during the encapsulation of QDs in liposomes and chitosan nanoparticles leading to loss of some florescence intensities, the encapsulation of the QDs in these bio-compatible environments was conducted using the QDs with the highest florescence intensity at 5 min reaction time. The preparation of the nanocomposites, characterization techniques and the corresponding loading efficiency of the QDs loaded in liposome vesicles (LVs) and CNP were all discussed previously in chapter two. We should also recall that due to the optimization of reaction conditions, the embedding of MPA-TGA-dual capped -CdTe multi-core-shell QDs in liposomes and CNP led to the generation of 14 and 12 different formulations, respectively corresponding to different reaction conditions. Therefore, in this chapter we discuss the florescence properties, morphology and physicochemical characterization of MPA-TGA-CdTe/CdSe/ZnSe multi-core-shell QDs loaded in liposomes and CNP.

## 5. Optical property, morphology and physio-chemical characterization of MPA-TGA-CdTe multi core-shell QDs loaded in liposome and CNP.

### 5.1. PL spectra of QDs and QDs loaded in liposomes (F1- F9).

The PL spectra in figure 32 shows the florescence properties of the interaction between multi-core-shell QDs and phospholipids at various formulations in accordance with Table 4 presented in chapter two. During the encapsulation of the QDs in liposomes, it is observed according to figure 32 that the florescence intensity of the QD-LVs quenches and is accompanied by a significant red shift in wavelength. The reduction in florescence intensity can be attributed to the transfer of energy from the surface of florescent QD to the surface of non-florescent phospholipids while the red-shift in wavelength might be due to the coating of the surface of the QDs with phospholipids. Similar observations were reported by Ye *et al* in 2013 during the encapsulation of CdTe QDs in liposomes for infra-red in-vivo imaging of mouse tissue. Chu and colleagues in 2010 also reported a similar observation during the loading of CdTe QDs in liposomes for sentinel lymph node mapping and Wang *et al* in 2011 reported the same observation during the cellular imaging of CdTe QDs loaded in liposome and intra-cellular study of the nanocomposite with three different cell lines [54-56]. It was explained by Chu and co-workers that the encapsulation of QDs in liposomes might be due to particles aggregation as a result of the fact that the interaction of QDs with LVs occurred in lesser alkaline media [55]. It is further observed that the interaction between QDs and phospholipids (100 mg) in F4 and F6 are slightly higher and similar than the other formulations in-terms of their florescence intensities. This result further illustrates that the stirring of QDs and lipids at these formulation (100 mg) for 15 and 45 min show better interaction compared to 30 min.

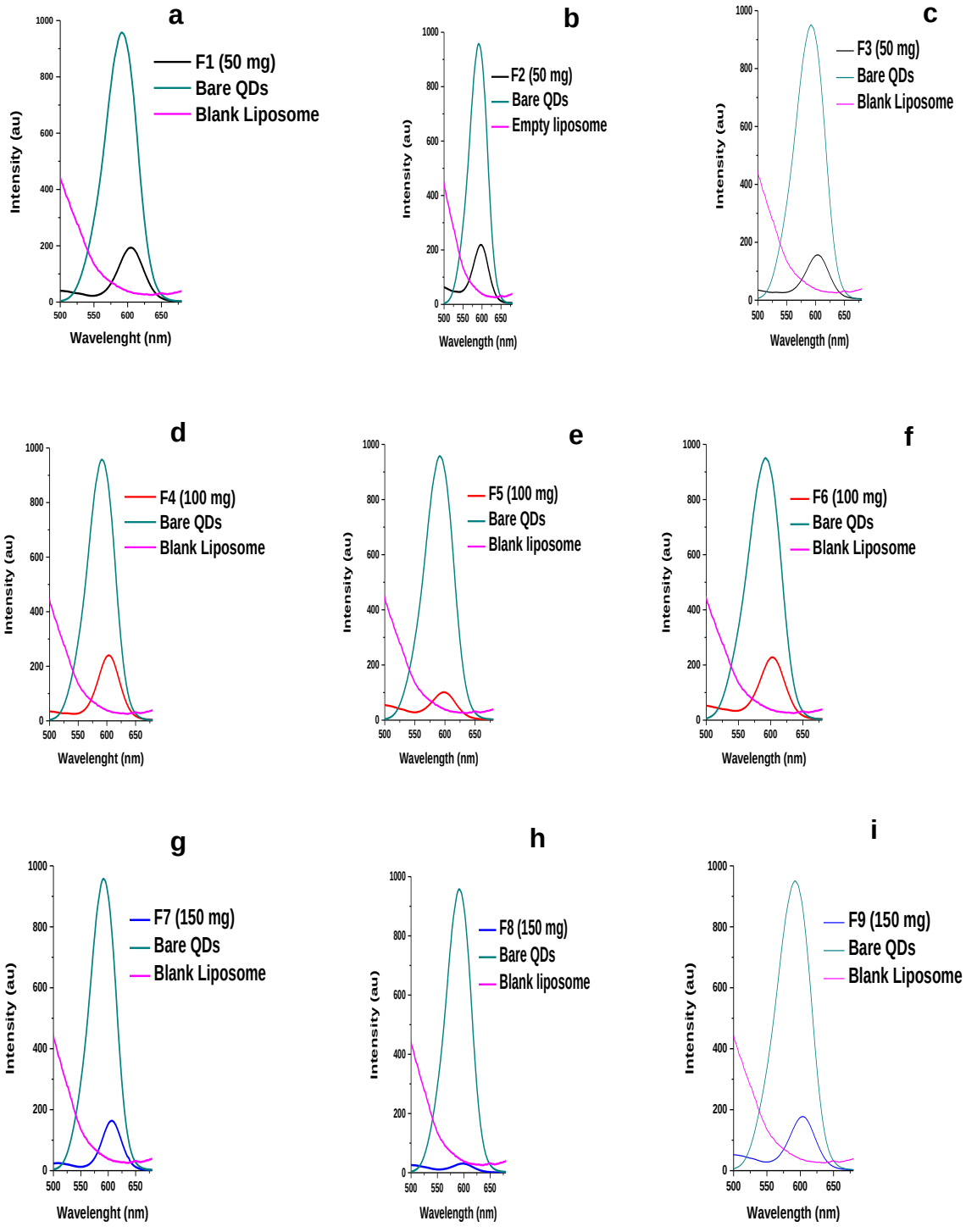
a
F1 (50 mg)
Bare QDs
Blank Liposome
Intensity (au)
Wavelenght (nm)
b
F2 (50 mg)
Bare QDs
Empty liposome
Intensity (au)
Wavelength (nm)
c
F3 (50 mg)
Bare QDs
Blank Liposome
Intensity (au)
Wavelength (nm)
d
F4 (100 mg)
Bare QDs
Blank Liposome
Intensity (au)
Wavelenght (nm)
e
F5 (100 mg)
Bare QDs
Blank liposome
Intensity (au)
Wavelength (nm)
f
F6 (100 mg)
Bare QDs
Blank Liposome
Intensity (au)
Wavelength (nm)
g
F7 (150 mg)
Bare QDs
Blank Liposome
Intensity (au)
Wavelenght (nm)
h
F8 (150 mg)
Bare QDs
Blank liposome
Intensity (au)
Wavelength (nm)
i
F9 (150 mg)
Bare QDs
Blank Liposome
Intensity (au)
Wavelength (nm)

j k

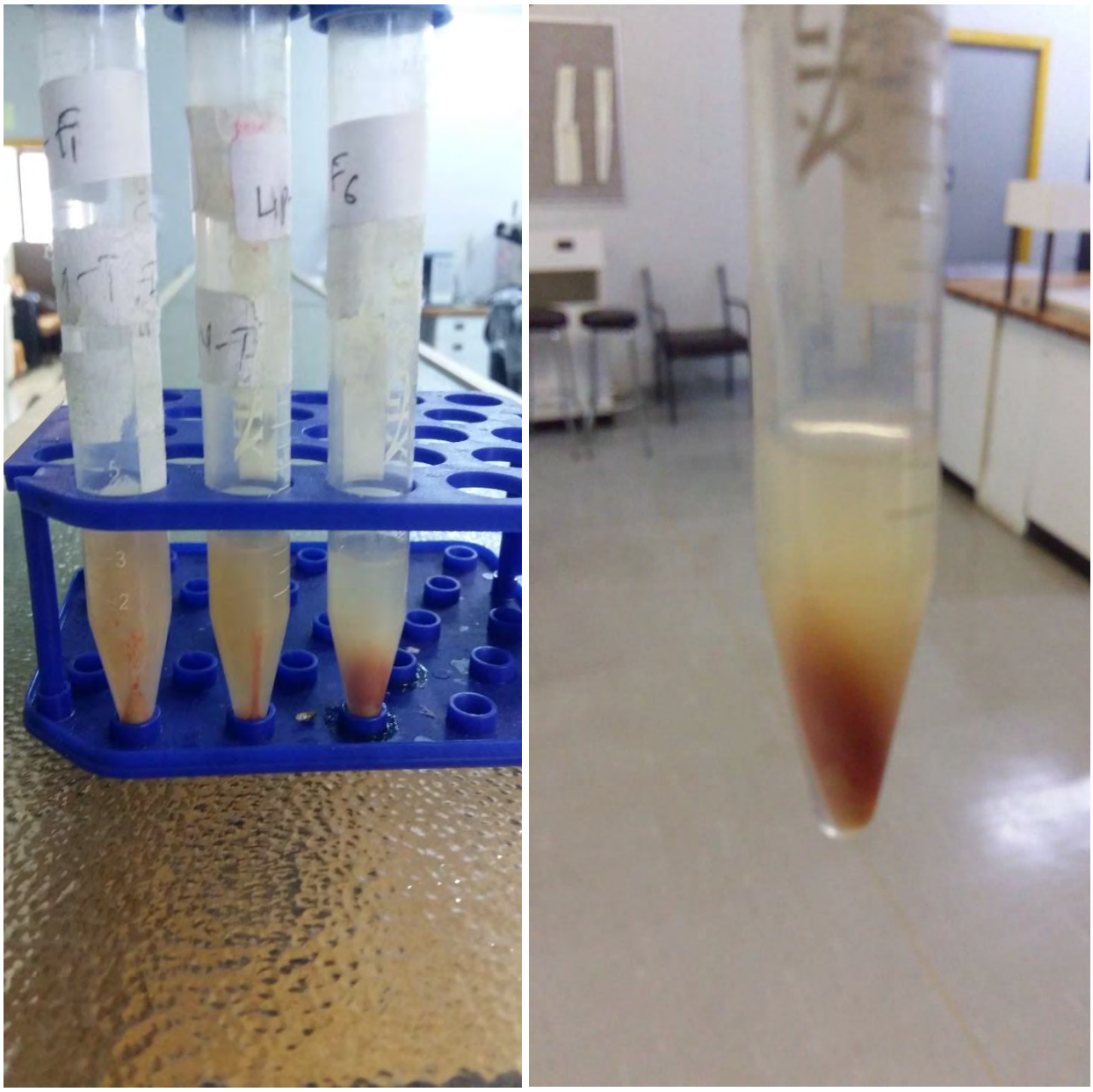


**Figure 32:** PL spectra of bare QDs, blank liposome and QD-LVs (F1- F9, a- i) at various amount of lecithin (50 mg, 100 mg and 150 mg) for various stirring time of 15 min, 30 min and 45 min. Images of QD-LVs under normal light (j and k).

We speculate the reason for stronger interaction to be due to a balanced equilibrium reaction which might have led to a formation of stronger co-ordination bonds between free $Zn^{2+}$ radical ions present at the surface of the QDs and the P=O group present in the hydrophilic headgroup of

the soya bean lecithin [56]. Although this observation will still be subjected to further investigation. After replicating the experiments for all the nine formulations discussed in figure 32 (a- i), it was observed that F6 demonstrated the highest loading content (22.7 ± 1.53) compared to the other remaining formulations (Table 9).

**Table 9: Loading efficiency of QD-LVs (F1- F9) and their zeta potential value.**

| **Formulations** | **Lecithin (mg)** | **Vol of QDs (ml) (4.2 mg/ml)** | **Stirring time (min)** | **Zeta potential (mV) (mean ± S.D)** | **Loading efficiency (%) (mean ± S.D)** |
|---|---|---|---|---|---|
| F1 | 50 | 3 | 15 | -59.2 ± 2.76 | 18.8 ± 4.64 |
| F2 | 50 | 3 | 30 | -58.9 ± 2.16 | 16.3 ± 5.16 |
| F3 | 50 | 3 | 45 | -71.2 ± 2.35 | 17.0 ± 2.41 |
| F4 | 100 | 3 | 15 | -49.7 ± 1.22 | 18.8 ± 4.73 |
| F5 | 100 | 3 | 30 | -35.2 ± 2.02 | 15.2 ± 3.30 |
| F6 | 100 | 3 | 45 | -52.2 ± 1.17 | 22.7 ± 1.53 |
| F7 | 150 | 3 | 15 | -13.8 ± 0.75 | 15.5 ± 1.62 |
| F8 | 150 | 3 | 30 | -28.1 ± 0.55 | 10.6 ± 5.3 |
| F9 | 150 | 3 | 45 | -34.1 ± 1.37 | 18.5 ± 0.69 |

| | | | | | |
|---|---|---|---|---|---|
| Bare liposome | 100 | | 45 | -47.8 ± 1.70 | - |
| Bare QDs | - | 3 | - | -38.5 ± 5.35 | - |

Figure 32 (j and k) show the image of QDs-LVs after centrifuging for 90 min at 4500 rpm. It is seen that the QDs settle down to the bottom of the centrifuging tube together with the liposomes indicating likely encapsulation of QDs in liposomes. To further increase the loading content of corresponding nanocomposite, we decided to interact the QDs at various volumes (1.5, 6, 9, 12 and 15 ml) with 100 mg of lecithin at stirring time of 45 min which is the actual reaction conditions for F6. This experiment led to the generation of four more formulations (F10- F14) as depicted in the PL spectra of figure 33 (a- e). This shows the interaction of QDs at different volumes with 100 mg of soya bean lecithin at 45 min stirring time.

### 5.1.2. PL spectra of QD and QD-LV (F10- F14) using various volumes of QDs.

Figure 33 (a - e) represent further interaction between different volumes of multi-core-shell QDs and 100 mg of soya bean lecithin at stirring time of 45 min. A significant quench in florescence intensity is accompanied by red-shift in wavelength, this is similar to what was observed in formulation F1 – F9 discussed in figure 32.

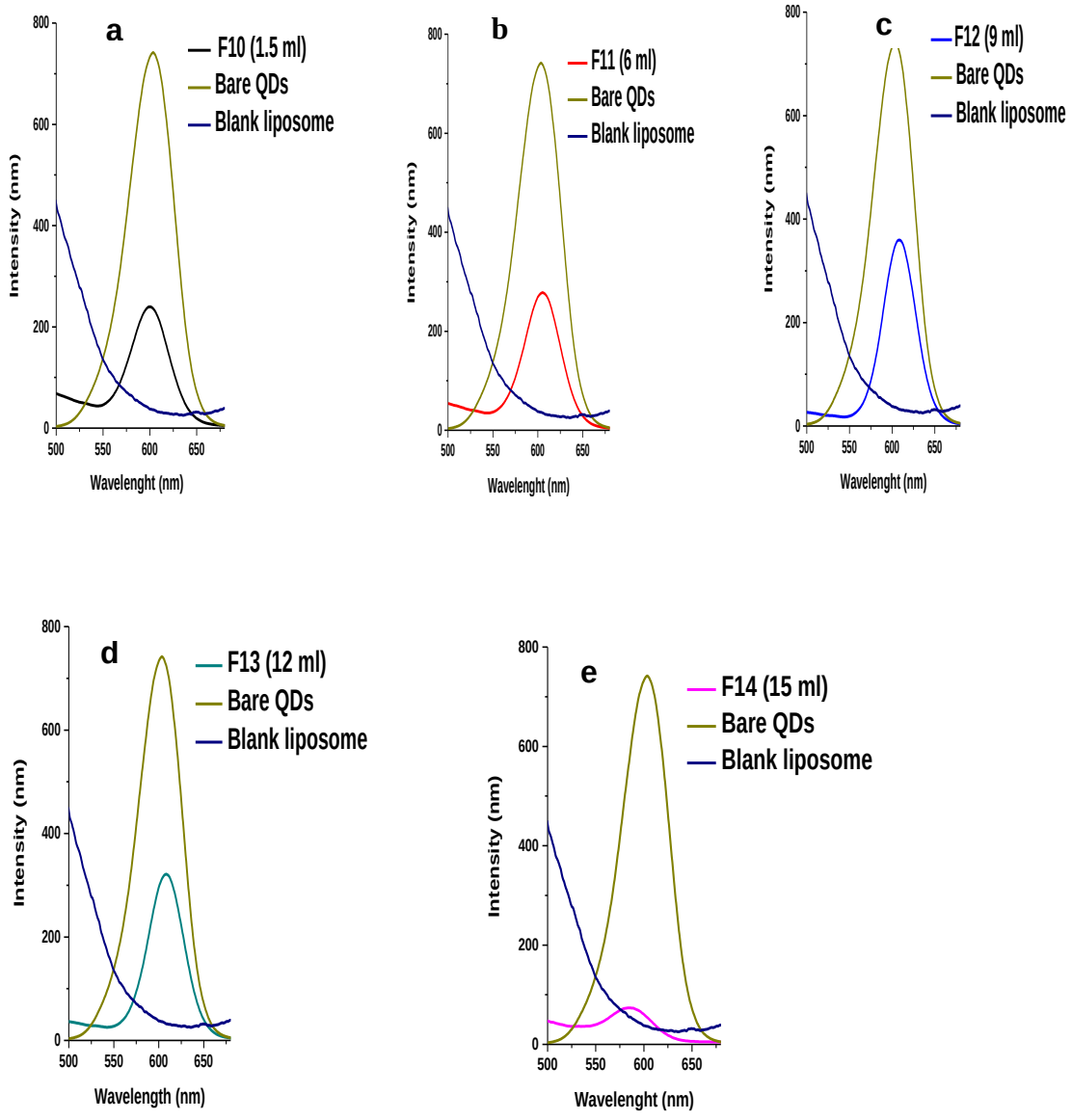


**Figure 33:** PL spectra of bare QDs, blank liposome and QD-LVs (F10- F15, a- e) at 100 mg of lecithin and stirring time of 45 min.

It is observed that as the volume of QDs increases from F11 (6 ml) to F12 (9 ml) the florescence intensities of QD-LVs also increase (figure a-c) signifying more QDs encapsulation in liposome. Slight reduction in florescence intensity can be observed at F13 which went down drastically at F14. This shows that the optimal volume or concentration of QDs reacting with phospholipids

had been at F12. Furthermore, when these formulations were replicated, it was observed that F12 demonstrated the highest loading content (41.5 ± 5. 84) according to Table 10.

**Table 10. Loading efficiency of QD-LVs (F10- F14) and their zeta potential value.**

| **Formulations** | **Lecithin (mg)** | **Vol of QDs (ml) (4.2 mg/ml)** | **Stirring time (min)** | **Zeta potential (mV) (mean ± S.D)** | **Loading efficiency (%) (mean ± S.D)** |
|---|---|---|---|---|---|
| F10 | 100 | 1.5 ml | 45 min | -69.8 ± 3.69 | 14.4 ± 12.8 |
| F11 | 100 | 6 ml | 45 min | -51.1 ± 2.48 | 26.5 ± 3.04 |
| F12 | 100 | 9 ml | 45 min | -34.3 ± 1.30 | 41.5 ± 5.84 |
| F13 | 100 | 12 ml | 45 min | -58.0 ± 1.26 | 36.1 ± 6.01 |
| F14 | 100 | 15 ml | 45 min | -71.9 ± 2.00 | 8.20 ± 1.20 |
| Bare liposome | 100 | | 45 min | -47.8 ± 1.70 | - |
| Bare QDs | - | 3 ml | - | -38.5 ± 5.35 | - |

Result in Table 10 reveal that as the volume of QDs interacting with lecithin is increasing, the loading content of QDs-LVs from F11 to F12 also increase but decreased from F13 to F14. This

corresponds to the result obtained for the PL spectra discussed in figure 33 (a- e). Ironically, the triplicate study of F10 demonstrated lesser loading content of QDs in liposomes compared to the loading content of F6 shown in Table 9. The interpretation of the result in this study is that reducing the volume of QDs below 3 ml might reduce the optimal ratio for interaction between the QDs and LVs. Furthermore, the nanocomposite in Table 9 and 10 also demonstrated higher zeta potential values which shows that they are highly stable and possess good surface property.

To further elucidate the encapsulation of multi-core-shell QDs in liposomes at various optimized reactions conditions, the graphical illustration in figure 34 was constructed. This shows the florescence following the interactions of QDs with lecithin at various formulations as a function time in triplicate.

### 5.1.3. Florescence study of QD-LVs (F1 to F9) for different amounts of lecithin (50, 100, 150 mg).

Figure 34 depicts the florescence behavior of F1 to F9 for different amounts of lecithin at stirring times of 15, 30 and 45 min and running the experiment in triplicate.

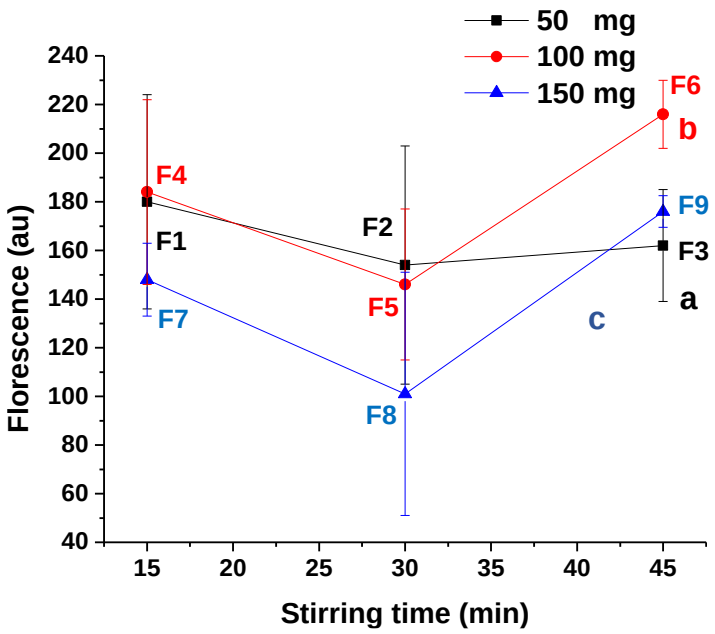


**Figure 34.** Florescence versus various stirring time (15, 30 and 45 mins) at different amount of lecithin. Black line (F1, F2 and F3) (a), Red line (F4, F5, and F6) (b) and blue line (F7, F8 and F9) (c).

The black line corresponds to F1 (15 min), F2 (30 min) and F3 (45 min) while the red line is F4 (15 min), F5 (30 min), and F6 (45 min), the blue line represents F7 (15 min), F8 (30 min) and F9 (45 min). Typically, the difference between each spectrum is the amount of lecithin used to interact with QDs. Hence, it can be inferred that as stirring time increases, the florescence intensity of the formulations generally decreased at 30 min and subsequently increased again at 45 min (figure 34 a, b and c). it is further shown that F6 and F9 demonstrated higher interactions than F3 at 45 min and that F6 shows higher level of interactions compared to F9. This observation is supported by higher florescence intensity at this reaction condition. This particular result corresponds to the highest value of loading efficiency obtained for F6 in Table 10. Thus, it becomes clear that the highest interaction between QDs and LVs is observed for F6 as shown in figure 34: these results are based on triplicate runs for the experiments.

### 5.1.4. Florescence study (F1 to F9) at different stirring time of 15, 30 and 45 min.

Similarly, when the florescence behavior of F1 to F9 is studied for different stirring times using 50 mg, 100 mg and 150 mg of lecithin with replicate runs of the experiment, it is observed that F6 still demonstrated the highest florescence intensity (figure 35). The black line represents F1 (50 mg), F4 (100 mg) and F7 (150 mg), the red line corresponds to F2 (50 mg), F5 (100 mg) and F8 (150 mg) and the blue line denotes F3 (50 mg), F6 (100 mg) and F9 (150 mg). The difference between each of the spectrum F1, F2 and F3 for example is the stirring time which corresponds to 15, 30 and 45 min.

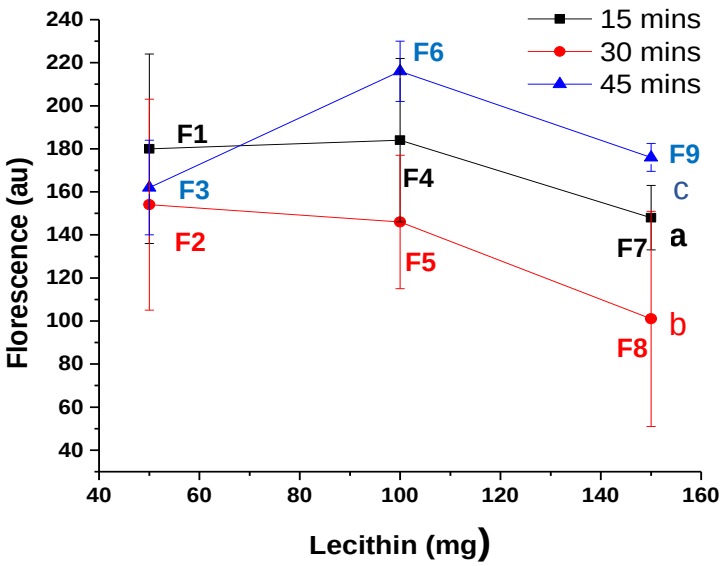


**Figure 35.** Florescence versus various amount of lecithin (50, 100 and 150 mg). Black line (F1, F4 and F7) (a), Red line (F2, F5, and F8) (b) and blue line (F3, F6 and F9) (c).

Therefore, it can be argued that as the amount of lecithin interacting with QDs increases to 100 mg at F4, F5 and F6, the florescence intensities only to decrease with more lecithin at 150 mg ad

depicted by F7, F8 and F9. This time, F6 demonstrated the highest interactions at 100 mg of lecithin compared to F4 and F5.

### 5.1.5. Florescence study (F10 to F14) at different stirring time using 100 mg of lecithin.

The illustration in figure 36 represent the interaction of QDs at various volumes of 100 mg of lecithin at 45 min stirring time after each reaction has been performed in triplicate. It was mentioned previously in section 5.1.1 that in order to optimize the amount of QDs loaded in the liposomes, the volume of QDs interacting with lecithin was varied using 1.5 ml (F10), 6 ml (F11), 9 ml (F12), 12 ml (F13) and 15 ml (F14) of QDs respectively.

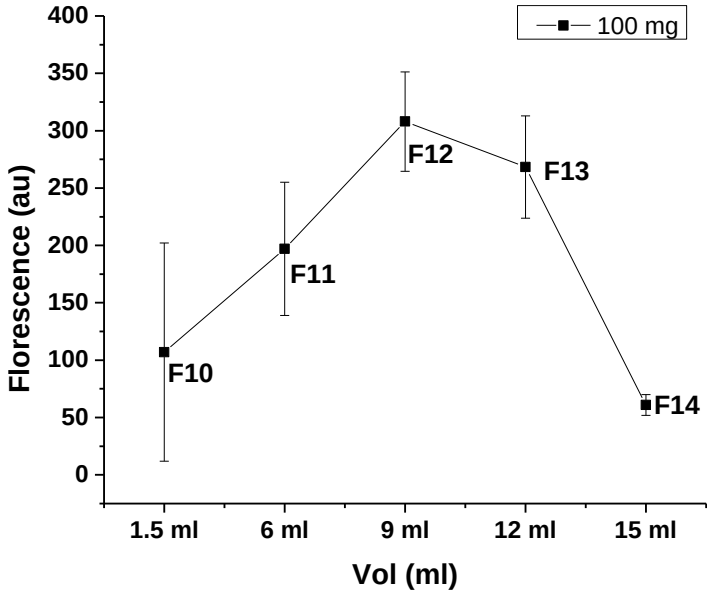


**Figure 36**. Florescence versus various volume of QDs (1.5, 6, 9, 12 and 15 ml).

It is observed in figure 36 that as the volume of QDs increases, the highest florescence intensity is observed at 9ml of QDs which corresponds to F12. At F13, the florescence intensity of the

QD-LVs decreased slightly and fell drastically at F14. It turns out that this result corresponds to the estimated loading efficiency calculated for these formulations in Table 10. Hence, it can also be concluded that upon replicating the encapsulation of the QDs in liposomes corresponding to F10, F11, F12, F13 and F14, the highest interactions between QDs and LVs can be found for F12 which also corresponds to the PL spectrum obtained in figure 33c.

### 5.1.6. Morphology.

#### 5.1.6.1. TEM micrograph of Bare liposome, Bare QDs and QDs-LVs.

It can be illustrated from figure 37a that the synthesized multi-core-shell QDs demonstrate spherical shape with individual particle separation. The average particle size distribution of the bare QDs can be estimated to be 9.83 nm ± 3.89 (figure 37b). Formation of empty liposome can be confirmed from figure 37c with an average size distribution of 294 nm ± 71.8 (figure 37d).

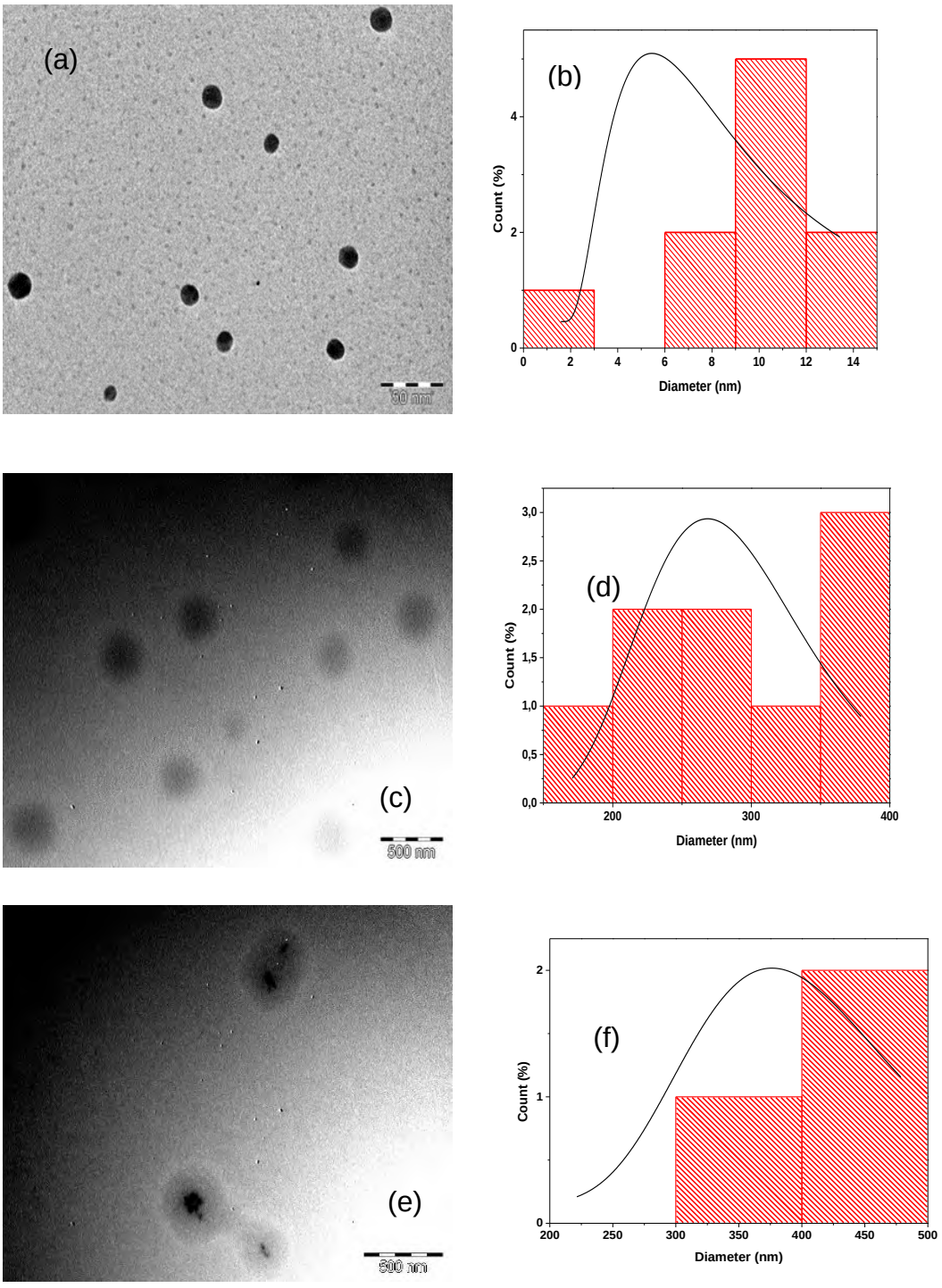


**Figure 37.** TEM images of Bare M-T-CdTe multi-core-shell QDs at 5 min (a) and size distribution (b), Empty liposome (c) and size distribution (d), loaded with QDs (e) and size distribution (f).

The loading of the CdTe/CdSe/ZnSe multi core-shell QDs in liposomes can be confirmed from figure 37e with an average size distribution of 412 nm ± 94.2. An increase in average particle size of the liposome loaded compared to empty liposome further proves the encapsulation of CdTe mutli-core-shell QDs in the liposomes. It can be further confirm that the QDs was not only loaded in liposomes but located at the aqueous core of the liposome vesicles showing its complete encapsulation in liposomes.

### 5.1.7. Physicochemical characterization.

#### 5.1.7.1. Thermogravimetric analysis of bare liposome and liposome loaded with QDs.

The loading of QDs in liposomes can further be investigated using thermogravimetry analysis (TGA) (figure 38), where the weight loss of the nanocomposite and liposomes are measured with increase in temperature. The initial drop in the profile of bare liposome and QD-LVs around 250 °C can be attributed to the loss of bound water in the materials.

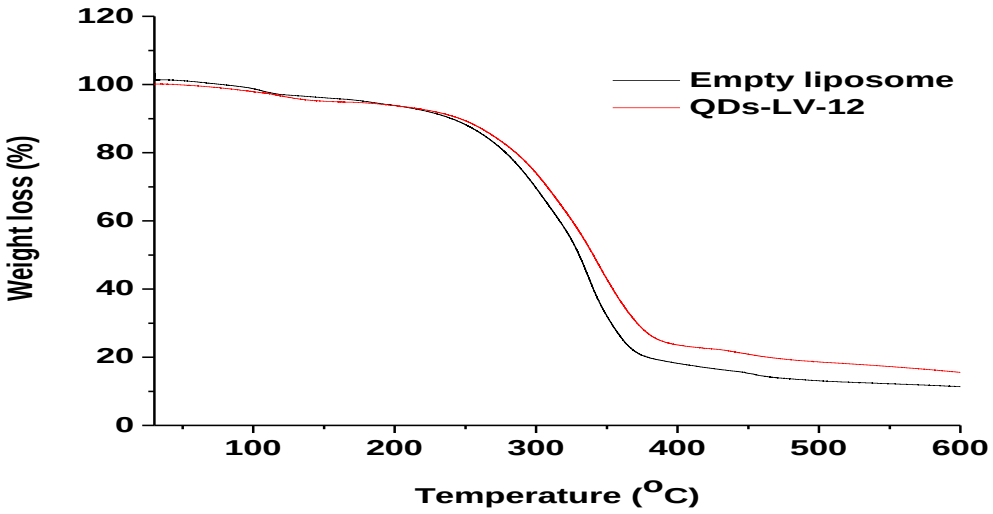


**Figure 38.** Thermogravimetric analysis of bare liposome versus liposome loaded with QDs (F12).

At 600 $^{0}$C, the value of weight remaining for QD-LVs is around 15.5 % while that of bare liposome can be found to be around 11.6 %. Therefore, when comparing their gravimetric result for QD-LVs to bare liposome, it can be concluded that the encapsulation of QDs in liposomes, slight show gain in weight over bare liposome demonstrating that an extra material has been loaded in the liposome vesicles.

### 5.1.7.2. EDS spectra of bare QDs, bare liposome and liposome loaded with QDs.

The images in figure 39 represent the elemental composition of bare QDs (a), bare liposome (b) and liposome loaded with QDs (c).

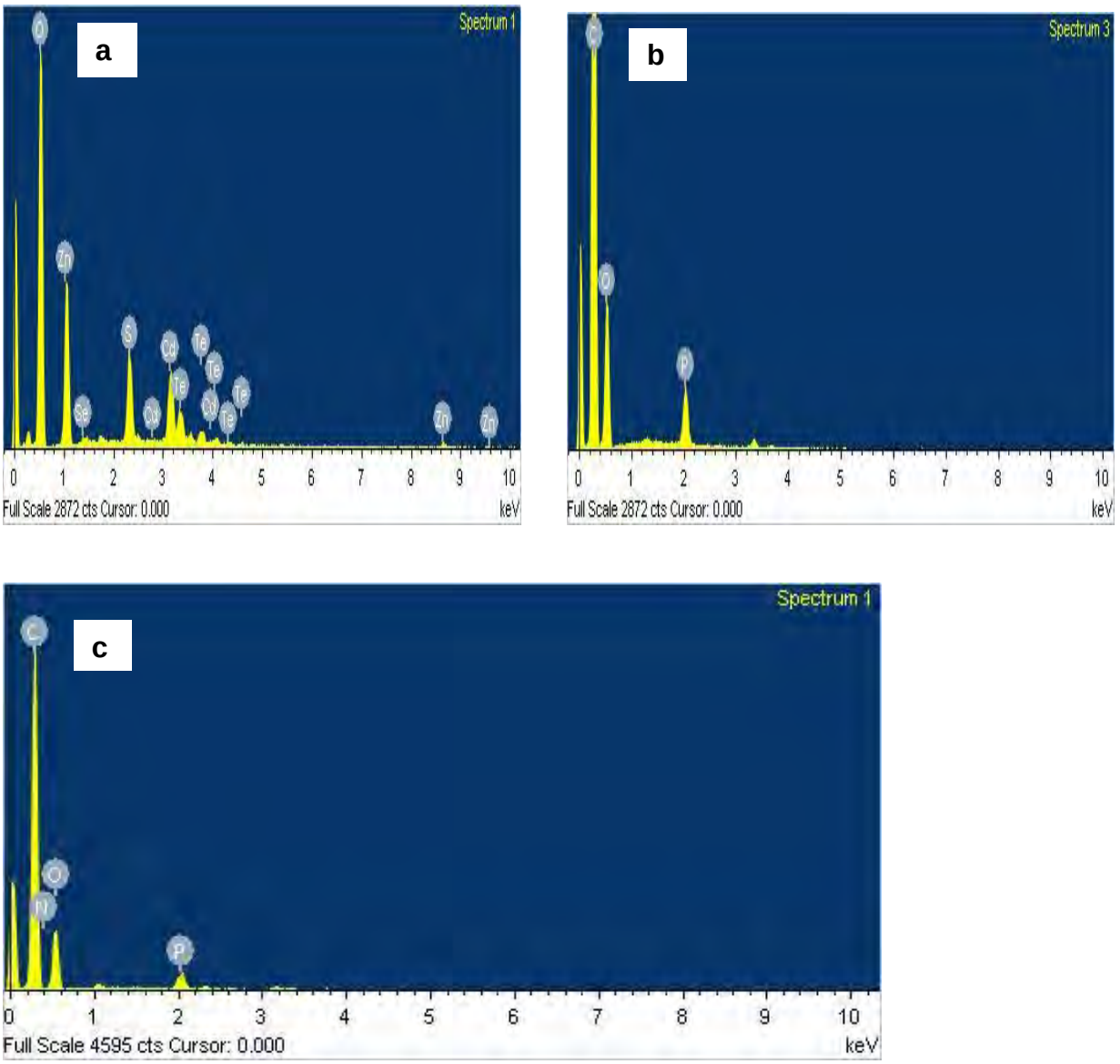


**Figure 39.** EDS spectra of bare QDs (a), bare liposome (b) and liposome loaded with QDs (F12) (c).

The successful synthesis of CdTe/CdSe/ZnSe mutli-core-shell QDs may be suggested from figure 39a due to the presence of Cd, Zn, Te and Se ions at the surface of the nanoparticle. The presence of phosphorous, oxygen and carbon in the spectrum also confirms the preparation of liposomes. The phosphorous is coming from the phosphate group present at the polar head of the structure while the carbon and oxygen are distributed all over the polar head and non-polar tail of

the phospholipids. In figure 39c is observed that the only available elements present at the surface of QD-LVs is carbon, phosphorous, oxygen and nitrogen. The nitrogen could be coming from the choline group present at the polar head of the phospholipids but the absence of $Cd^{2+}$, $Zn^{2+}$, $Te^{2-}$ and $Se^{2-}$ ions signifies the fact that the multi-core-shell QDs seems to be completely encapsulated in the aqueous core of the liposomes. Because the EDS only analyze the surface of a material to reveal its elemental composition, it may be difficult to detect the QDs elements at the surface due to their deeper encapsulation in the aqueous core of the liposome. This result also confirms the TEM image in figure 38c which shows the complete encapsulation of QDs in the aqueous core of the liposome.

## 5.2. Optical property, morphology and physio-chemical characterization of MPA-TGA-loaded in chitosan nanoparticle (CNP).

### 5.2.1. PL spectra of QDs and QD-CNP (F1 -F14).

The PL spectra in figure 40 (a-l) illustrates the loading of multi-core-shell QDs in CNP at various formulations. As shown in Table 7, each formulation is a representation of a specific optimized reaction condition. Therefore, twelve formulations were generated from the interactions between QDs and CNP and they are displayed here,

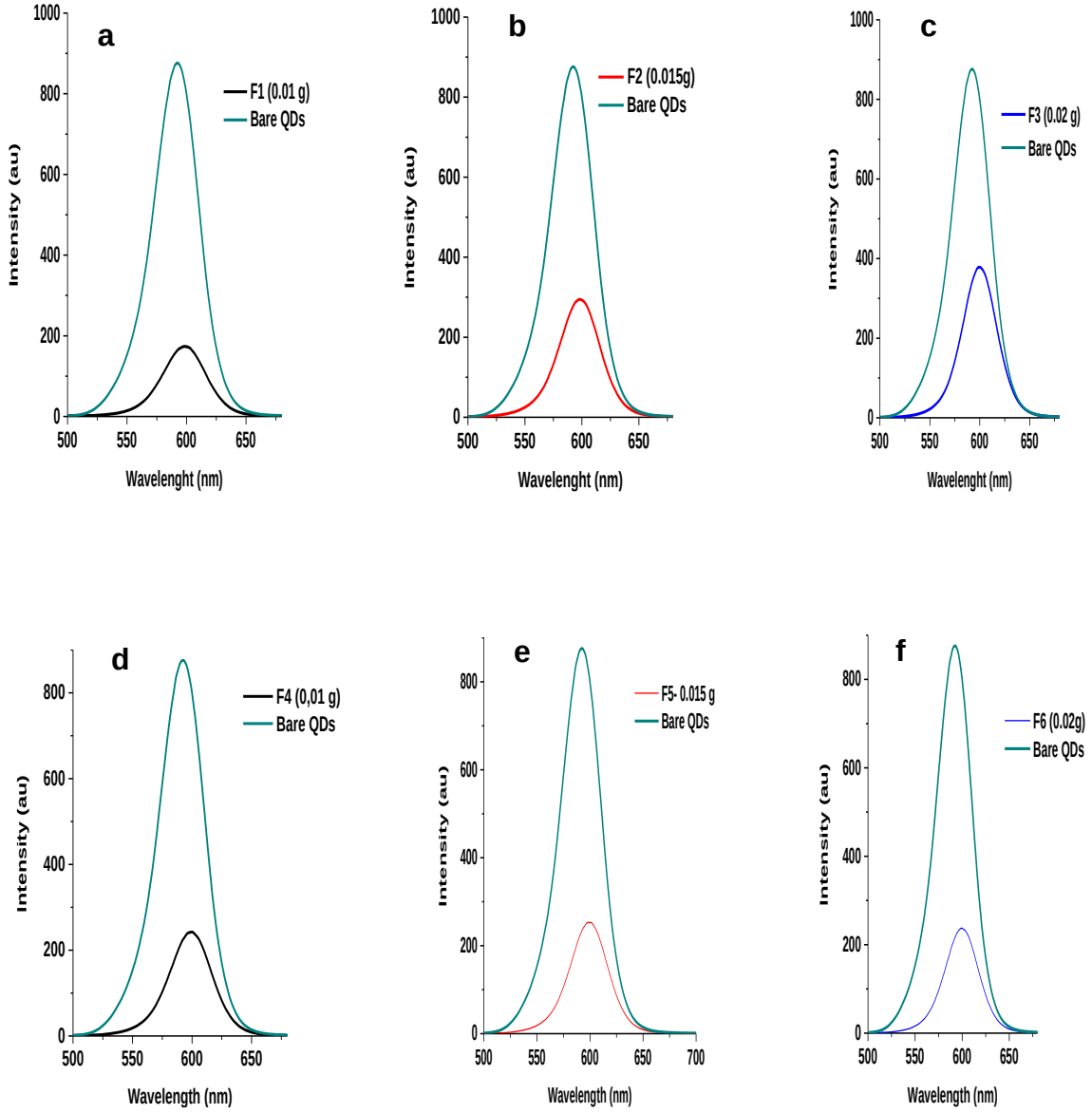
a
F1 (0.01 g)
Bare QDs
Intensity (au)
Wavelenght (nm)
b
F2 (0.015g)
Bare QDs
Intensity (au)
Wavelenght (nm)
c
F3 (0.02 g)
Bare QDs
Intensity (au)
Wavelenght (nm)
d
F4 (0,01 g)
Bare QDs
Intensity (au)
Wavelength (nm)
e
F5- 0.015 g
Bare QDs
Intensity (au)
Wavelength (nm)
f
F6 (0.02g)
Bare QDs
Intensity (au)
Wavelength (nm)

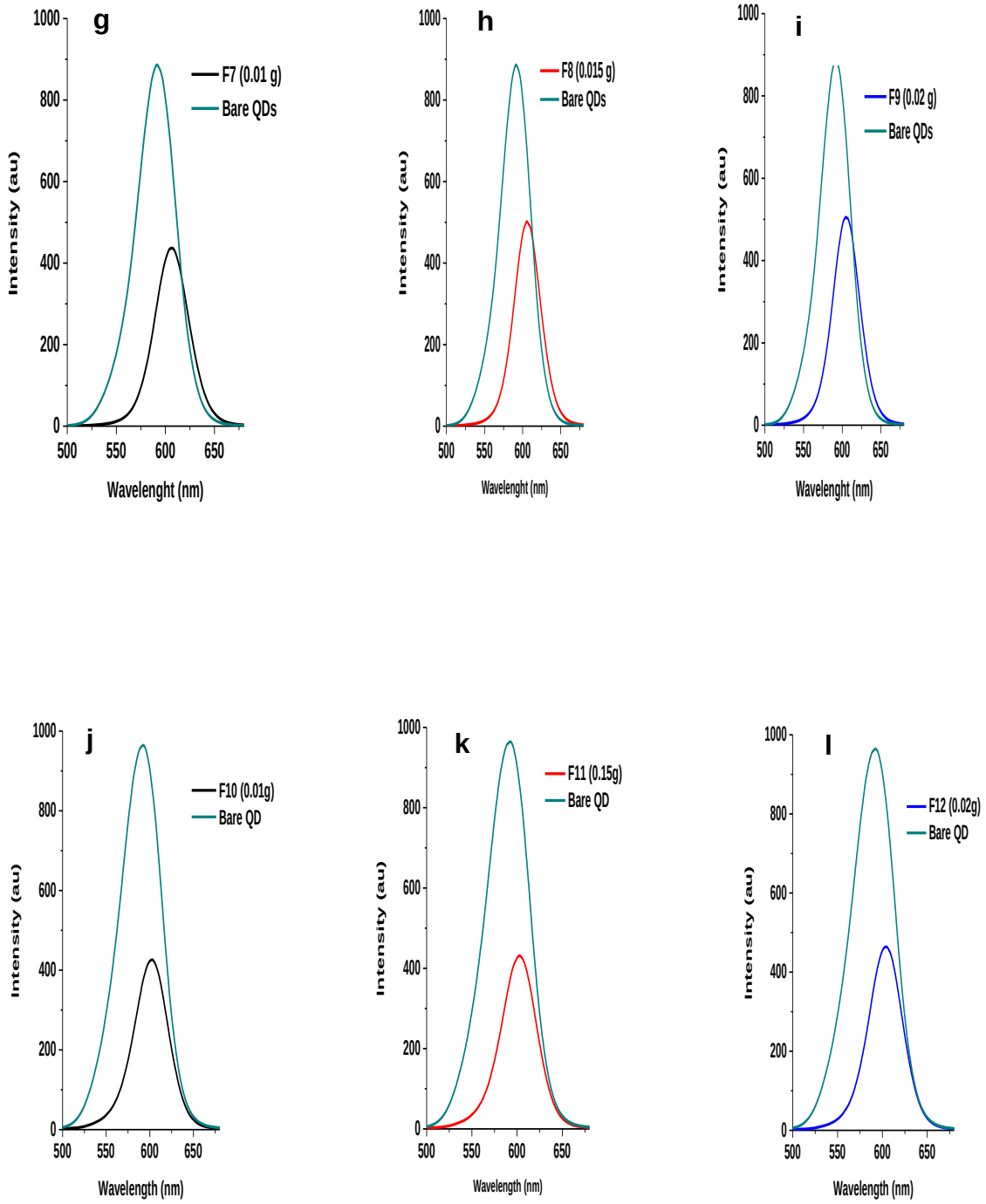


**Figure 40:** PL spectra of bare QDs, and QD-CNP (F1- F12, a- l) at various amount of chitosan (0.01g, 0.015g, 0.02g) and at different volumes of QDs (6ml, 9ml, 12ml and 15 ml).

It is observed that the florescence pattern of all formulation in figure 40 resembles that of QD-LVs discussed in figure 32 and 33. The resemblance corresponds to the slight shift in wavelength and florescence quenching which is also experienced in QD-LVs. The reduction in florescence intensity may also be attributed to the transfer of energy from the surface of florescent QDs to non-florescent CNP. Similar observation was also reported by Ghormade *et al* in 2014 during the encapsulation of CdTe QDs in CNP for the imaging of Mouse fibroblast cell line NIH- 3T3 [58]. The shift in wavelength observed in all formulation may be due to agglomeration of the QDs as a result of their encapsulation in CNP polymer matrices [75]. Furthermore, the ability for the QDs to be either directly conjugated to the surface of the CNP or embedded within the polymer matrices might be due to their electro-static interaction with the $COO^-$ ions at the surface of the QDs and the protonated amino group at the surface of the CNP [58, 75- 77]. It was previously emphasized in chapter two that chitosan is known to be cationic in nature which makes it to bind easily to any negatively charged molecule [75-76]. This property tends to increases its bio-compatibility with bio-molecules and leads to easier conjugation with cell membranes [58]. However, it is observed in F1- F3 that as the amount of chitosan (0.01- 0.02 g), interacting with QDs increases, at F3 the highest florescence intensity is observed. This might be due to the interaction of more amino group with carboxylate ions as a result of the use of higher amount of chitosan (0.02g) to interact with 6 ml of QDs. It can be observed that there is no significant difference in the PL intensity of F4-F6 when 9 ml of QDs interact with CNP (figure 40 d, e and f). A slight increase in florescence intensity between F7 and F8 can be seen when the volume of QD interacting with CNP is further increased to 12 ml (figure 40 g and h). However, there seems to be no significant difference between the florescence intensities of F8 and F9 (figure 40; h, i). The florescence intensities of F10, F11 and F12 appear to slightly decrease when the volume of

QDs interacting with CNP was increased to 12 ml (figure 40; j-l). In general, it is observed that except F6, the interaction of QDs with CNP using 0.02 g of chitosan contributes to increase in the florescence intensity of the nanocomposites. This can be noted from the PL spectra of F3, F9 and F12 (figure 40 c, i and l) and F9 seems to demonstrate the overall best interaction between QD and CNP. This can be further verified through the graphical illustration of their corresponding replicated results in figure 41.

### 5.2.2. Florescence study of QDs and QD-CNP (F1- F12) at various volume of QDs.

The graphical illustration in figure 41 depicts the interaction of QDs with CNP; each experiment conducted in triplicate for each formulation. The difference between the graphical lines is the volume of QDs reacting with the chitosan. It can be observed that as the amount of chitosan interacting with QDs increases, significant increases in florescence is experienced for F1 to F3 (figure 41a) and similarly for F7 to F9 (figure 41c). But for F10 to F12 (figure 41d), the florescence intensity of the nanocomposites first decreased and later increased slightly.

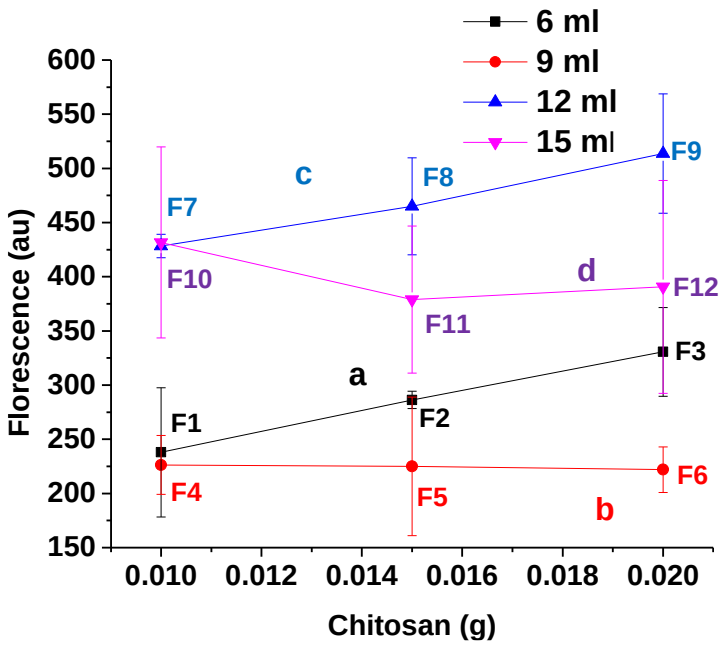


**Figure 41.** Florescence versus various amount of chitosan (0.01, 0.015 and 0.02 g). Black line (F1, F2 and F3) (a), Red line (F4, F5, and F6) (b), Blue line (F7, F8 and F19) (c), Purple line (F10, F11 and F12) (d).

A slight decrease in florescence can be observed as the amount of chitosan increases for F4 to F6 (figure 41d). Hence, it is clear that F9 still demonstrated the highest florescence intensity even after the embedding of QDs in CNP was replicated.

### 5.2.3. Florescence study of QDs and QD-CNP (F1- F12) at various amount of chitosan.

Figure 42 also illustrate the florescence study of the interaction between QDs with CNP for replicate studies of each formulation. Each of the graph is differentiated by the amount of chitosan interacting with various volumes of QDs. It is observed that for each graph the trend in (figure 42; a-c) is similar to florescence behavior for F7, F8 and F9 which demonstrated the

highest florescence intensity when compared to the others. Their similarity relates to the fact that as the volume of QDs interacting with CNP increases, slight decrease in florescence is first observed at 9 ml of QDs (F4, F5 and F6) this later increased at 12 ml of QDs (F7, F8 and F9). Further increase in the volume of QDs to 15 ml led to a significant decrease in florescence intensity at F10, F11 and F12.

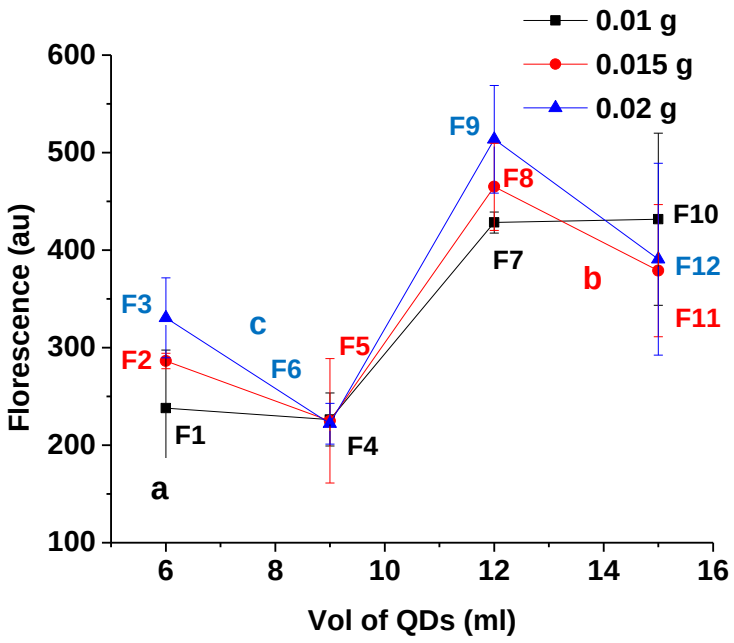


**Figure 42**. Florescence versus various volumes of QDs (6 ml, 9 ml, 12 ml and 15 ml). Black line (F1, F4, F7 and F10) (a), Red line (F2, F5, F8 and F11) (b) and blue line (F3, F6, F9 and F12) (c).

The reason for the decrease in emission intensity at F10, F11 and F12 might be due to the availability of too many QDs trying to compete with the protonated amino group, this might lead to the quenching of the florescence intensity of the corresponding nanocomposite. As observed

in figure 42, the triplicate result for F9 depicts the highest florescence intensity when 12 ml of QDs interacted with 0.02 g of chitosan and this also corresponds to the highest loading content shown in Table 11.

**Table 11. Loading efficiency of QD-CNP (F1- F12) and their zeta potential value.**

| **Formulations** | **Chitosan (g)** | **Vol of QDs (ml) (4.2 mg/ ml)** | **Zeta potential (mV) (mean ± S.D)** | **Loading efficiency (%) (mean ± S.D)** |
|---|---|---|---|---|
| F1 | 0.01 | 6 | 38.8 ± 1.35 | 29.2 ± 8.0 |
| F2 | 0.015 | 6 | 38.2 ± 4.33 | 32.7 ± 0.77 |
| F3 | 0.02 | 6 | 40.1 ± 6.48 | 37.7 ± 3.84 |
| F4 | 0.01 | 9 | 36.9 ± 0.15 | 25.8 ± 2.54 |
| F5 | 0.015 | 9 | 39.5 ± 2.40 | 25.3 ± 5.73 |
| F6 | 0.02 | 9 | 39.2 ± 1.57 | 25.3 ± 1.93 |
| F7 | 0.01 | 12 | 46.0 ± 6.10 | 48.8 ± 1.02 |
| F8 | 0.0 15 | 12 | 40.8 ± 1.65 | 53.1 ± 4.15 |
| F9 | 0.02 | 12 | 45.6 ± 1.92 | 58.5 ± 5.17 |
| F10 | 0.01 | 15 | 58.1 ± 8.12 | 44.8 ± 7.48 |
| F11 | 0.015 | 15 | 38.8 ± 0.35 | 39.3 ± 5.75 |
| F12 | 0.0 2 | 15 | 38.0 ± 1.96 | 40.5 ± 8.33 |
| Bare CNP | 0.02 | | 49.7 ± 2.51 | |
| Bare QDs | | | -38.5 ± 5.35 | |

The high zeta potential values of the QD-CNP nanocomposite from Table 11 also indicate that these compounds are stable and can be kept for quite some time. However, the highest zeta potential value for QD-CNP corresponds to F10 (58.1 ± 8.12). This value is low compared to QD-LVs-F14 in table 10 which demonstrated the highest zeta potential value of -71.9 ± 2.00. This indicates that QD-LVs are more stable than QD-CNP a fact which favors their potential use in biological applications.

### 5.2.4. Morphology.

#### 5.2.4.1. TEM micrograph of Bare CNP and QD-CNP.

Figure 43 depicts the morphology of bare CNP and QD-CNP with their corresponding size distribution. The TEM image of empty CNP in figure 43a shows that the particles appear to be spherical in shape with an average size distribution of 10.2 ± 1.12.

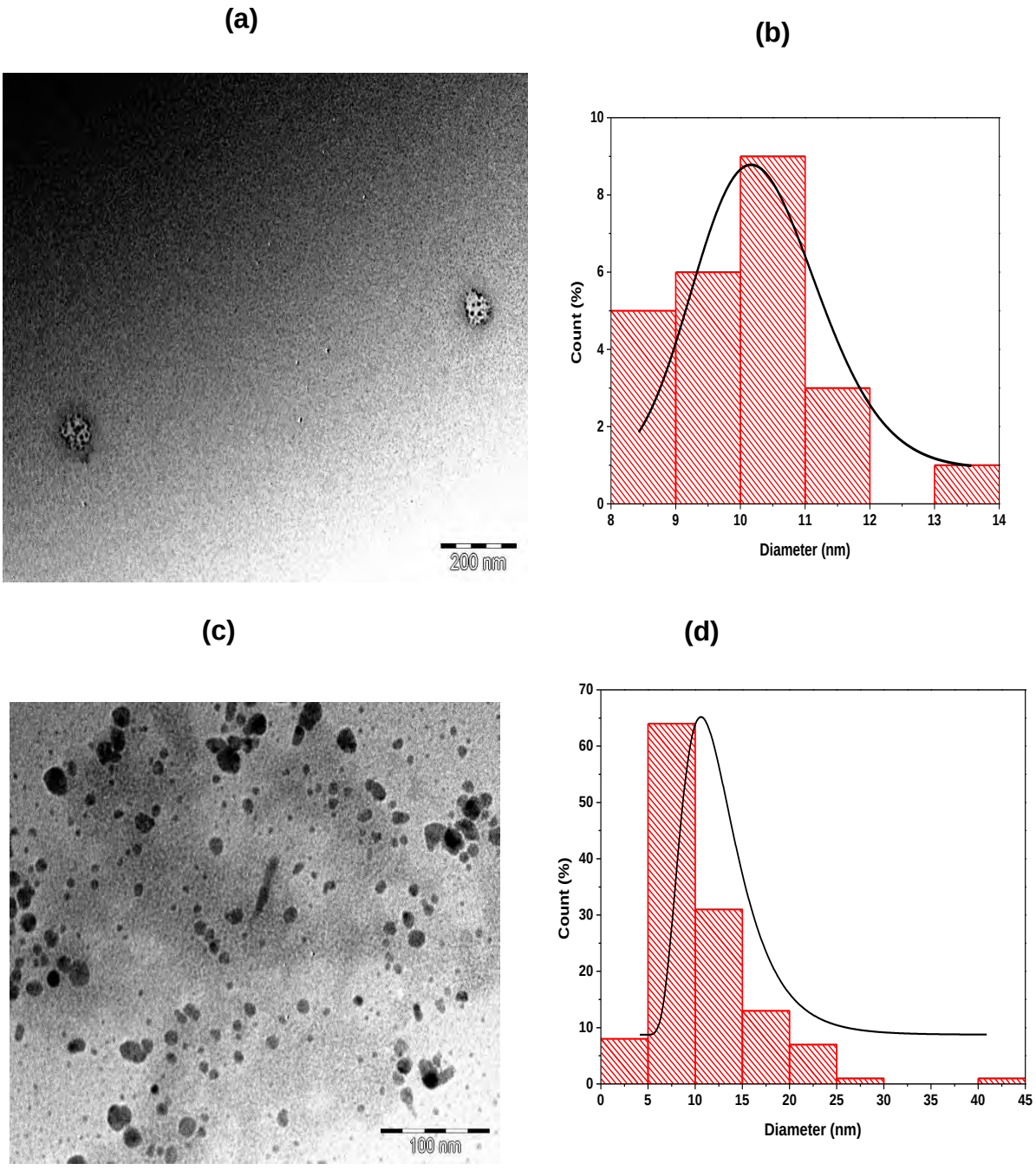


**Figure 43.** TEM image of Bare CNP (a) and CNP loaded with QDs (c) (F9). Size distribution of Bare CNP (b) and CNP loaded with QDs (d).

The loading of QDs in CNP can clearly be observed in figure 43 (c) with an average size distribution of 10.72 ± 5.55 (figure 43d). It is observed that the mean size of QD-CNP is bigger than the estimated mean size for bare QDs (9.83 ± 3.89) shown in figure 37 (a) and bare CNP. This interprets the encapsulation of multi-core-shell QDs in chitosan nanoparticles.

### 5.2.5. Physicochemical characterization.

#### 5.2.5.1. Thermogravimetric analysis of empty CNP and CNP loaded with QDs.

Thermogravimetry analysis (TGA) was used to determine the loading of the QDs in the polymeric CNPs and this is presented in figure 44. The initial drop in the profile of CNPs and QD-CNP composites (F3 and F9) can be attributed to the loss of bound water to the material. A sharp decline in weight loss can be observed for CNP around 246.5 °C with the degradation of the principal chains of chitosan beginning at 200 °C. Similar observation was reported by Ghormade *et al* in 2015 and Kumar *et al* in 2013 during the embedding of CdTe QDs in chitosan [58, 77]. As temperature increases from 30 – 600 $^{o}$ C, the rate at which the nanocomposite is losing weight is slow compared the bare CNP.

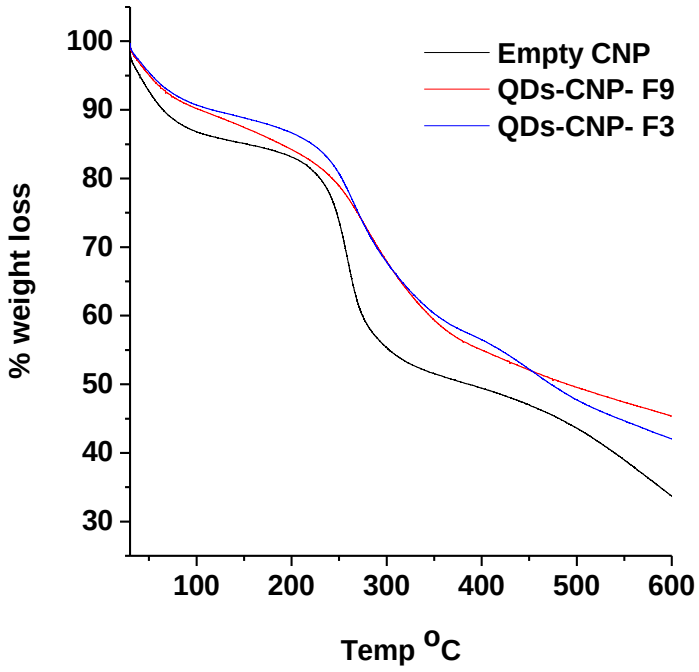


**Figure 44.** Thermogravimetric analysis of bare CNP and QD-CNP (F9) and CNP-QDs (F3).

The remaining weight for QD-CNP at 600 $^{0}$C for F3 is around 42 % and F9 is 45.4 %. This is comparable to the result for empty CNP which was found to be around 33.7 %. This result may be attributed to the entrapment of QDs in the CNP in both formulations. The reason why the present weight loss of F9 at 600ºC is found at 45.4 % compared to F3 which is recorded at 42 % is due to the difference amount of QD used (12 ml) with CNP compared to F3 in which 9 ml of QDs was used to interact with CNP. This result confirms that the QDs loading content in CNP for F9 is higher than F3. This observation is in good agreement with the calculated loading efficiency of QDs- CNP as shown in Table 11.

### 5.2.5.2. FTIR spectra of CNP, QDs and CNP loaded with QDs.

Fourier transform infrared spectroscopy (FTIR) spectra of the bare CNPs (a), QDs-embedded in chitosan nanoparticles (b) and bare- QDs (c) are shown in figure 45. For the IR spectrum of bare CNPs, the characteristic bands for chitosan were observed at 2844 $cm^{-1}$ OH of acid group, 1633 $cm^{-1}$ (amide I), 1535 $cm^{-1}$ (amide II), 1380 $cm^{-1}$ (amide III), 1066 and 1024 $cm^{-1}$ (COC) group.

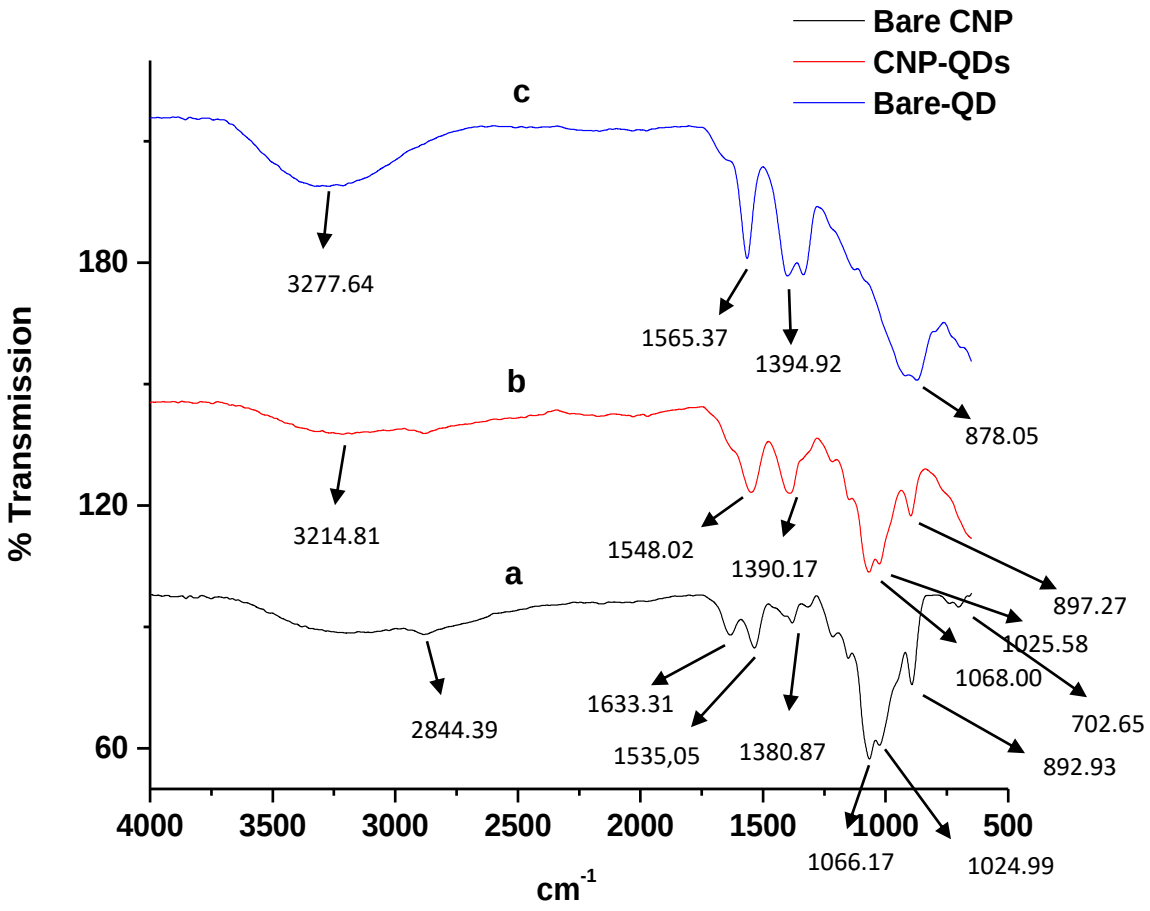


**Figure 45.** FTIR spectra of bare CNP (a), QD-CNP (b) and bare QDs (c).

The characteristic IR bands for the carboxyl group of the thiol-capped CdTe QDs (c) were seen at 3214 $cm^{-1}$ (O-H stretching), 1565 $cm^{-1}$ (C=O stretching), 1394 $cm^{-1}$ (COC stretching) and 878 $cm^{-1}$ (C–O bending). The spectra for QDs-embedded chitosan nanoparticles (b) showed the appearance of absorption bands of carboxyl groups at 1548 $cm^{-1}$, amide group of chitosan at 1390 $cm^{-1}$ and COC stretch at 1025 $cm^{-1}$.

It can be seen that the amide peaks at 1633 $cm^{-1}$ of bare chitosan (a) disappeared on CNP-QDs (b). This disappearance might be due to interaction between the positively charged amine group of the chitosan and the negatively charged carboxylate group at the surface of the QDs. it is also observed that the carboxyl groups at 1548 $cm^{-1}$ on QD-CNP (b) shifted to corresponding peak at 1565 $cm^{-1}$ coming from bare CNP (a). Then the amide group at 1380 $cm^{-1}$ for bare CNP (a) blue shifted to 1390 $cm^{-1}$ on interaction to QD-CNP (b). This observation collectively indicates some interaction between CNP and QDs confirming the embedding of QDs in the CNP polymeric matrices.

#### 5.2.5.3. XRD pattern of CNP, QDs and CNP loaded with QDs

Figure 46 describe the XRD patterns of the bare QDs (a), QD-CNP (b) and bare CNP (c). It can be observed carefully that the XRD pattern of the three compounds indicate a difference in the physical state of the compounds and materials. While empty CNP show a broad amorphous profile, the bare QDs shows a clear pattern of crystallinity and the QD-CNP also depict some crystalline peaks. The characteristic peaks of QDs at 26º and 46º in the range of 20º – 60º are found in the QD-CNP pattern and this confirms the presence of QDs in CNP. These XRD data supports earlier TGA results discussed in figure 44 concerning the change in the physical structure of QDs loaded in CNP.

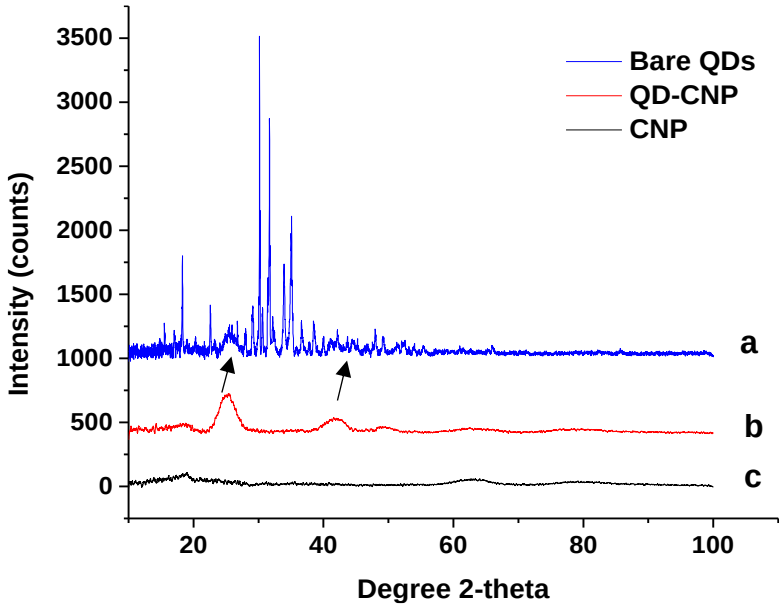


**Figure 46.** XRD pattern of bare QD (a), QD-CNP (b) and bare CNP (c).

### 5.2.5.4. EDS spectra of QDs, CNP and CNP loaded with QDs.

The elemental composition of bare QDs, empty CNP and CNP loaded with QDs is shown in figure 47. As mentioned previously connection with figure 39, the synthesis of CdTe/CdSe/ZnSe can be confirmed in figure 47a, while the presence of C, O and N at the surface of empty chitosan nanoparticles indicates the existence of the polymer (figure 47b). Image c shows the presence Zn, Cd, Se and Te ions which are all coming from CdTe multi-core-shell QDs while C, O and N come from CNP. This confirms that there is an interaction between the QDs and CNP

following the embedding of the QDs in the CNP. The phosphorous strong signal identified in image b and c might be due to some phosphate material which were not completely washed off from the chitosan. The sulphur signal observed in image c could be coming from the thiol group of the stabilizing agent used in the passivation of the QDs. However, comparing the EDS result of QDs-CNP to QD-LVs reported in figure 39c, it seems clear that it is easier to detect the presence of QDs in chitosan than in liposome.

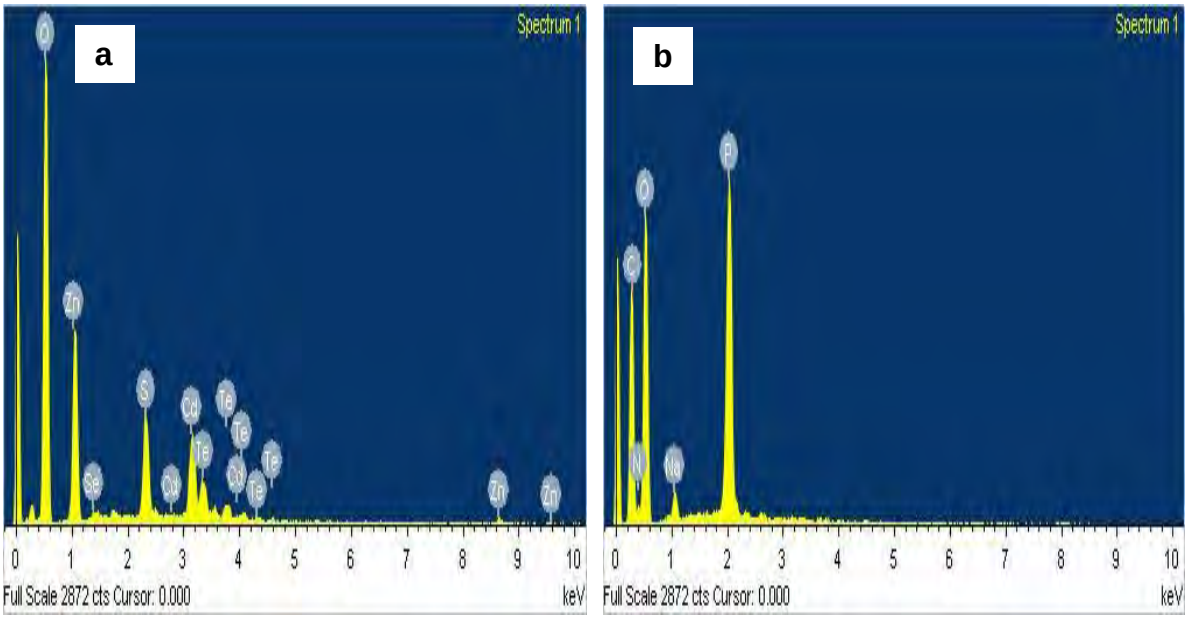

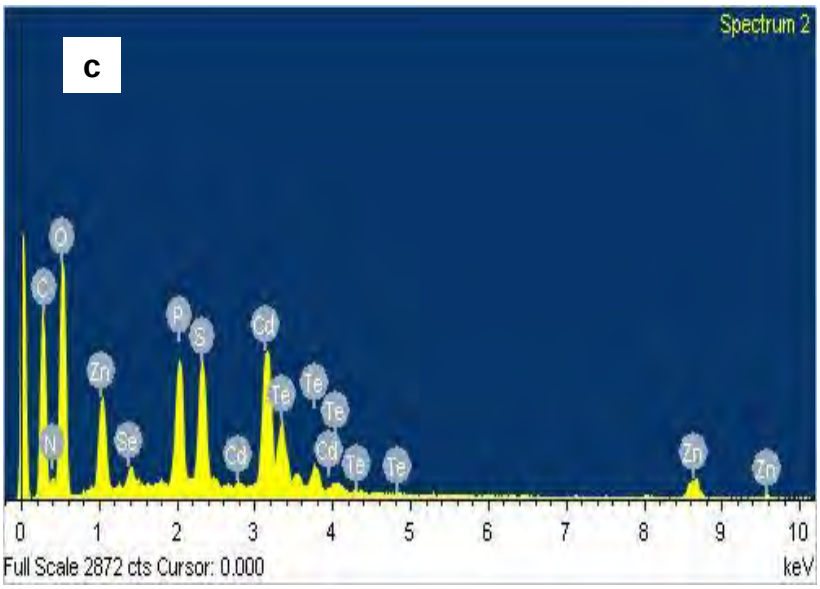


**Figure 47.** EDS spectra of raw QDs (a), empty CNP (b) and CNP loaded with QDs (c).

The reason for the easier detection in one case and not the other may be the fact that the encapsulated QDs in chitosan nanoparticle seem to be closer to the surface compared to liposomes which envelops them completely. Therefore, it may be difficult for beam of electrons during the analysis to easily get to the QDs loaded in liposomes because they are most likely embedded within the aqueous core of the liposome and electrons are limited to some lower penetration for solid samples [86]. Therefore, the thickness of coating compared to the covering demonstrated by chitosan nanoparticles appears to be stronger for the former which might have explain enhanced photo-stability of QDs loaded in liposome as observed in figure 48.

### 5.2.5.5. Exposure of QDs, QD-LVs and QD-CNP to UV irradiation.

Figure 48 describe the photostability study of QD-LVs and QD-CNP upon exposure of their surface to UV irradiation for 10 h. It is observed that as illumination time increases, bare QDs demonstrate a slight increase in florescence at 2 h which gradually decreases for 10 h. The increase in florescence as explained in figure 26, was said to be attributed to photo-etching effects and surface re-combination processes of the photo-degenerated charge carriers while the gradual reduction in florescence intensity was said to be due to the oxidation of metal nanoparticles present at the surface of the QDs [81- 85]. However, it is also observed that while the florescence of QD-LVs is increasing the florescence of QD-CNP was decreasing as illumination time increased.

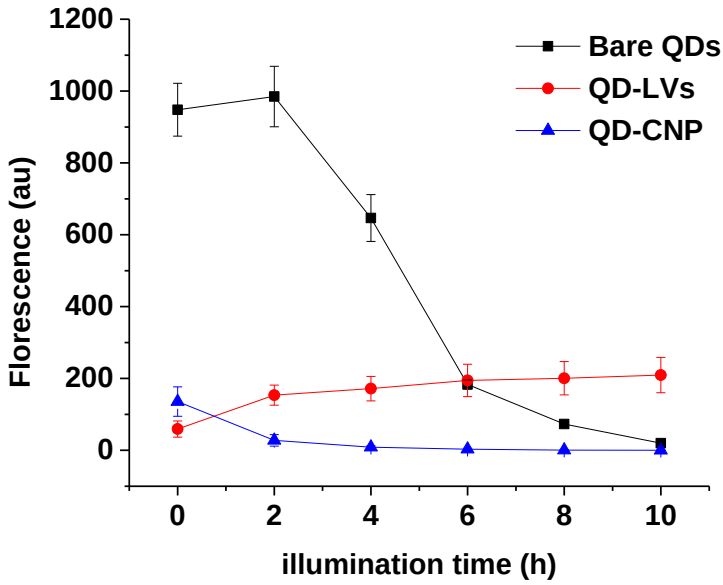


**Figure 48.** UV illumination study of bare QDs (a), QD-LVs (b) and QD-CNP (c).

The reason for this observation has been illustrated by the EDS spectra in figure 47 in which the encapsulated QDs in CNP can be found very close to the surface compared to the QDs loaded in the liposome (figure 39c). Thus, the QDs embedded in CNP are easily exposed to UV irradiation in such a way that the metal nanoparticles present at the surface of the QDs can easily oxidized. The enhanced florescence intensity observed for QD-LVs as illumination time increases could be due to the formation of strong covalent bonds between the phosphorous in the lipids and the metal nanoparticle. Similar observation was also demonstrated by Ye and co-workers during the encapsulation of CdTe QDs in liposomes for the near-infrared in-vivo imaging of mouse tissue [54].

# CHAPTER 6.

## 6. Cytotoxicity and cellular imaging studies of compounds with both HeLa and Vero cells.

Our aim in the chapter is to investigate the cell viability and cellular imaging studies of the compounds discussed in the previous chapter. As mentioned in previous sections, the main purpose of the whole study is to further enhance the biocompatibility of CdTe core-shell-shell QDs or multi core-shell QDs and make them more useful as florescence labels in cellular imaging. It was earlier said towards the end of chapter one that some recent studies have disapproved the coating of the surface of CdTe QDs with less toxic ZnSe/ZnS shell. The coating is done properly to prevent the toxic Cd metal ion from causing damage to cells during biological investigation. As an example, recall that Monaheng *et al* proved this point when their

synthesized CdTe/CdSe/ZnSe core-shell-shell QDs showed some toxicity towards Chinese Hamster Ovary cells at almost all concentrations [48].

As a result, it was vital to explore further encapsulation of the synthesized CdTe core-shell-shell or multi-core-shell QDs in liposomes and chitosan nanoparticles (CNP) which was reported in chapter five.

In order to determine which environment is best suitable to these multi-core-shell QDs, cytotoxicity and florescence imaging studies of the nanocomposite was investigated using two different cells lines which are HeLa and Vero cells. The HeLa cells represent cancer cells while the Vero cells are normal cells. As pointed out earlier in section 2.2, three samples were selected from end of the list of prepared formulations of QD-LVs and QD-CNP, this led to a total of 10 samples that were screened for the cytotoxicity investigation. The formulation with the highest loading content which corresponds to F12 (QDs-LV) and F9 (QDs-CNP) were the main compounds selected for the cytotoxicity investigation and florescence imaging studies. Added to this formulation are F1 and 11 for QDs-LVs and F3 and 4 for QDs-CNP. The formulations added to the best sample were selected for the validation of the experiments most importantly, the cell viability studies. The concentration of the compounds used for the cytotoxicity studies according to section 2.2 ranges from $2.56 \times 10^{-7}$ mg/ml. – 0.5 mg/ml.

It was estimated from the study that the compound with the concentration > 0.5 mg/ml that did not kill at least 50 % of the cell is regarded to show minimal toxicity. Hence, the following $IC_{50}$ graphs were constructed to demonstrate the cytotoxicity study of the all the 10 compounds that interacted with both HeLa and Vero cells.

### 6.1. $IC_{50}$ Graphs of compounds with HeLa cells.

The cytotoxicity study showing the $IC_{50}$ graphs of 10 various compounds upon interaction with HeLa cells is illustrated in figure 49. it is observed from figure 49 (a, b) that the interaction of both empty liposome and CNP with the cells demonstrated lower toxicity. This is due to the fact that more than 50 % of the cell survived at their highest concentration. The result shows that these compounds do not contain impurities that may pose some toxicity to the cells, this confirms their high bio-compatibility as reported from various literature [8- 9].

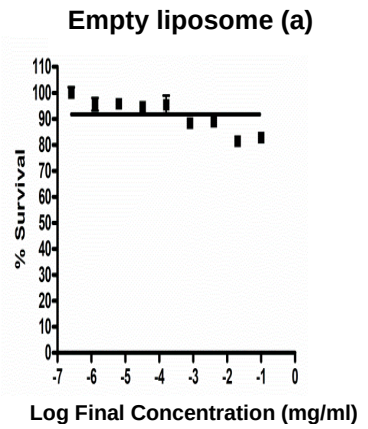
Empty liposome (a)
% Survival
Log Final Concentration (mg/ml)

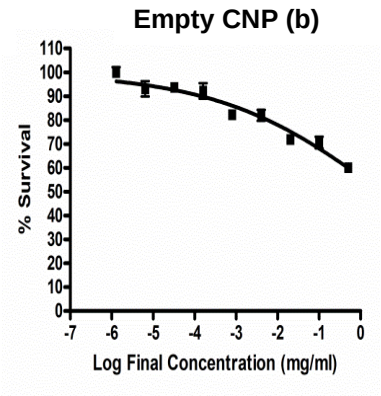
Empty CNP (b)
% Survival
Log Final Concentration (mg/ml)

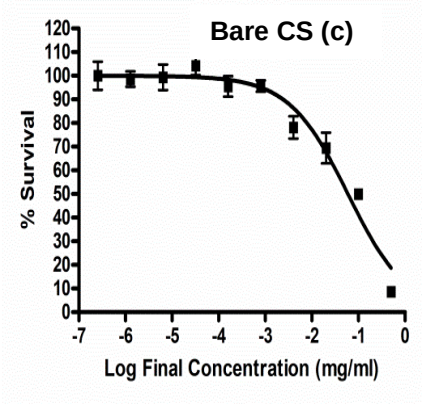
Bare CS (c)
% Survival
Log Final Concentration (mg/ml)

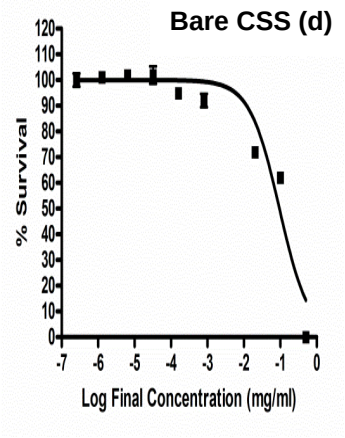
Bare CSS (d)
% Survival
Log Final Concentration (mg/ml)

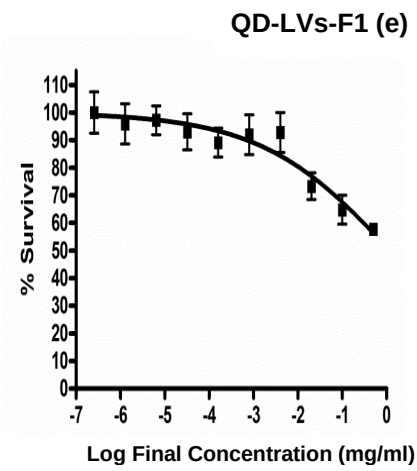
QD-LVs-F1 (e)
% Survival
Log Final Concentration (mg/ml)

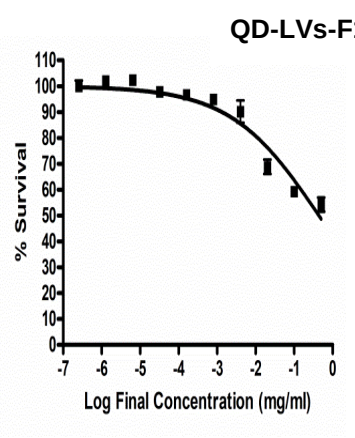
QD-LVs-F11 (f)
% Survival
Log Final Concentration (mg/ml)

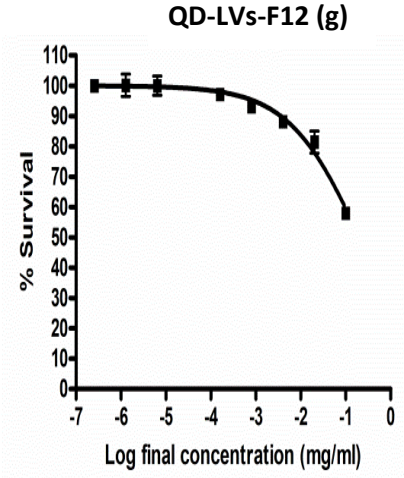
QD-LVs-F12 (g)
% Survival
Log final concentration (mg/ml)

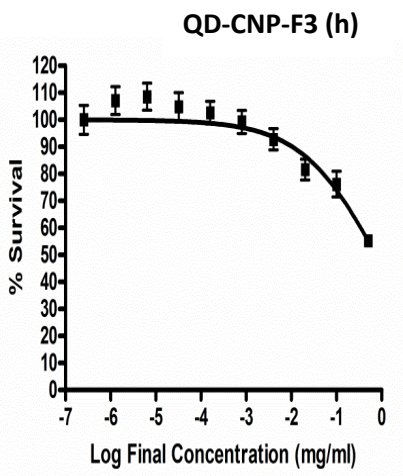
QD-CNP-F3 (h)
% Survival
Log Final Concentration (mg/ml)

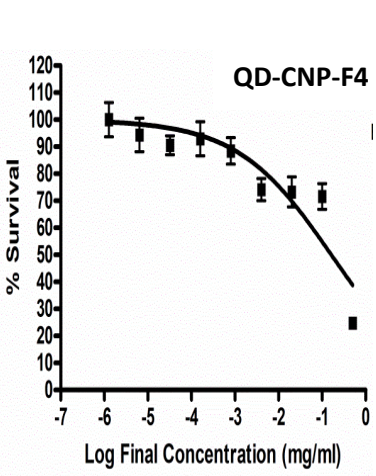
QD-CNP-F4 (i)
% Survival
Log Final Concentration (mg/ml)

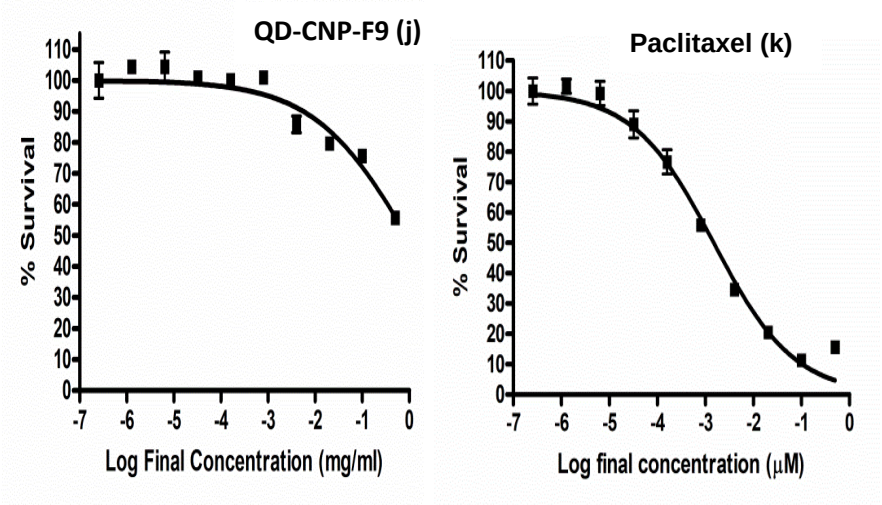


**Figure 49.** $IC_{50}$ graphs of 10 compounds (a- j) with anti-cancer drugs (k) as the controls after interactions with HeLa cells at various concentration ranging from 0.5 mg/ml – $2.56^{-7}$ mg/ml. Note: CS and CSS is core-shell and core-shell-shell.

High mortality is recorded during the interaction of CS and CSS with the cells as shown in figure 49 (c, d). The study reveals that in each case about 80 % of cell death occurred at their highest concentration which could be due to the release of high amount of toxic Cd metal ions from the QDs into the nearby solutions. In the case of CSS, the result observed confirms the work reported by Monhange *et al* which emphasized that coating the surface of CdTe QDs with less toxic ZnSe or ZnS shell is not enough to prevent highly toxic Cd metal ions from escaping into the nearby solutions [48].

Table 12 shows the highest concentration of various compounds where 50 % of the cell survived. However, it is observed that the interaction of CSS with the cells still demonstrate lower toxicity compared to CS. This is because the highest concentration of 50 % cell survival for CSS is found to be 0.09381 mg/ml while that for CS can be observed at 0.05916 mg/ml. The reason for the

lower toxicity generated by CSS compared to CS is thought be due to the slight coating of ZnSe shell at the surface of CdTe/CdSe core-shell QDs.

Furthermore, from the $IC_{50}$ graphs in figure 49 (e- j) it is observed that except QD-LVs-F11 and QD-CNP-F4, the interactions of the various composites with the cells demonstrate slight toxicity at their highest concentration. This can be observed with QD-LVs-F1, QD-LV-F12, QD-CNP-F3 and QD-CNP-F9. This means that the encapsulation of the multi-core-shell QDs in both liposomes and CNP at these formulations reduced the toxicity of the nanoparticles. However, as observed from the $IC_{50}$ graphs in figure 49f the percentage of cell survival for QD-LVs-F11 is around 48 % (52 % cell death) while that of QD-CNP-F4 shows 40 % cell survival (60 % cell death) (figure 49i) at their highest concentration. This indicates that QD-LVs-F11 still demonstrates minimal toxicity compared to QD-CNP-F4. This is also confirmed from the $IC_{50}$ values for QD-LV-F11 on Table 12 which is closer to 0.5 mg/ml compared to QD-CNP-F4 $IC_{50}$ value of 0.1618 mg/ ml (note that the $IC_{50}$ value shows the highest concentration at which 50 % of the cell survived). This result interpreted to mean that the rate at which the toxic Cd metal ion escapes into the solution is higher for QD-CNP-F4 than QD-LVs-F11. The reason why QD-LVs-F11 is demonstrating lesser toxicity is ascribed to the fact that the lipid shell is providing enough covering at the surface of the multi-core-shell QDs compared to the one provided by the polymer. The explanation to this was also mentioned during the EDS analysis of QD-LVs and QD-CNP composites in figure 47. This result might also support the reason why poor photo-stability studies was also encountered upon exposure of QD-CNP to UV irradiation as discussed in figure 48. Furthermore, it is further observed that the interaction of Paclitaxel control with the Hela cells in figure 49k led to about 98 % apoptosis which demonstrate the therapeutic

effectiveness of the anti-cancer drug towards cancer cells. This control is essential to ensure that the study is bench worked.

**Table 12. $IC_{50}$ value of compounds with the control.**

| | | | HeLa | | | Vero | | |
|---|---|---|---|---|---|---|---|---|
| **S/N** | **Sample name** | **Solvent** | **$IC_{50}$ (mg/ml)** | **$IC_{50}$ (ug/ml)** | **R2** | **$IC_{50}$ (mg/ml)** | **$IC_{50}$ (ug/ml)** | **R2** |
| **1** | Empty CNP Empty | Acetic-acid | >0.5 | >500 | N/A | >0.5 | >500 | N/A |
| **2** | Liposome | De-ion water | >0.5 | >500 | N/A | >0.5 | >500 | N/A |
| **3** | QD-CNP (F9) | Acetic acid | >0.5 | >500 | N/A | >0.5 | >500 | N/A |
| **4** | QD-LVs (F11) | De-ion water | 0.4364 | 436.4 | 0.9186 | >0.5 | >500 | N/A |
| **5** | Bare QD(CSS) | De-ion water | 0.09381 | 93.81 | 0.9226 | 0.05835 | 58.35 | 0.8805 |
| **6** | Bare-QDs(CS) | De-ion water | 0.05916 | 59.16 | 0.9248 | 0.04536 | 45.36 | 0.9432 |
| **7** | QD-LVs (F1) | De-ion water | >0.5 | >500 | N/A | >0.5 | >500 | N/A |
| **8** | QD-LVs (F12) | De-ion water | >0.5 | >500 | N/A | >0.5 | >500 | N/A |
| **9** | QD-CNP (F3) | Acetic acid | >0.5 | >500 | N/A | >0.5 | >500 | N/A |
| **10** | QD-CNP (F4) | Acetic acid | 0.1618 | 161.8 | 0.7699 | >0.5 | >500 | N/A |
| | **control** | | **$IC_{50}$ (uM)** | **$IC_{50}$ (nM)** | **R2** | **$IC_{50}$ (uM)** | **$IC_{50}$ (nM)** | **R2** |
| **11** | Paclitaxel control | | 0.001485 | 1.485 | 0.9734 | >0.5 | >500 | N/A |

## 6.2. $IC_{50}$ Graphs of compounds with Vero cells.

The illustration in figure 50 represent the cytotoxicity studies of 10 various compounds upon interactions with Vero cells. It is clearly observed that the interaction of empty liposome and CNP with the Vero cells in figure 50 (a, b) led to more than 50 % of cell survival at their highest concentration. This indicates that the two compounds demonstrate lower toxicity to the normal cells which make them to show good bio-compatibility as evidenced by their interactions with HeLa cells.

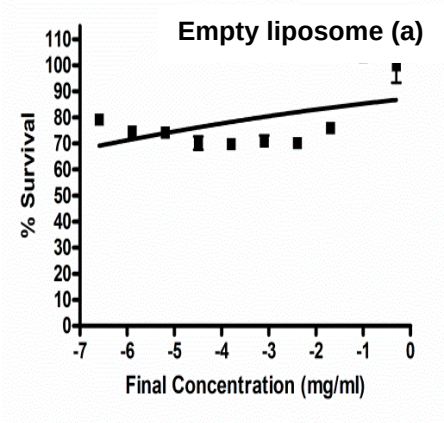


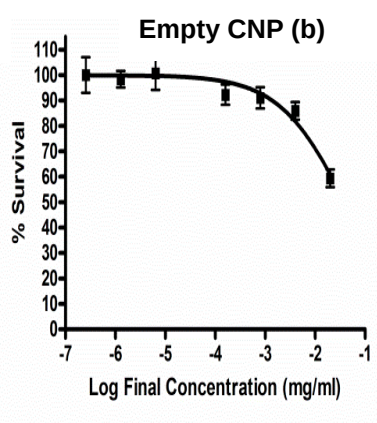


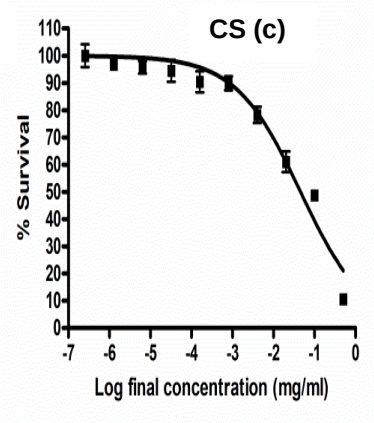


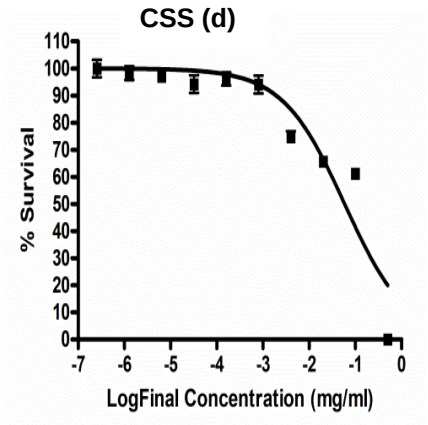


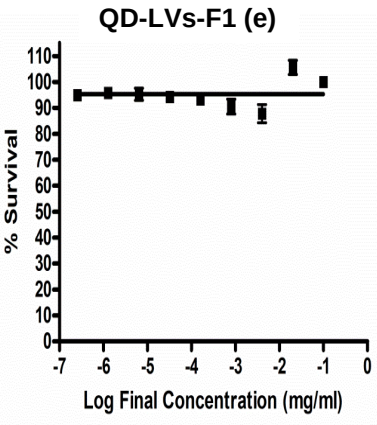


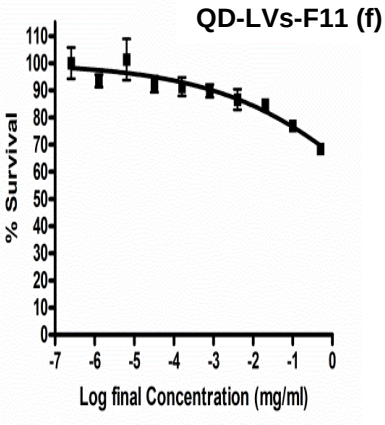

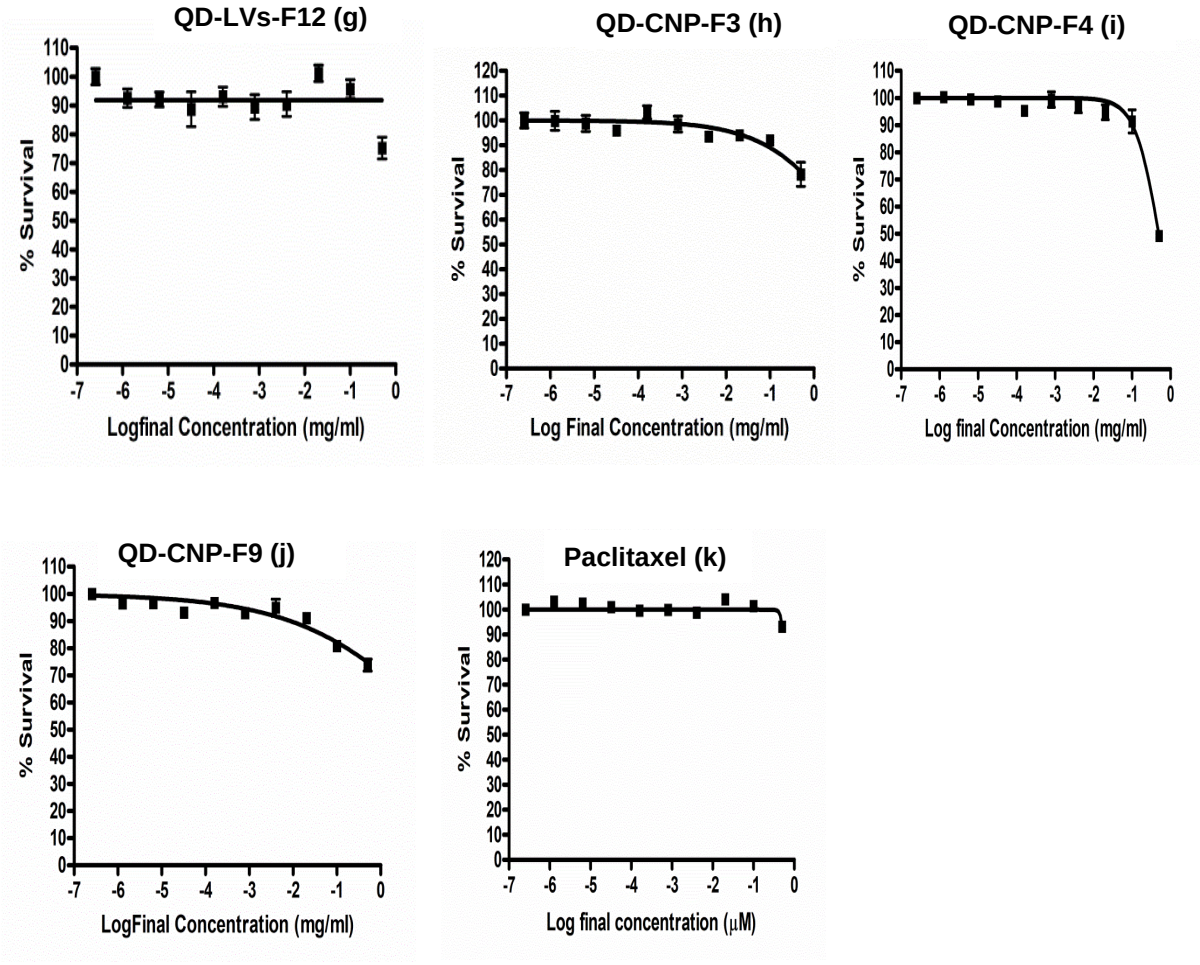


**Figure 50.** $IC_{50}$ graphs of 10 compounds (a- j) with anti-cancer drugs (k) as the controls after interactions with HeLa cells at various concentration ranging from 0.5 mg/ml – $2.56^{-7}$ mg/ml. Note: CS and CSS is core-shell and core-shell-shell.

In contrast to the toxicity demonstrated with the HeLa during the interactions of CS and CSS as discussed in figure 49 (c, d), these compounds also show approximately 80 % cell death (20 % cell survival) with Vero cells at their highest concentration as indicated in figure 50 (c, d). This suggests that the release of more toxic Cd metal ion into the solution might have affected the rate of survival of the cells leading to high mortality. Regarding CSS QDs, the effects on the cells depict that covering the surface of the CdTe QDs with less toxic ZnSe shell is not sufficient to stop the leaching of the toxic Cd metal ions into the solution. However, the result from the $IC_{50}$

value in Table 12 indicated that the multi-core-shell QDs (CSS) still demonstrated less toxicity compared to CS QDs. According to this table, the highest concentration than did not kill 50 % of the cell for bare CSS QDs is 0.05835 mg/ml while that for bare CS is 0.04536 mg/ml. Furthermore, it is seen from figure 50 (e- j) that the interaction of the nanocomposites with the cells demonstrated at least 50 % of cell survival at their highest concentration indicating that these compounds show less toxicity. The result proves that upon their exposure to normal cells, the encapsulation of the synthesized multi-core-shell QDs in both liposomes and chitosan nanoparticles improves the biocompatibility of the QDs and thereby enhancing their use in biological applications. This also supports their estimated $IC_{50}$ value according to Table 12 which shows that more than 50 % of the cells survived at a concentration > 0.5 mg/ml. However, another observation that is seen clearly is that QDs-LVs-F11 and QDs-CNP-F4 at their highest concentration show lesser toxicity to Vero cells compared to HeLa cells according to the $IC_{50}$ graphs in figure 49 and 50 (f, i), together with $IC_{50}$ values in Table 12. Although it can be seen that QD-CNP-F4 depicts more toxicity with both cells compare to QDs-LV-F11. Meanwhile, we must recall, that the toxicity shown by the liposome composite is still minimal compared to the chitosan composite. Nevertheless, this gives us an insight especially with QDs-CNP-F4 that the Cd metal ions may not only be the actual cause of cell deaths but the generation of free radicals by the QDs may also lead to apoptosis.

CdTe QDs has been identified from various literature as the potential source of free radical generation and this increases the level of their toxicity during in-vitro or in-vivo studies [87- 89]. In a study conducted by Zhang *et al* in 2015, it was discovered that the administration of CdTe QDs significantly increased the level of lipid peroxides marker malondialdehyde (MDA) in the livers of treated mice and also caused cytotoxicity in AML 12 cells in a dose- and time-

dependent manner. All these are said to have been due to the generation of reactive free radicals by the QDs [90]. Also in 2013, Xie and colleagues studied the oxidative damage effects induced by CdTe QDs in the liver of mice. At a specific concentration they discovered a significant increase in MDA concentration in the tissue of the liver compared to those of the control group [91]. The exposure of human hepatocellular carcinoma HepG2 cell to CdTe-QDs were investigated by Nguyen *et al* in 2013. It was discovered in these studies that CdTe QDs causes cytotoxicity in HepG2 cells in a dose- and time-dependent manner and treated cells showed an increase in reactive oxygen species (ROS) [89]. Therefore, all these observations derived from various literature indicates that the toxicity demonstrated by most especially QD-CNP-F4 on HeLa cell may be due to free radical generation caused by the encapsulated QDs leading to oxidative stress. Even though the composites were screened with the cells at the same range of concentration, the HeLa cells seems to find it difficult to restrict the impact of oxidative stress imposed by the QDs compared to Vero cells. This might have led to some cell death as observed in the HeLa cells compared to the Vero cells. Hence, it can be concluded from this cytotoxicity study that encapsulating CdTe multi-core-shell QDs in liposome shows more biocompatibility compared to chitosan nanoparticle, because QDs-CNP-F4 shows the highest toxicity among all the composite.

### 6.3. Cellular uptake studies of Bare CdTe multi-core-shell QDs, QDs-LVs and QDs-CNP using Hela cells.

The cellular uptake studies and internalization of bare CdTe multi-core-shell QDs, liposome and chitosan nanoparticles composite were elucidated using florescence microscopy through a random selection of liposome and chitosan composite (QDs-LV-F12 and QD-CNP-F9). These composites were selected due to their high loading efficiency compared to the other formulations.

The images of the compounds were captured upon interaction with HeLa cells using the green/visible and red/Infra-red channels of the florescence microscopy. The nuclear staining was achieved using diamindino-2-phenylindole (DAPI) to track the uptake and internalization of the compounds into the cell cytoplasm (figure 51 c,d,g, h, k, i). Following 24 h of exposure, the interaction of bare QDs with the cells showed strong fluorescence especially in the green and red channels (figure 51 b and c). Firstly, it appears that some of the QDs are sitting around the cell membrane (figure 51 a and b) but the morphology of staining appears to be consistent with location in endocytic vesicles as observed from the labelling of the nucleus with DAPI (figure 51 c and d).

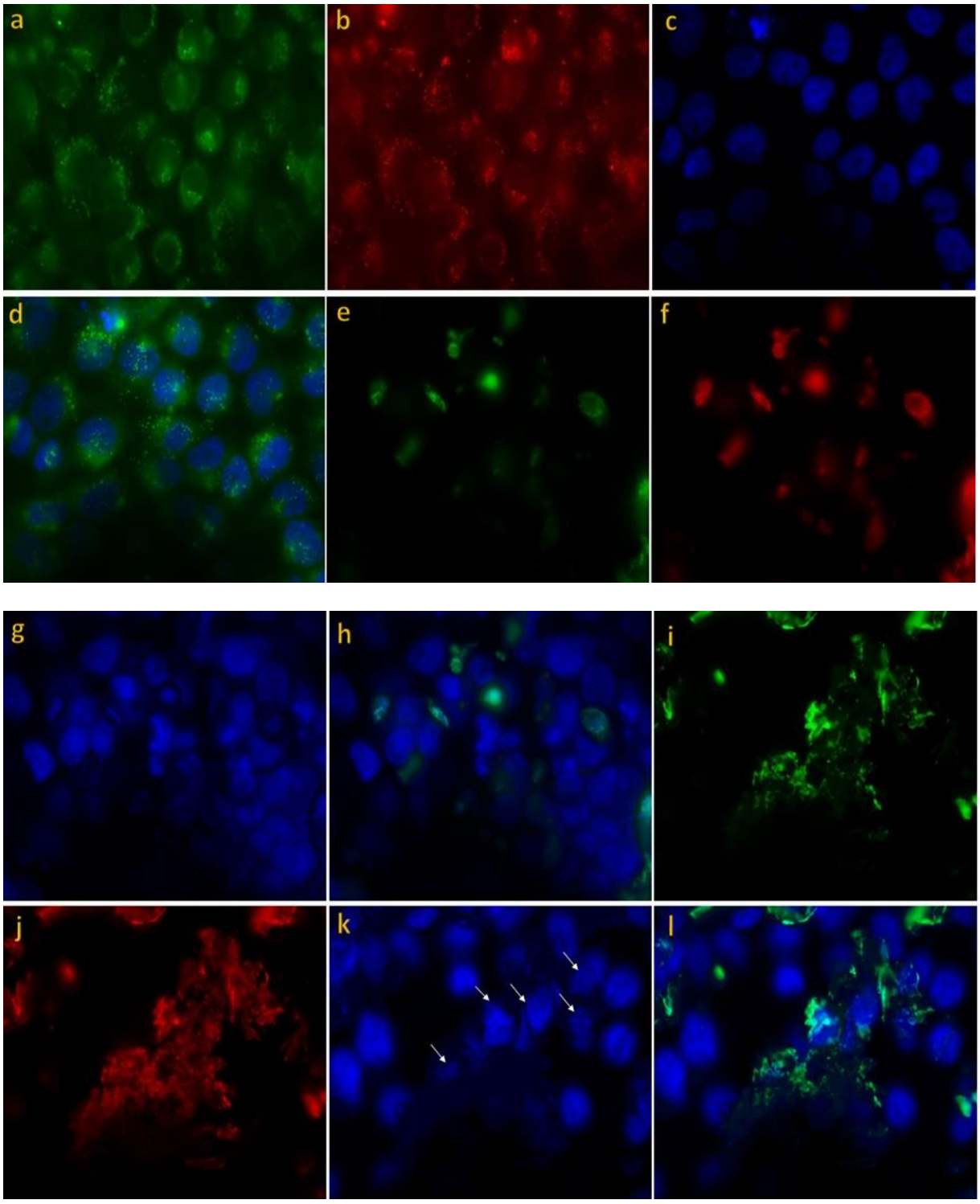
a
b
c
d
e
f
g
h
i
j
k
l

**Figure 51**. Florescence imaging studies of bare QDs (a and b), QD-LVs-F12 (e and f) and QDs-CNP-F9 (i and j) with Hela cells using the green/ visible and red/infra-red florescence channels. Hoechst 33342 staining of the nucleus and merged images corresponding to bare QDs (c and d), QD-LVs-F12 (g and h) and QD-CNP-F9 (k and l).

The internalization and cell uptake of QDs-LVs-F12 and QDs-CNP-F9 can be observed in green and red channel of the florescence microscopy (figure 51 e-f, i-j). The amorphous staining caused by the QDs-LV-F12 is shown clearly in figure 51 g with a slight distortion in morphology of the nucleus. Larger amorphous staining is observed in figure 51 k corresponding to QDs-CNP-F9 leading to more distortion of the nucleus morphology. However, in 2014, Ghormade *et al* also reported similar amorphous staining pattern during the exposure of NIH3T3 mouse embryonic fibroblast cell lines to green fluorescent CdTe QDs loaded in CNPs [58]. In their study, DAPI was further used to stain the cell nucleus to confirm the internalization of the composite into the cells. The amorphous staining caused by these composites upon exposure to HeLa cells in our study may be attributed to aggregation of particles during the encapsulation of QDs in liposomes and Chitosan nanoparticles (CNP). This was also observed from the TEM images and florescence spectra results discussed in figure (32- 33, 37 and 40).

The merged images of the composite displayed in figure (h and l) shows that the liposome and chitosan composite can be found around the nucleus, this observation depicts their localization and internalization in the cell cytoplasm. The uptake and internalization of liposome and chitosan composites can possibly be attributed to the endocytosis uptake mechanism [54, 92- 93]. While the coating of the surface of the QDs with phospholipid for QDs-LVs-F12 allows its easy diffusion across the cell membrane into the cytosol, the presence of positively charged chitosan

surface creates an interaction with the cell membrane which allows easy location of QDs-CNP-F9 in the cytosol [58].

Although the internalization of bare QDs into the cells did not change the morphology of the nucleus but the huge toxicity earlier displayed by this compound figure 49 and 50; limits its bio applicability in various applications.

However, the distortion in the nucleus morphology observed from the amorphous staining of the composite, which is more dominant in figure 51 k (see white arrows) for QDs-CNP-F9 is still under investigation. Since large amorphous staining can be observed for QDs-CNP-F9 compared to QDs-LV-F12 it is concluded that the encapsulation of multi-core-shell QDs in liposome showed better biocompatibility compared to CNP. It must be recalled that the cytotoxicity studies discussed previously from figure 49- 50 and also in Table 12 prove that liposome composite demonstrate minimal toxicity compared to chitosan composite. All these results provide clear evidence that in order to use CdTe multi-core-shell QDs as tracer or imaging device in applications such as drug delivery it is advisable to encapsulate this compound in more biocompatible environment such as liposome.

## 7. Conclusion.

The summary of this whole project discusses how the biocompatibility of CdTe multi-core-shell QDs can be further improved to allow their continual use in florescence imaging studies. In chapter two (2.6.1 – 2.6.2), the synthesis of these hetero-structured compound was firstly initiated by synthesizing their corresponding cores, which were then dual capped with combinations of five different thiol co-capping ligands using a one pot synthetic method under open-air atmospheric conditions. These conditions were successfully applied to make high-quality QDs with good fluorescence properties. The synthesized QDs shows good stability over at least 6 to 12 months with no special treatment. In chapter three (3.1 – 3.4) it was revealed that the physio-chemical techniques used during the construction of these cores provided straightforward evidence of successful dual-capping of the QDs. The QDs capped with GSH exhibited much more enhancement in surface passivation than those capped with other capping agents. In addition, the use of Thio-glycolic acid/Mercaptopropionoic acid (TGA/MPA) in a dual capping system was found to provide increased intensities due to the supply of enough negative charges by the thiols to the surface of the nano-crystals. A follow up study on the pH-florescence dependent studies reveals that MPA-TGA and L-cysteine-TGA dual-capped QDs exhibited interesting pH-dependent luminescence properties. Hence, these showed that the QDs could be deemed as potential pH responsive nano-devices that would be useful for fluorescence quenching evaluations.

In a further attempt to convert the synthesized CdTe core into a multi-core-shell system, in chapter two (2.6.3 – 2.6.5), the cores were upgraded to core-shells through the coating of CdSe shell at the surface of CdTe core and finally to multi-core-shell QDs. During the synthesis of these QDs, optimization of the reaction conditions was achieved by varying the concentration of

reduced selenium in the reaction vessels to give various mole ratios of Te:Se, starting from 1: 0.2 up to 1:1. However, in chapter four (4.1- 4.3), it was reported that almost all the CdTe dual capped core-shells showed their highest emission intensities at 1:0.2 of Te:Se following 3 hrs reaction time compared to other mole ratios for equal reaction times. It was highlighted that the use of TGA as one of the dual stabilizing agents in the case of GSH-TGA, L-cysteine-TGA and MPA-TGA demonstrated enhanced fluorescence compared to GSH-MPA and L-cysteine-MPA. Nevertheless, the combination of MPA-TGA to stabilize the surface of the QDs was observed to produce higher fluorescence intensities at all mole ratios of Te/Se this can virtually be observed for all its reaction times compared to the other four dual capped thiols: L-cysteine-TGA, GSH-MPA, L-cysteine-MPA and GSH-TGA.

Furthermore, the synthesis of five dual capped CdTe multi core-shells QDs with enhanced optical properties was achieved with a minimum reaction time of 5 mins and maximum time of 35 mins in chapter two (2.6.6- 2.6.8). It was pointed out in chapter four (4.4 – 4.7) that upon optimization of the reaction condition, the largest shift in wavelength at 3 hrs for the core-shell and 35 min for the multi-core-shell corresponded to 21 ml injection of Zn and Se ions, respectively. The change in injection time intervals from 5 min to 30 min contributed no significant differences in wavelength shift compared to the shift caused by variation in the amount of Zn and Se ion. It was further observed that multi core-shell dual capped with glutathione (GSH) demonstrated a significant shift in wavelength only after 14 and 21 ml injection of Zn and Se ions respectively. Injections at 7 ml of Zn and Se ions only enhanced their fluorescence intensity with no significant shift in their wavelength. The positive effects of using TGA as a co-stabilizing agent was also observed during the shell growth from 25 – 35 mins by comparing the fluorescence intensity of GSH-TGA-CdTe core-shell-shell to GSH-MPA-CdTe

core-shell-shell. The same observation can be made with L-cysteine-TGA-CdTe core-shell-shell compared to L-cysteine-MPA-CdTe core-shell-shell at the similar reaction time. The main observation is that for all the thiol-dual caps, the highest emission maxima occur at 35 mins reaction time corresponding to 21 ml injection of the Zn and Se ions for MPA-TGA dual cap (PLQY 16 %). A further fluorescence enhancement with PLQY of 23 % was observed during the continuous exposure of MPA-TGA-CdTe multi-core-shell QDs at 35 mins reaction times to UV radiation for 18 hrs. Similarly, the exposure of MPA-TGA-CdTe core-shell QDs to UV radiation at 3 hrs reaction time led to an increase in its PLQY from 73 % to 89 %. The EDS result also confirmed the fabrication of CdTe multi core-shell QDs by revealing the presence of Zn and Se ions. Therefore, the aim of converting our synthesized CdTe core-shell QDs to a multi-core-shell QDs proved a success. We concluded that the synthetic approach followed in this study can be used to produce CdTe multi-core-shell heterostructures emitting at longer emission wavelengths, this is achievable within a short reaction time. Hence, this method of synthesis can be applied to the synthesis of similar QDs due to effective energy conservation which contribute towards green chemistry. The use of dual capping thiol especially TGA to stabilize the surface of synthesized core-shell and multi-core-shell QDs also assisted in the improvement of the surface chemistry of the synthesized chalcogenides.

To further improve the biocompatibility of the rapidly synthesized CdTe multi-core-shell QDs, the synthesized QDs were encapsulated in liposome vesicles (LVs) and chitosan nanoparticles (CNP) in chapter two (2.2- 2.5). Each encapsulation led to the generation of about 14 formulations for QD-LVs and 12 formulations for QD-CNPs which were done in triplicates. It was observed that QD-LVs-F12 and QD-CNP-F9 demonstrated the highest loading efficiency of 41.5 ± 5.84 and 58.6 ± 5.17 respectively

In chapter five (5.1 – 5.2.5.5), the photoluminescence spectra of all the composites confirms an interaction between the QDs and the delivery systems. Morphology from the TEM images reveals the shape and the difference in size of the bare QDs, empty liposome and QDs loaded in LVs and CNP. The TEM images also confirm the encapsulation of the QDs in the liposomes and CNP. The FTIR spectra for the QD-CNP demonstrate an interaction between the CNP and QDs through the changes in the absorption bands of various functional groups present at the surface of the compounds. Results from the XRD pattern of QD-CNP also show the amorphous behavior demonstrated by the empty CNP and the crystalline pattern depicted by the QDs and QDs loaded in CNP. The EDS differentiate the elemental composition of the bare QDs from QDs-LVs and QDs-CNP confirming the embedding of the QDs in this delivery systems. The TGA results all confirm enhanced thermal stability of the composites compared to the bare QDs and this confirms the encapsulation of the QDs in the liposomes and CNP. While QD-CNP composite demonstrated poor photo-stability under UV irradiation, QDs-LVs show enhanced photo-stability compared to bare QDs, this is due to the encapsulation of the QDs in the aqueous core of the liposomes.

In chapter two (2.2- 2.5), we further explained that the cytotoxicity and florescence imaging studies of the composites and their counter parts were conducted in other to investigate the environment which is more bio-compatible for the QDs. This was carried out using HeLa and Vero cells. It was estimated from the toxicity study that the compound with the concentration > 0.5 mg/ml that did not kill at least 50 % of the cell is regarded to show minimal toxicity. In chapter six (6.1 - 6.3) we reported that apart from the bare core-shell and multi-core-shell QDs that demonstrate high mortality, the empty liposome and CNP showed low toxicity to both cells ($IC_{50}$ > 0.5 mg/ml). While QDs-LVs at F1 and F12 demonstrated lower toxicity with the cells

($IC_{50}$ > 0.5 mg /ml), QD-LVs-F11 showed more toxicity with HeLa cells ($IC_{50}$ = 0.4364 mg/ml) and reduced toxicity was observed with Vero cells ($IC_{50}$ > 0.5 mg/ml). Similarly, at least 50 % of the cells survived for QD-CNP at F3 and F9 at concentration greater than 0.5 mg/ ml but QD-CNP-F4 were found to demonstrate huge toxicity with HeLa cells ($IC_{50}$ = 0.1618 mg/ ml) compared with QDs-LV-F11 even though they were found to be less toxic with Vero cells ($IC_{50}$ > 0.5 mg/ml). It also implied that during the cytotoxicity studies, cell deaths might have also occurred due to the generation of free radicals also known as reactive oxygen species (ROS) by the encapsulated QDs in both liposomes and CNP as supported from literature. While Vero cells might have withstood the effects of lipid peroxidation caused by free radicals, oxidative stress generated from lipid peroxidation might have contributed to cell death in the HeLa cells during interaction with some species.

Therefore, the cytotoxicity results show that liposomes seem to advance the biocompatibility of the multi-core-shell QDs compared to CNP. This was revealed by the $IC_{50}$ value of the QD-LVs-F11 and QD-CNP-F4.

Result from the cellular uptake studies also show that both liposome and chitosan composite are well taken up by the cells. Their location around the nucleus indicate that they can be found in the cytoplasm. The slight change in the morphology of the nucleus was found to be more predominant with QDs-CNP-F9. Large amorphous staining of the cell vesicles can also be found with chitosan composites (QDs-CNP-F9) compared to liposome composite (QDs-LVs-F12). The internalization of bare QDs in HeLa cells was also observed with no change in the nucleus morphology but the huge toxicity displayed by this compound limits its' biocompatibility. Therefore, these results provide clear evidence that encapsulating CdTe multi-core-shell QDs in liposome shows better biocompatibility compared to chitosan nanoparticles.

It must also be noted that all the synthesized thiol dual capped core-shell and multi-core-shell QDs discussed in this study demonstrated good photostability for several months without aggregations. Some of them are still stored at room temperatures in our lab up to this present moment.

Nevertheless, to further improve on some of the various challenges encountered during this study, we plan to further investigate in the future how we can improve the florescence properties of this QDs upon encapsulating them in liposomes and chitosan nanoparticles. This will assist us to reduce the problem of florescence quench being observed in most of the composite discussed in this study. The slight change in the morphology of the nucleus which was more predominant with chitosan composite will also be examined.

We also aim to conduct some lipid peroxidation study in other to be sure that the generation of free radicals by the QDs might also be responsible for the cell death which was mostly attributed to chitosan composites.

It must be noted that we recently took advantage of the good electronic properties displayed by some of the synthesized core-shell QDs in this study and used them for applications in memory devices. This was a collaboration work recently done with some other research groups that was not presented in this study.

Another study we plan to execute very soon is to encapsulate some drugs together with the multi-core-shell QDs in liposomes for the purpose of drug delivery applications in the treatment of micro-organism or virus infected cells. This is essential due to enhanced biocompatibility displayed after embedding the multi-core-shell QDs in liposomes. It further gives us an

assurance that liposomes can be used to simultaneously encapsulate both CdTe multi-core-shell QDs and model drugs for both diagnosis and therapeutic evaluations.

## 8. References.


1. Oluwafemi S.O, Daramola O.A and Vuyelwa N (2014) A facile green synthesis of type II water soluble CdTe/CdS core shell nanopartices. *Mat Lett*, 133, 9-13.
2. Jing L, Kershaw S.V, Li Y, Huang X, Rogach AL and Gao M (2016) Aqueous based semiconductor nanocrystals. *Chem. Rev*, 116, 10623−10730.
3. Daramola O.A, Siwe Noundou X, Nkanga C.I, Tseki P.F, Krause R.W.M (2020) Synthesis of pH Sensitive Dual Capped CdTe QDs: Their Optical Properties and Structural Morphology. *J Fluoresc,* 30, 557- 564.
4. Yuanyuan W, Kefeng C and Yao Xi (2011) Synthesis and photoluminescence properties of water-soluble CdTe/CdS core/shell quantum dot. *Micro and Nanoletters*, 6, 43-141.
5. Raju S.P, Hareesh K, Chethan P.S, Dhole S.D and Sanjeev G (2017) ZnS shell growth on thiol capped CdTe quantum dots using gamma irradiation. *AIP*, 1832, 1-4.
6. Zhang Y and Li Yan X.P (2009) Microwave-assisted synthesis of water-dispersed CdTe/CdSe core/shell type II quantum dots. *Small*, 5, 185-189.
7. Muthu M.S, Kulkarni S.A, Raju A, Feng S.S (2012) Theranostic liposomes of TPGS coating for targeted co-delivery of docetaxel and quantum dots. *Biomaterials*, 33, 3494- 3501.
8. Lazarovits Y.Y, Chen Y.Y, Sykes E.A and Chan W.C.W (2015) Nanoparticles- blood interactions: the implication on solid tumor targeting. *Chem. Commun*, 51, 2756-2767.
9. Luk B.T, Ronnie H. F and Liangfang Z (2012) Lipid- and Polymer-Based Nanostructures for Cancer Theranostics. *Theranostics,* 12, 1117-1126.
10. Crosby, G.A and Demas, J.N. (1971) Measurement of quantum yields *Review J Phys Chem*,75, 991-1024.

11. Szuha, Bernard F. (1989). "Chapter 7". Lecithins: Sources, Manufacture & Uses. *The American Oil Chemist's Society,* 12, 400- 683.
12. Liu Y.F and Yu J.S (2009) Selective synthesis of CdTe and high luminescence CdTe/CdSe quantum dots: The effect of Ligands. *J. Colloid Interface Sci*, 333, 690-698.
13. Fang Z, Liu L, Xu L.L, Yin X.G and Zhong X.H (2008) Synthesis of highly stable dihydrolipoic acid capped water-soluble CdTe nanocrystals. *Nanotechnology,* 19, 23- 30.
14. Wang H, Chen Q, Tan Z, Yin X and Wang L (2012) Electrochemiluminescence of CdTe quantum dots capped with glutathione and thioglycolic acid and its sensing of $pb^{2+}$. *Electrochim., Acta,* 72**,** 28-31.
15. Daramola O.A, Siwe-Noundou X, Tseki P.F, Krause R.W.M (2021) Rapid Synthesis of Thiol-Co-Capped-CdTe/CdSe/ZnSe Core Shell-Shell Nanoparticles: Their Optical and Structural Morphology. *Nanomater*, 11, 1174- 1193.
16. Ruosheng Z, Jincheng L, Qiang W, Tingting Z, Song H and Xuanming L (2009) Aqueous synthesis of type-II CdTe/CdSe core–shell quantum dots for fluorescent probe labeling tumor cells. *Nanotechnology*, 20, 1-8.
17. Gaponik N and Andrey L.R (2010) Thiol-capped CdTe nanocrystals: progress and perspectives of the related research fields. *J. Phys. Chem,* 12, 93-8685.
18. Daramola O.A, Xavier Siwe N, Krause R.W.M.K and Marks J.A (2017) Facile synthesis of glutathione-l-Cysteine co-capped CdTe core shell system: Study on optical and structural morphology. *J. nanosci. Nanotechnol,* 17, 1-7.
19. Wu S, Jun D, Jie Z, and Shurfen Z (2011) A simple and economical one-pot method to synthesize high-quality water soluble CdTe QDs.*J. Mater. Chem,* 22, 14573-14578

20. Kim J, Huy B.T, Sakthivel K, Choi H.J, Joo W.H, Shin S.H, Lee M.H and Lee Y.I (2015). Highly fluorescent CdTe quantum dots with reduced cytotoxicity- A Robust biomarker. *Sens BioSensing Res*, 3, 46-52.

21. Gao X, Cui Y, Levenson R.M and Chung L.W (2004) In vivo cancer targeting and imaging with semiconductor quantum dot. *Nat Biotechnology*, 22, 76-969.

22. Chang S.Q, Kang B, Dai Y.D, Zhang H.X, Chen D (2011) One-step fabrication of biocompatible chitosan coated ZnS and ZnS: $Mn^{2+}$ quantum dots via a γ-radiation route. *Nanoscale Res. Lett*, 6, 591–597.

23. Oberdörster G, Oberdörster E, Oberdörster J (2005) Nanotoxicology: an emerging discipline evolving from studies of ultrafine particles. *Environ. Health Perspect*, 113, 823–839.

24. Zhang Y, Li Y, Yan X. P (2009) Aqueous Layer-by-Layer Epitaxy of Type-II CdTe/CdSe Quantum Dots with Near-infrared Fluorescence for Bioimaging Applications. *Small* 5, 185−189.

25. Kale S, Kale A, Gholap H, Rana A, Desai R, Banpurkar A, Ogale S, Shastry P (2012) Quantum dot bio-conjugate: as a western blot probe for highly sensitive detection of cellular proteins. *J. Nanopart. Res*, 14,732–736.

26. Gerion D, Pinaud F, Williams S.C, Parak W.J, Zanchet D, Weiss S, Alivisatos A.P (2001) Synthesis and properties of biocompatible water-soluble silica-coated CdSe/ZnS semiconductor quantum dots. *J. Phys. Chem.* B, 105, 8861–8871.

27. Mengying L, Huameng Z, Hongyan Z, Pan S, Kuiyu Y, Meng W, Zaizheng D, Shukun X (2010) Preparation and purification of l-cysteine capped CdTe quantum dots and its self-recovery of degenerate fluorescence,.*Luminescence,* 130, 1935-1940

28. Nie Q.L, Tan W.B, Zhang Y (2006) Synthesis and characterization of monodisperse chitosan nanoparticles with embedded quantum dots. *Nanotechnology*,17,140–144.

29. Wang Y and Chen L (2011) Quantum dots, lighting up the research and development of nanomedicine. *Nanomed. Nanotechnol. Biol. Med*, 7, 385–402.

30. Song KK, Lee S (2001) Highly luminescent (ZnSe)ZnS core-shell quantum dots for blue to UV emission: synthesis and characterization. *Curr. Appl. Phys.*1,169–173.

31. Khadem-Abbassi K, Rinnert H, Balan L, Doumandji Z, Joubert O, Masteri-Farahani M and Schneider R (2019) $CdTe_{0.5}S_{0.5}$/ZnS Quantum Dots Embedded in a Molecularly Imprinted Polymer for the Selective Optosensing of Dopamine. *Nanomaterials*, 9, 693- 700.

32. Wang J, Li N, Shao F and Han H (2015) Microwave-assisted synthesis of high-quality CdTe/CdS@ZnS–$SiO_2$ near-infrared-emitting quantum dots and their applications in $Hg^{2+}$sensing and imaging. *Sensors and Actuators B*, 207, 74–82

33. Yang S.S, Ren C.L, Zhang Z.U, Hao J.J, Hu Q and Chen, X.G (2010) Aqueous synthesis of CdTe/CdSe core/shell quantum dots as pH sensitive fluorescence probe for determination of ascorbic acid. *J Fluoresc*, 21, 1123-1129.

34. Chen X, Liang L, Yongxian L, Jianna Y, Yichen T and Xiuli W (2015) Microwave-Assisted Synthesis of Glutathione-Capped CdTe/CdSe near-infrared Quantum Dots for cell imaging. *Int. J. Mol. Sci*, 16, 11500-11508.

35. Zhang H, Sun P, Liu C, Gao H, Xu Z, Fang J, Wang M, Liu J and Xu S (2011) L-Cysteine capped CdTe/CdS quantum dots: preparation, characterization and immune-labelling of Hela cells. *Luminescence*, 26, 86- 92.

36. Samanta A, Deng Z and Liu Y (2012) Aqueous Synthesis of Glutathione-Capped CdTe/CdS/ZnS and CdTe/CdSe/ZnS Core/Shell/Shell Nanocrystal Heterostructures. *Langmuir*, 21, 8205–8215.

37. Zeng R, Zhang T, Liu J, Hu S, Wan Q, Liu X, Peng Z and Zou B (2009) Aqueous synthesis of type-II CdTe/CdSe core–shell quantum dots for fluorescent probe labeling tumor cells. *Nanotechnology*, 20, 1-8.

38. Fontana J, Yin H, Chen Y, Florez R, Brismar H and Fu Y (2017) Transport and release of colloidal 3-mercaptopropionic acid-coated CdSe–CdS/ZnS core-multishell quantum dots in human umbilical vein endothelial cells. *Int J Nanomedicine*, 12, 8615-8629

39. He Z, Zhu H, Zhou P (2012) Microwave-assisted aqueous synthesis of highly luminescent carboxymethyl chitosan-coated CdTe/CdS quantum dots as fluorescent probe for live cell imaging. *J Fluoresc*, 22, 193–199.

40. Saikia D, Chakravarty S, Sarma N. S, Bhattacharjee S, Datta P and Adhikary N. C (2016) Aqueous synthesis of highly stable CdTe/ZnS Core/Shell quantum dots for bioimaging. *Luminescence*, 32, 401- 408.

41. Green M, Williamson P, Samalova M, Davis J, Brovelli S and Dobsond P (2009) Synthesis of type II/type I CdTe/CdS/ZnS quantum dots and their use in cellular imaging. *Journal of Material Chemistry*, 19, 8341- 8346.

42. Taniguchi S, Green M, Rizvib S.B and Seifalian, A (2011) The one-pot synthesis of core/shell/shell CdTe/CdSe/ZnSe quantum dots in aqueous media for in vivo deep tissue imaging. *J. Mater. Chem*, 21, 2877- 2882.

43. Aldeek F, Lavina B, Jacques L and Raphael S (2008) The influence of capping thioalkyl acid on the growth and photoluminescence efficiency of CdTe and CdSe quantum dots. *Nanotechnology*, 19, 1-9

44. Yu Y, Xu L, Chen J, Gao H, Wang S, Fang J and Xu S (2012) Hydrothermal synthesis of GSH-TGA co-capped CdTe quantum dots and their application in labelling colorectal cancer cells. *Colloids Surface., B*, 95, 53-247.

45. Adegoke O and Nyokong (2013) T. Probing the sensitive and selective luminescent detection of peroxynitrite using thiol-capped CdTe and CdTe@ZnS quantum dots. *J.Lumin*, 134, 448-44.

46. Vuyelwa N, Sundararajan P, Sandile P.S, Tetsuya K and Oluwatobi S.O (2017) Simple green synthesis of amino acid functionalised CdTe/CdSe/ZnSe core-multi shell with improved cell viability for cellular imaging. *Mat Lett*, 189, 168-171.

47. Zhang Y.Y, Kim J.Y, Kim Y and Jang D.J (2012) Controlled optical properties of water-soluble CdTe/CdS/ZnS quantum dots. *J Nanopart Res*, 14,1117- 1126.

48. Monaheng N.M, Parani S, Gulumian M and Oluwafemi O.S (2019) Eco-friendly synthesis of glutathione-capped CdTe/CdSe/ZnSe core/double shell quantum dots: their cytotoxicity and genotoxicity effects on Chinese hamster ovary cells. *Toxicol Res (Camb)*, 6, 869- 874.

49. Wang A, Zheng Y and Peng F (2014) Thickness-Controllable Silica Coating of CdTe QDs by Reverse Microemulsion Method for the Application in the Growth of Rice. *Journal of Spectroscopy*, 20, 345- 350.

50. Modlitbová P, Kleparnik K, Farka Z, Pořízka P, Skládal P, Novotný K, and KaiserJ (2018) Time-Dependent Growth of Silica Shells on CdTe Quantum Dots. *Nanomaterials*, 8, 439-450.

51. Ruan J, Wang K, Song H, Xu X, Ji J and Cui D (2011) Biocompatibility of hydrophilic silica-coated CdTe quantum dots and magnetic nanoparticles. *Nanoscale Res Lett*, 6, 299-310.

52. Wolcott A, Gerion D, Visconte M, Sun J, Schwartzberg A, Chen S, and Jin Z. Zhang (2006) Silica-Coated CdTe Quantum Dots Functionalized with Thiols for Bioconjugation to IgG Proteins. *The Journal of Physical Chemistry* B, 11, 5779-5789.

53. Bhushan S. P, Vladimir V. C and Vladimir P. T (2015) New Developments in Liposomal Drug Delivery. *Chem. Rev,* 115, 10938−10966.

54. Ye C, Wang Y, Li C, Yu J and Hu Y (2013) Preparation of liposomes loaded with quantum dots, fluorescence resonance energy transfer studies, and near-infrared in-vivo imaging of mouse tissue. *Microchim Acta,* 180, 117–125.

55. Wang J.Y, Zhao J.F, Wang P.N, Yang W.L and Chen J.Y (2011) Liposome encapsulation of thiol-capped CdTe quantum dots for enhancing the intracellular delivery. *J Fluoresc*, 21, 1635- 1642.

56. Chu M, Zhuo S, Xu J, Sheng Q, Hou S and Wang R (2010) Liposome-coated quantum dots targeting the sentinel lymph node. *J Nanopart Res,* 12, 187–197.

57. Galante R, Rediguieri C.F, Kikuchi I.S, Vasquez P.A.S, Colaço R, Serro A.P and Pinto T.J (2016) About the Sterilization of Chitosan Hydrogel Nanoparticles. *PLoS ONE,* 12, 862- 880.

58. Ghormade V, Gholap H, Kale S, Kulkarni V, Bhat S, Paknikar K (2015) Fluorescent cadmium telluride quantum dots embedded chitosan nanoparticles: a stable, biocompatible preparation for bio-imaging. *J Biomater Sci Polym Ed*, 26, 42-56.

59. Rouhani A, Mina Shakeri S and Bashari A (2018) Recent advances in application of chitosan and its derivatives in functional finishing of textile. *The Impact and Prospects of Green Chemistry for Textile Technology (The textile book series)*,13, 107- 113.

60. Younes I, Rinaudo M (2015) Chitin and chitosan preparation from marine sources. Structure, properties and applications. *Mar. Drugs*, 13, 1133-1174.

61. Nessaa F, Masumb S.M, Asaduzzamana M, Roya S.K, Hossaina M.M and Jahanc M.S (2010) A process for the preparation of chitin and chitosan from prawn shell waste. *Bangladesh J. Sci. Ind. Res*, 45, 323-330.

62. Hussain M.R, Iman M and Maj T.K (2013) Determination of degree of deacetylation of chitosan and their effect on the release behavior of essential oil from chitosan and chitosan-gelatin complex microcapsules. *Ija-Era*, 6, 4-12.

63. No H.K, Meyers S.P (1995) Preparation and characterization of chitin and chitosan—a review. *J. Aquat. Food Prod. Technol*, 4, 27-52.

64. Muzzarelli R, Baldassarre V, Conti F, Ferrara P, Biagini G, Gazzanelli G, Vasi V (1988) Biological activity of chitosan: ultrastructural study. *Biomaterials,* 9,247–252.

65. Jigar M.J, Sinha V.K (2007) Ceric ammonium nitrate induced grafting of polyacrylamide onto carboxymethyl chitosan. *Carbohyd Polym,* 67, 427–435.

66. Wang P.F, Wu S.H.K, Shi X.Y, Deng B.M, Sun C (1998) The aggregation behavior of chitosan bioelectric in aqueous solution using a fluorescence probe. *J Mater Sci,* 33,1753–1757.

67. Xie W.M, Xu P.X, Wang W, Liu Q (2002) Preparation and antibacterial activity of a water-soluble chitosan derivative. *Carbohyd Polym* 50, 35–40.

68. Huang M, Khor E, Lim L.Y (2004) Uptake and cytotoxicity of chitosan molecules and nanoparticles: effects of molecular weight and degree of deacetylation. *Pharm. Res*, 21, 344–353.

69. Hamidi M, Azadi A, Rafiei P (2008) Hydrogel nanoparticles in drug delivery. *Adv Drug Delivery Rev*, 60, 49- 55.

70. Sarkar S.D, Farrugia B.L, Dargaville T.R, Dhara S (2013) Physico-chemical/biological properties of tripolyphosphate cross-linked chitosan-based nanofibers. *Mater Sci Eng C Mater Biol Appl*, 33, 54- 66

71. Li J, Huang Q (2012) Rheological properties of chitosan tripolyphosphate complexes: From suspensions to microgels. *Carbohydr Polym*, 2, 7- 15.

72. Dutta P.K., Dutta J and Tripathi V.S (2004) Chitin and Chitosan: Chemistry, Properties and Applications. *CSIR,* 63, 20- 31.

73. Riccardo A.A (1988) Carboxymethylated chitins and chitosans. *Carbohydr. Polym,* 8, 1- 21.

74. Qiang M, Zi H, Na Y, Yang L, Xing G. (2014) A novel carboxymethyl chitosan–quantum dot-based intracellular probe for $Zn^{2+}$ ion sensing in prostate cancer cells. *Acta Biomaterialia*, 10, 868–874.

75. Parani, S, Lakshmi B. S & Pandian K (2012) Biopolymer Encapsulation of CdTe Quantum Dot for In Vitro Controlled Drug Delivery Release of 6-Mercaptopurine. *Advanced Materials Research*, 584, 258–262.

76. Li L, Chen D, Zhang Y, Deng Z, Ren X, Meng X, Fangqiong Tang1, Ren J and Zhang L (2007) Magnetic and fluorescent multifunctional chitosan nanoparticles as a smart drug delivery system. *Nanotechnology*, 18, 405- 411.

77. Kumar H, Srivastava R, Dutta P.K (2013) Highly luminescent chitosan-l-cysteine functionalized CdTe quantum dots film: Synthesis and characterization. *Carbohydrate Polymers*, 97, 327-334.

78. Lihong J, Stephen V.K, Yilin L, Xiaodan H, Yingying L, Andrey L.R and Mingyuan G (2016) Aqueous based semiconductor nanocrystals. *Chem. Rev,* 116, 10623−10730

79. Zhang J, Li J, Zhang J.X, Xie R.G and Yang W.S (2010) Aqueous synthesis of ZnSe nanocrystals by using glutathione as ligand: The pH-mediated coordination of $Zn^{2+}$ with glutathione, *J. Phys. Chem*, 114, 11087−11091.

80. Krezel A and Bal W (1999) Coordination chemistry of glutathione, Acta Biochim. *Polym*. 146, 567−580.

81. Lan G. Y, Lin Y. W, Huang Y. F and Chang H. T (2007) Photo-assisted synthesis of highly fluorescent ZnSe (S) quantum dots in aqueous solution. *J. Mater. Chem*, *17*, 2661–2666.

82. Shavel A, Gaponik N and Eychmüller A (2004) Efficient UV-blue photoluminescence thiol-stabilized water-soluble alloyed ZnSe (S) nanocrystals. *J. Phys. Chem*. B, *108*, 5905–5908.

83. Talapin D.V, Gaponik N, Borchert H, Rogach A.L, Haase M, Weller H (2002) Etching of colloidal InP nanocrystals with fluorides: Photochemical nature of the process resulting in high photoluminescence efficiency. *J. Phys. Chem. B*, *106*, 12659–12663.

84. Hosnedlova B, Vsetickova M, Stankova M, Uhlirova D, Ruttkay-Nedecky B, Ofomaja A, Fernandez C, Kepinska M, Baron M, Ngoc B.D, Nguyen H.V, Thu H.P.T, Sochor J, Kizek R (2020) Study of Physico-Chemical Changes of CdTe QDs after Their Exposure to Environmental Conditions. *Nanomaterials*, *10*, 847- 865.

85. Derfus A.M, Chan W.C, Bhatia S.N (2004) Probing the cytotoxicity of semiconductor quantum dots. *Nano Lett 4*, 11–18.

86. Yougui, Liao.; Practical Electron Microscopy and Database (2006) www.globalsino.com/EM/.

87. Chessman K. H and Slater T.F (1993) An introduction to free radicals' chemistry. *Med Bull*, 49, 1– 8.

88. Lobo V, Patil A, Phatak A and Chandra N (2010) Free radicals, antioxidants and functional foods: Impact on human health. *Pharmacogn* revised, 8, 324-991.

89. Nguyen k, Seligy V, Rippstein P and Tayabali A (2010) Cadmium Telluride quantum dot nanoparticles cause oxidative stress and apoptosis in mammalian cells. *European Cells and Materials*, 20, 187-200.

90. Zhang T, Hu Y, Tang M, Kong L, Ying J, Wu T, Xue Y and Pu Y (2015) Liver toxicity of cadmium telluride quantum dots (CdTe QDs) due to oxidative stress in vitro and in vivo. *Int. J. Mol. Sci*, 16, 23279-23299.

91. Xie G, Du Q, Zheng M, Chen W, Liu N, Lu Y, Huang P and Sun Z (2013) Oxidative damage effects induced by CdTe QDs in mice liver. *Journal of Hygiene Research*, 1, 39-43.

92. Huang M, Khor E, Lim LY (2004) Uptake and cytotoxicity of chitosan molecules and nanoparticles: effects of molecular weight and degree of deacetylation. *Pharm. Res*. 21, 344–353.

93. Cho Y, Shi R, Ben Borgens RB (2010) Chitosan nanoparticle-based neuronal membrane sealing and neuroprotection following acrolein-induced cell injury. J. *Biol. Eng*, 4, 2–11.

## 9. Recommendation.

(a) Based on this studies, it is highly recommended that the as-synthesized CdTe multi-core-shell nanocomposite can be used as a device for various applications in cellular imaging with high performance efficiency and low toxicity.

(b) It is also recommended that encapsulation of various drugs models such as anti-cancer, anti-microbial and anti-viral drugs in liposomes and Chitosan nanoparticles also need to be investigated for comparative bio-compatibility studies. In-fact this study is gradually under investigation in our labs.

## 10. Academic Presentations.

(a) Nano world conference- 2018.

Doubletree by Hilton hotel Philadelphia International Airport USA. Oral presentation on the facile synthesis of pH and light sensitive thiol-dual capped CdTe QDs.

(b) International conference on Advanced and Nano-materials- 2019.

Delta Hotel by Marriott Montreal, Canada. Oral presentation on the rapid synthesis of MPA-TGA dual capped CdTe multi core-shell.

## 11. Articles Published within the PhD thesis.

(a) Daramola O.A, Siwe Noundou X, Potlaki F.T, Krause R.W.M (2021) Rapid synthesis of thiol-co-capped-CdTe/CdSe/ZnSe multi-core-shell QDs: their optical and structural morphology. *Nanomaterials* 11, 1174-1193. (Q1 journal, IF 4.0).

(b) Daramola,O.A, Siwe Noundou X, Nkanga, C.I, Krause R.W.M (2020). Synthesis of pH Sensitive Dual Capped CdTe QDs: Their Optical Properties and Structural Morphology. *J Fluoresc* 30, 557–564. (Q2 journal, IF 1.85).

## 12. Recent articles published in 2021 outside the PhD thesis

(c) Zolile Wiseman Dlamini, Sreedevi Vallabhapurapu, Olamide Abiodun Daramola *et al*., (2022) Resistive Switching in CdTe/CdSe Core–Shell Quantum Dots Embedded Chitosan-Based Memory Devices. Journal of Circuits, Systems, and Computers. (Available online in April)

(d) Zolile Wiseman Dlamini, Sreedevi Vallabhapurapu, Olamide Abiodun Daramola *et al.*, Conduction and Resistive Switching in Dropcast CdTe/CdSe Core-Shell Quantum Dots Embedded Chitosan Composite. Springer Nature (December 2021). (Recently accepted manuscript).

## 13. Articles in-preparation

(e) Encapsulation of MPA-TGA- co-capped-CdTe/CdSe/ZnSe multi-core-shell QDs in liposomes and chitosan nanoparticles; their comparative biocompatibility studies using Hela and Vero cells.